

NASA CR-73221

ETD-261

AVAILABLE TO THE PUBLIC

DESIGN AND TEST OF AN EARTH ASPECT SENSOR

By Harold A. Elliott and Jack C. Heffington

Distribution of this report is provided in the interest of information exchange. Responsibility for the contents resides in the author or organization that prepared it.

Prepared under Contract No. NAS2-3281 by
QUANTIC INDUSTRIES, INC.
Electro-Optical Division
1011 Commercial Street
San Carlos, California 94070

for

NATIONAL AERONAUTICS AND SPACE ADMINISTRATION
Ames Research Center



FACILITY FORM 602	N 68-30223	
	(ACCESSION NUMBER)	(THRU)
	175	1
	(PAGES)	(CODE)
	CR-73221	31
	(NASA CR OR TMX OR AD NUMBER)	(CATEGORY)

NASA CR-73221

ETD-261

DESIGN AND TEST OF AN EARTH ASPECT SENSOR

By Harold A. Elliott and Jack C. Heffington

Distribution of this report is provided in the interest of information exchange. Responsibility for the contents resides in the author or organization that prepared it.

. Prepared under Contract No. NAS2-3281 by
QUANTIC INDUSTRIES, INC.
Electro-Optical Division
1011 Commercial Street
San Carlos, California 94070

for

NATIONAL AERONAUTICS AND SPACE ADMINISTRATION
Ames Research Center

CONTENTS

	<u>Page No.</u>
I. Summary	1
II. Introduction	5
A. Motivation	5
B. Statement of Problem	5
III. Study Tasks	7
A. The Earth Aspect Sensor Mission	7
1. Description of Mission	7
2. Fundamental Detection and Discrimination Problems	7
3. A Typical Mission	8
4. Conclusions of Mission Study	18
B. Target Radiation Study	18
1. The Visible Region (0.353 to 1.0 Micron)	19
2. The Ultraviolet Region (0.2 to 0.3 Micron)	31
3. The Near-Infrared (IR) Region (1 to 4 Microns)	33
4. The Emitted-Infrared Region (>4 Microns)	35
5. Comparison of Ultraviolet, Visible, Near-IR, and Emitted-IR Sensing	38
6. Comparison of Discrimination Techniques	40
7. Decisions Reached as a Result of the Target Radiation Study	40
C. Detector Investigation	41
1. Detector Review and Evaluation	41
2. Detector Tests	49
IV. EAS System and Hardware Concepts	57
A. Optical Concepts	57
1. Pulse-Width Concept	57
2. Pulse-Amplitude Concept	59
3. Direct-Digital Concept	61
4. Star Sensor for Indirect Earth Aspect Sensing	61
5. Evaluation of Optical Concepts	66
B. Signal-Processing Concepts	66

CONTENTS (concl.)

	<u>Page No.</u>
V. EAS Detailed Design	75
A. Optics	75
1. System Operation	75
2. Packaging	75
3. Objective Lens	78
4. Reticle	80
5. Condensing Lenses	80
6. Filters	80
7. Detector	85
8. Sun Sensor	85
B. Electronics	88
1. System Operation	88
2. Derivation of Servo Error Signal	96
3. Derivation of Servo Transfer Function	99
4. Digital Integrator	102
VI. Testing	105
A. Testing of Circuits	105
B. System Testing	106
C. Target Simulator	108
VII. Major Remaining Testing and Design Tasks	113
Appendix A - Definition of D*	115
Appendix B - Specification Data, Multiplier Phototube Model 543F-04-14	117
Appendix C - Optical Concepts Based on Pulse-Width Measurement	121
Appendix D - Signal-Processing Concepts	131
Appendix E - Operating Range	147
Appendix F - Wide-Angle FOV Concepts	155
Appendix G - Sun Shielding	163
References	167

LIST OF ILLUSTRATIONS

<u>Figure No.</u>	<u>Title</u>	<u>Page No.</u>
1	Solar Probe Trajectory in Rotating (Fixed Earth), Sun-Centered Coordinate System (With Venus and Mercury)	10
2	Solar Probe Trajectory in Rotating (Fixed Earth), Sun-Centered Coordinate System (With Mars and Jupiter)	11
3	Probe-Mercury Distance and Mercury Phase	12
4	Probe-Venus Distance and Venus Phase	13
5	Probe-Earth Distance and Earth Phase	14
6	Probe-Mars Distance and Mars Phase	15
7	Probe-Jupiter Distance and Jupiter Phase	16
8	Trajectory of Probe in Vicinity of Earth	17
9	Curves of Constant V-Band Earth Magnitudes as Functions of Phase Angle and Distance from Observation Point (out to 5 AU)	24
10	Curves of Constant V-Band Earth Magnitudes as Functions of Phase Angle and Distance from Observation Point (out to 10 AU)	25
11	Irradiance Ratios Versus Wavelength (Earth, Mars, Venus, Mercury)	28
12	Irradiance Ratios Versus Wavelength (Earth, Moon, Jupiter, Saturn)	29
13	Spectral Irradiance from Earth and Moon in IR Region	36
14	Visible (Reflected) and IR Radiant Energy from the Moon as a Function of Phase Angle	37
15	Noise Characteristics of Typical Silicon Photovoltaic Detectors	42
16	Spectral-Response Characteristics of Silicon Photovoltaic Detectors	44
17	Spectral-Response Characteristics of Representative Photomultiplier Tubes	45
18	Detector Test Equipment	50
19	Detector Test Equipment Schematic	51
20	Photomultiplier Output for One Complete Cycle of Chopper Wheel	53
21	Silicon Detector Output During and Just After Exposure to Sun	55

LIST OF ILLUSTRATIONS
(cont.)

<u>Figure No.</u>	<u>Title</u>	<u>Page No.</u>
22	Optical Schematic, Pulse-Width Concept	58
23	Optical Schematic, Pulse-Amplitude Concept, Two-Channel Version	60
24	Direct-Digital Concept	62
25	Optical Schematic, Canopus Tracker	64
26	Reticle Schematic, Canopus Tracker	65
27	Non-Coherent Signal Processing for Split-Rectangle Pulse-Width Optics	69
28	Coherent Signal Processing for Trapezoidal Pulse-Width Optics	71
29	EAS Optical Schematic	76
30	EAS Optical Head	77
31	Objective Lens	79
32	Reticle	81
33	Condensing Lenses	82
34	Relative Response of Silicon Detector to Various Targets	84
35	Silicon Photovoltaic Detector	86
36	Sun Sensor	87
37a	EAS Block Diagram	90
37b	EAS Schematic	91
38	Pulse Sequence Before Earth Acquisition	93
39	Pulse Sequence After Earth Acquisition in Phase	94
40	Pulse Sequence After Servoing on Pulse Width	95
41	Spectral Characteristics of Gating Waveform at Nominal Spin Rate	101
42	System Test Setup	107
43	Record of System Test	109
44	Breadboard of EAS Coherent Signal-Processing Electronics	110
45	Target Simulator	111
C-1	Three-Substrate, Split-Rectangle Detector Array (One Channel)	122
C-2	X-Detector and Superimposed-Triangle Detector Patterns	123

LIST OF ILLUSTRATIONS
(concl.)

<u>Figure No.</u>	<u>Title</u>	<u>Page No.</u>
C-3	Optical Schematic, Prism/Filter Approach	125
C-4	Optical Schematic, Separate-Color-Detector Approach	127
C-5	Optical Schematic, Single-Detector Approach	128
D-1	Signal Processing for Three-Substrate Split-Rectangle Array	132
D-2	Signal Processing for Wedge/Filter Approach	135
D-3	Signal Processing for Separate-Color-Detector Approach	138
D-4	Signal Processing for Single-Detector Approach	139
D-5	Signal Processing for Pulse-Amplitude Concept (Variable-Transmission Neutral-Density Filters)	140
D-6	Signal Processing for Binary-Coded-Mask Direct-Digital Concept	142
D-7	Signal Processing for Pulse-Counting Direct-Digital Concept	143
D-8	Signal Processing for Star Sensor	145
E-1	Operating Range, Non-Coherent Electronics, Solid-State Detector	150
E-2	Operating Range, Coherent Electronics, Solid-State Detector	151
E-3	Operating Range, Coherent and Non-Coherent Electronics, Photomultiplier Tubes	152
E-4	Effect of Exponential Decay of Solid-State Detector Output on Operating Range, Coherent Electronics	153
F-1	Optical Schematic, Three-Channel Wide-Angle Optics Using Solid-State Detectors	156
F-2	Optical Schematic, Wide-Angle Optics Using Fiber-Optics Condenser (With Photomultiplier Tube)	157
F-3	Optical Schematic, Wide-Angle Optics with Light-Pipe Condenser	158
F-4	Spherical Objective Lens for Wide-Angle Optics	160
F-5	Cylindrical Condensing Lenses for Wide-Angle Optics	162
G-1	Solar-Glare Shield	165

LIST OF TABLES

<u>Table No.</u>	<u>Title</u>	<u>Page No.</u>
I	Planetary Magnitude and Phase Laws	21
II	Additional Planetary Phase Laws	22
III	Planetary Mean Colors	26
IV	Planetary Reflectivity Ratios	27
V	Bright Star Magnitudes	30
VI	Lunar Ultraviolet Data	34
VII	Comparison of Ultraviolet, Visible, Near-IR and Emitted-IR Sensing and Discrimination	39
VIII	Tabulation of Detector Properties	48
IX	Comparison of Optical Concepts	67
X	Comparative Rating of Different Versions of a Pulse-Width Optical Approach Using Color Discrimination	73

I. SUMMARY

This contract effort has led to a feasibility demonstration of an Earth Aspect Sensor in its electronic breadboard form. The reader is referred to Section VII, "Major Remaining Testing and Design Tasks." The existing design can lead to a light-weight, long range, solid-state attitude sensor for use on a spinning spacecraft. Basically, the device measures the angle between the vehicle spin axis and the line of sight to the earth; outputs can be used either for vehicle attitude control or for attitude measurement in conjunction with payload experiments. Key features of the sensor are:

- 1) Ability to operate at great distances from the earth (up to 50 million miles with the present design).*
- 2) All solid-state design, including detector (a photovoltaic cell is used instead of a photomultiplier).
- 3) Ability to discriminate between the earth and other bodies by measuring target color.
- 4) Accuracy of $\pm 1/2$ degree in a ± 15 degree field of view.
- 5) Light weight (2.8 lb).
- 6) Low power requirement (1.5 watts).

Early attempts to define general design considerations and restraints led to the examination of possible missions on which the sensor might be employed. Three typical missions were studied: a solar probe and two planetary probes (Mars and Venus). All missions carried technically possible launch dates but did not necessarily indicate actual planning by NASA. Several interesting problems appeared early in this study, perhaps the most striking being the extreme variation in range over which the sensor might be required to perform. The maximum range could be in excess of 1 astronomical unit (approximately 93 million miles).

Another interesting result of the study was the determination that the sun will interfere with earth sensing in regions of space where the angle between the earth and the sun, as viewed from the spacecraft, becomes as small as the field of view (plus a margin for the system detector to recover after exposure to the sun). Such interference would exist to some degree for any sensor of earth radiation because of the extreme relative brightness of the sun.

*Assuming a fully illuminated earth, or zero-degree phase. Phase is defined as the angle subtended at a planet by lines to the vehicle and to the sun.

The second step in the earth aspect sensor development program was a detailed study of the radiation characteristics of the earth and of other planets that could be bright enough to interfere with operation of the sensor. A comparison of ultraviolet, visible, near-infrared, and emitted-infrared sensing revealed that the visible region (0.3 to 1.0 micron) was the best choice. From a comparison of target discrimination by means of brightness, angular size, position with respect to the vehicle spin phase, and color, it was concluded that color discrimination was the most feasible; the earth, as viewed from space, is substantially bluer than any other planets of comparable brightness.

On the basis of the above findings, effort was initiated on optical and electronic design. Numerous concepts were generated and evaluated, culminating in an optical system based on measurement of the width of the earth pulse and utilizing solid-state silicon photovoltaic detectors, combined with a spin-coherent electronic signal-processing system with digital integration. The optical system consists of an objective lens, corrected over a wide spectral region, that images the earth onto a trapezoidal-shaped reticle; and a series of condensing lenses that form an image of the objective-lens aperture stop onto a circular, silicon photovoltaic detector. The detector is split along its diameter, and separate outputs are available from each half. One half is covered with a red filter, while the other half is covered with a blue filter. The condensing lenses insure complete defocusing of the earth image so that light from the earth will be spread equally over both the red and blue halves of the detector.

The sensor is mounted on the vehicle with the optical axis perpendicular to the vehicle spin axis. As the vehicle spins, images of the stars, the earth, and the other planets pass across the trapezoidal reticle, producing approximately square output pulses from the two detector halves. The width of these pulses is a measure of the angle between the vehicle spin axis and the line of sight to the targets. When the earth passes the field of view, the earth-pulse width is proportional to the earth-aspect angle to be measured.

The solid-state silicon photovoltaic detector was selected for the sensor rather than a photomultiplier tube for three basic reasons. First, the photomultiplier is subject to deterioration when exposed to high-intensity pulses, as will be the case in most applications of the sensor, in which the sun will pass through the field of view once each vehicle revolution. Second, a photomultiplier with its associated high-voltage power supply is relatively bulky and heavy, both undesirable features for deep-space probes where payload weight is very limited. Finally, the reliability for a long period in orbit would be higher with a solid-state detector since it requires no high voltages. Having selected the solid-state detector for these reasons, it was then necessary to

utilize a spin-coherent electronic system because the solid-state detector, having only a fraction of the detectivity of a photo-multiplier, gives a lower signal-to-noise ratio than desired.

In the signal-processing electronics, locally generated pulses are matched in both width and phase to the very weak earth pulses from the signal preamplifier. The matching is accomplished with two all-electronic servo loops, one to control the time at which the locally generated pulses occur, the second to control the duration of the locally generated pulses. A third channel provides an earth-present indication, and hemisphere-determination logic is also available. With this kind of processing, the effective time constant is equal to the time constant of the various servo loops involved. Digital-integration techniques permit times constants of almost any desired length.

The program resulted in the design and fabrication of an optical head and an electronic signal-processing breadboard for the earth aspect sensor. Preliminary testing of the breadboard demonstrated that the system is capable of searching for and locking on the earth at ranges of up to 50 million miles with an accuracy of $\pm 1/2$ degree and a field of view of ± 15 degrees.

Accuracy and field of view are governed chiefly by the geometry of the optical system, while range is a better indicator of electronic performance. Further electronic development could be expected to result in still greater range. Accuracy can be improved by independently varying the angular sensitivity of the system, which can be increased merely by changing the geometry of the reticle that determines the field of view. For a fixed noise figure, the noise equivalent angle decreases. Effectively, the accuracy for a given range will increase while the field of view will decrease. For example, the present design would be capable of ± 0.1 degree accuracy over a ± 3 degree tilt range of the spin axis, or of ± 0.03 degree accuracy over a ± 1 degree tilt range, at 50 million miles.

The expected size, weight, and power of the sensor, utilizing integrated electronic circuits, are listed below.

	Size	Weight	Power
Optics	1" dia. \times 4"	0.8 lb	-
Electronic Package	3" \times 5" \times 2"	2 lb	1.5 W

In the development of the sensor for a feasibility demonstration, considerable attention was given to the reduction of electronic noise and drift, but no attempt was made to optimize either the optics or the electronic package for weight or size. The numbers above, however, are careful estimates of a flight-system package, based on the actual breadboard sensor.

II. INTRODUCTION

A. Motivation

The development of the earth aspect sensor was originally initiated because of concern over possible problems in the orientation of the Pioneer series of spacecraft. The Pioneer, a spinning, solar-orbiting vehicle, requires a two-step orientation maneuver after separation to achieve the desired attitude. The scientific experiments require that the spin axis be normal to the ecliptic plane. This orientation will allow the narrow-beam, high-gain antenna pattern to intersect the earth.

Step 1 orientation takes place automatically in a closed-loop fashion upon boom deployment. It establishes the spin axis normal to the vehicle-sun line to maximize solar power.

Step 2 orientation is commanded in an open-loop fashion from the ground. This maneuver precesses the spin axis around the vehicle-sun line. A partial step 2 is necessary just after completion of step 1 to prevent the dead zone of the omnidirectional antenna from covering the earth and interrupting communication. Step 2 may not be completed until some time later, however, because of the trajectory of the vehicle. It is desirable to achieve final orientation quickly in the event of a premature pneumatic- or command-subsystem failure. A sensor permitting a rapid and sure orientation would certainly contribute to the probability of a successful mission. The earth is a convenient reference for spacecraft attitude determination; hence the earth aspect sensor.

The sensor was developed by Quantic Industries, Inc., for NASA/Ames Research Center, Contract NAS2-3281, under the direction of the Vehicle Guidance and Control Branch of the System Engineering Division.

B. Statement of Problem

The attitude information to be sensed by the earth aspect sensor is the average angle (termed θ) between the spin axis of the vehicle and the line connecting the vehicle and the geocenter of the earth, measured in the plane containing the vehicle spin axis and the earth. Precession, or wobble, of the vehicle spin axis (resulting in rapid oscillation of the angle θ) can cause errors in sensor operation; however, most spinning spacecraft are carefully balanced and usually have a wobble-damping device to remove the dynamic effect after a short period of time.

The requirements placed on the sensor were: 1) $\pm 1/2$ degree accuracy; 2) a large dynamic range beginning at 50,000 miles; 3) simplicity and reliability. The average weight of scientific experiments on a Pioneer is about 5.5 lb each, and power consumption is somewhat more than 1 watt.

The design goals were changed somewhat about mid-way through the program. At that time, an earth aspect sensor design compatible with the Pioneer requirements was ready for breadboarding, and an engineering model would have been complete within several months. However, the notable success of two Pioneers launched at that time indicated that the orientation procedure worked well, at least in those two cases. With the Pioneer orientation problem apparently surmounted, effort in the earth aspect sensor development program was directed toward a sensor of greater capability, specifically with regard to operating range. The system range design goal was set at 50 million miles.

III. STUDY TASKS

A. The Earth Aspect Sensor Mission

1. Description of Mission

The earth aspect sensor (EAS) was designed for a class of missions rather than for a specific mission. This class includes missions in which a spin-stabilized probe leaves the immediate vicinity of the earth and enters a solar orbit. This would include solar probes, planetary probes, or any other deep-space mission in the solar system, with the restriction that the orbital plane will lie in or close to the plane of the ecliptic. The primary function of the EAS is to detect the earth and determine the angle between the spin axis of the probe and the line of sight to the earth. The EAS mission has been concisely stated in the work statement as follows:

"The earth aspect sensor is to be a device placed aboard a spin-stabilized, heliocentric orbiting, deep-space vehicle from which a certain angle may be computed for vehicle orientation purposes. That angle is the one formed by the intersection of the vehicle spin axis and the line from the vehicle to the earth's geocenter; i.e., the 'earth look angle.'

"A secondary purpose of the sensor is to determine the celestial hemisphere into which the spin axis is pointing as defined by the ecliptic plane."

2. Fundamental Detection and Discrimination Problems

In order for an EAS to fulfill its function, it must be able to cope to some extent with certain fundamental problems of detection and discrimination, as listed below. These problems will be encountered by the EAS on all missions to a greater or lesser degree, depending on the specific trajectory.

1) Obtaining adequate signal-to-noise ratio when the distance is large from the probe to the earth.

2) For a sensor relying on reflected sunlight, obtaining sufficient signal when only a small fraction of the illuminated portions of the earth are visible to the sensor.

3) Discriminating against the moon and other planets even when their over-all brightness, as seen from the position of the probe, is much greater than that of the earth.

4) Discriminating against the planets or the moon when their angular separation from the earth, as subtended at the probe, is small.

5) Discriminating against bright stars which may have color indices similar to that of the earth and which, under certain conditions, may have an apparent magnitude similar to that of the earth.

6) Detecting the earth when its angular separation from the sun, as subtended at the probe, is small.

During the course of the program, various EAS concepts were studied, and it became apparent that none of these could completely overcome all the above-mentioned problems.* The resultant version of the EAS is therefore a compromise; at certain times during some missions, operation of the EAS will be submarginal.

As is discussed in detail in Section V, the version of the EAS developed during this program will be able to discriminate very well against possible interfering targets (items 3 and 4 above), but this was accomplished at the expense of range (item 1). The device operates in the visible spectral region and therefore is limited by the constraints of item 2. However, it need not discriminate against bright stars (item 5), because this effect is masked by item 1.

3. A Typical Mission

In order to gain a better appreciation of the problems that might be encountered, three missions were selected for detailed study: a solar probe, a Venus probe, and a Mars probe. Although these missions were not or will not necessarily be scheduled, they have been considered and appear technically feasible. The analysis of one of these flights, a solar probe with a 5 May 1967 launch date, is described below.

* A device is described in Section IV which in principle is completely independent of all the above problems as long as the mission is in or near the ecliptic plane. However, it does not operate by sensing the earth but rather two stars (one of which would be Canopus). Since further investigation of this device was deemed to be outside the scope of the present contract, the effort was not carried beyond the concept stage.

First, the predicted trajectory of the probe was plotted, and the position of the probe at regular time intervals was indicated. Then the orbits of the planets were plotted on the same graph, and their positions at regular time intervals were indicated. The planetary-coordinate information was obtained from reference 1. These plots are shown in Figure 1 (Mercury, Venus, and Earth) and Figure 2 (Earth, Mars, and Jupiter).

Based on these plots for the probe and for each planet, plots were made of probe-planet distance and planetary phase (Figures 3 through 7). (Phase is defined as the angle subtended at the planet by lines to the probe and to the sun. A phase angle of 0 degrees therefore indicates a fully illuminated target.)

An earth-centered plot was then made of the trajectory of the probe as it leaves the vicinity of the earth (Figure 8), with the purpose of determining the phase angle and distance of closest approach to the moon.

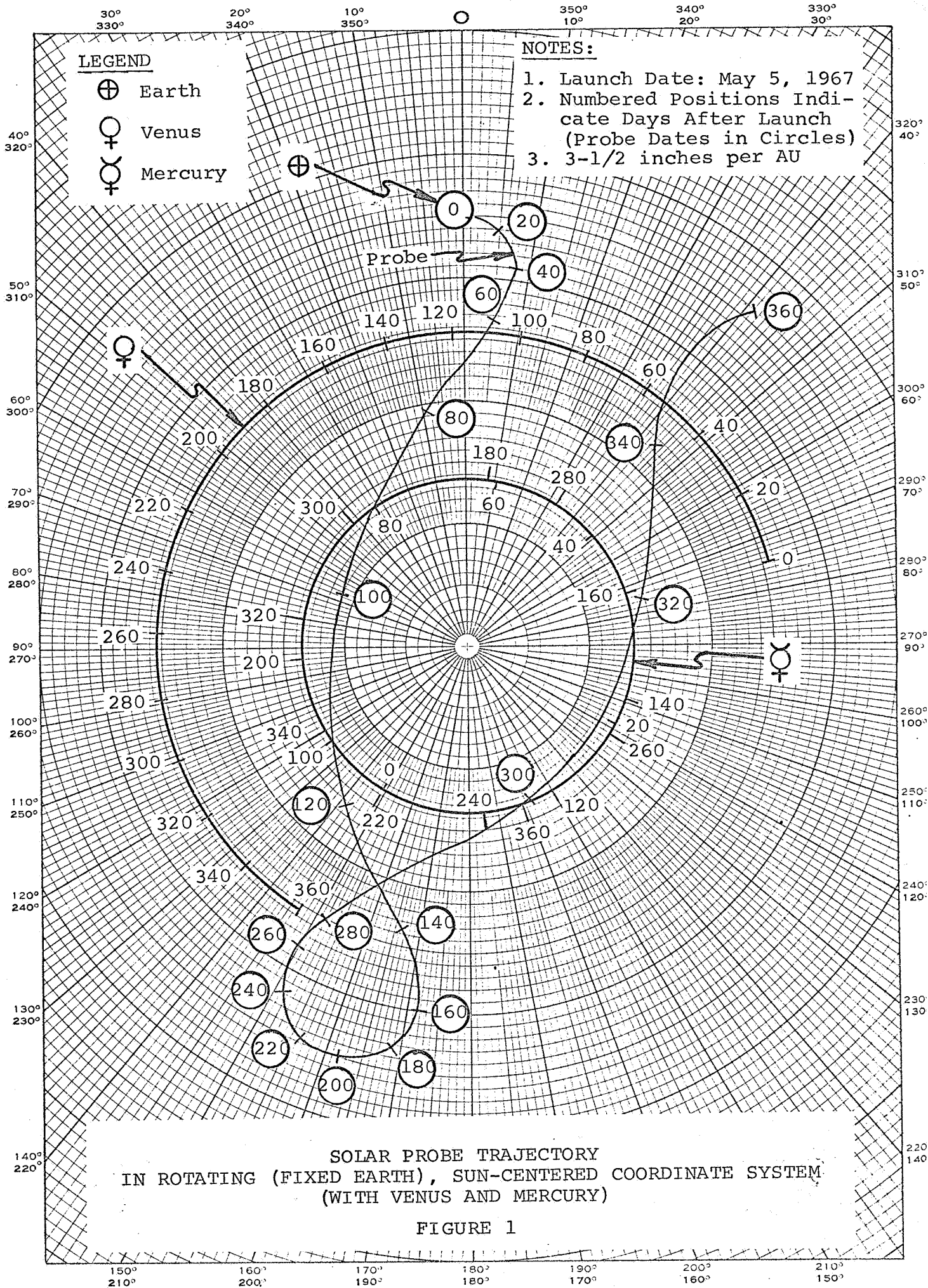
A few additional comments should be made regarding the plots and the calculations leading to them. In all cases, inclinations to the ecliptic were ignored, and circular orbits were assumed. In addition, the probe trajectory was plotted on a sun-centered rotating coordinate system (earth remaining fixed). Saturn coordinates were tabulated but not plotted. However, this planet's phase angle remains small and the percentage variation in probe-Saturn distance is small during the mission. The planets beyond Saturn were not considered since they are very faint and should pose no interference problem to EAS's for missions now under active study.

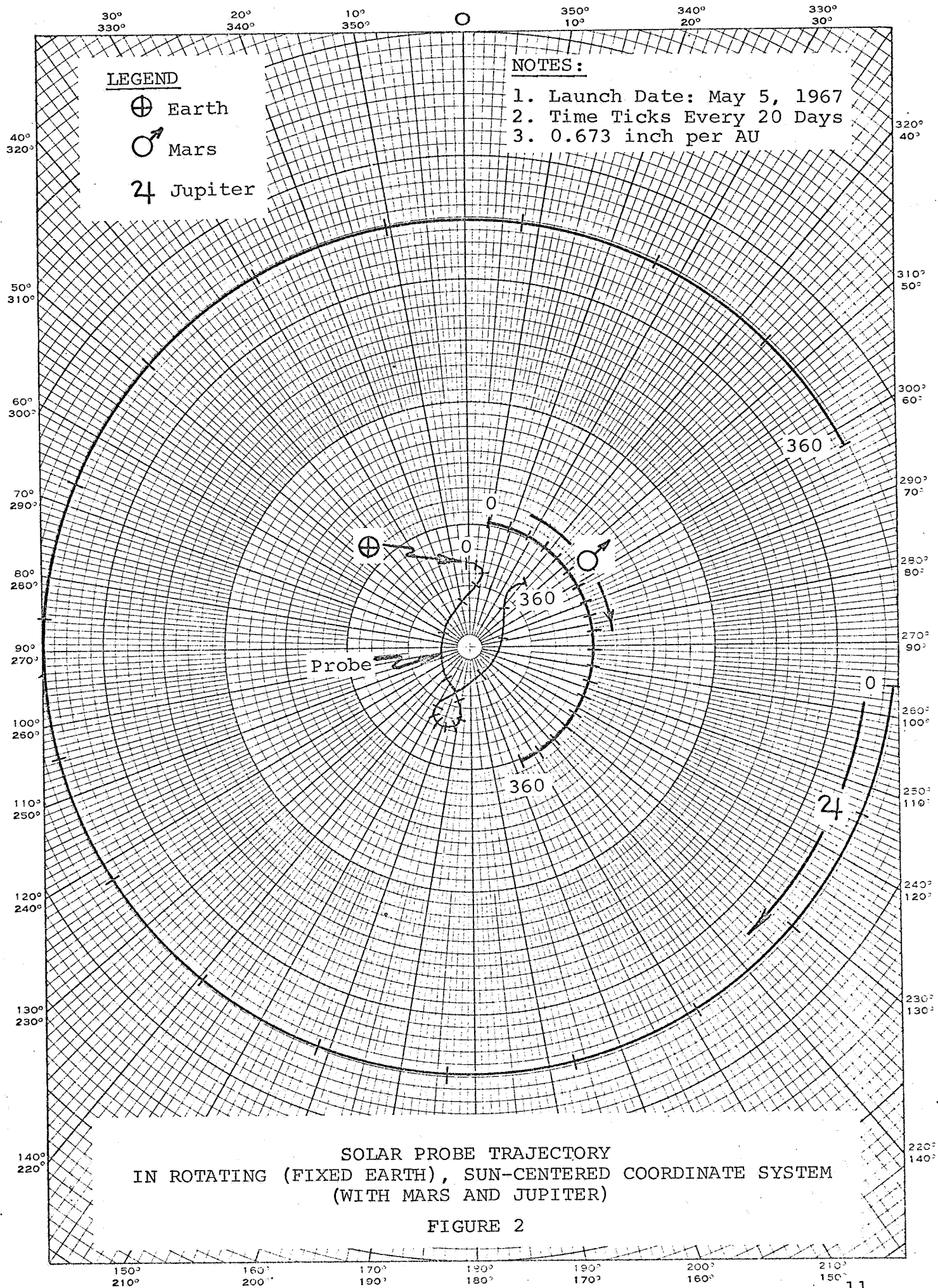
In the probe parking orbit, the earth will always appear brighter than the moon except for a period during each circuit in the region where the earth phase angle is 180 degrees. During probe injection and the period immediately following, the phase angle of the earth will always be smaller than that of the moon and the probe-earth distance will always be less than the probe-moon distance; thus, the earth will always appear brighter.

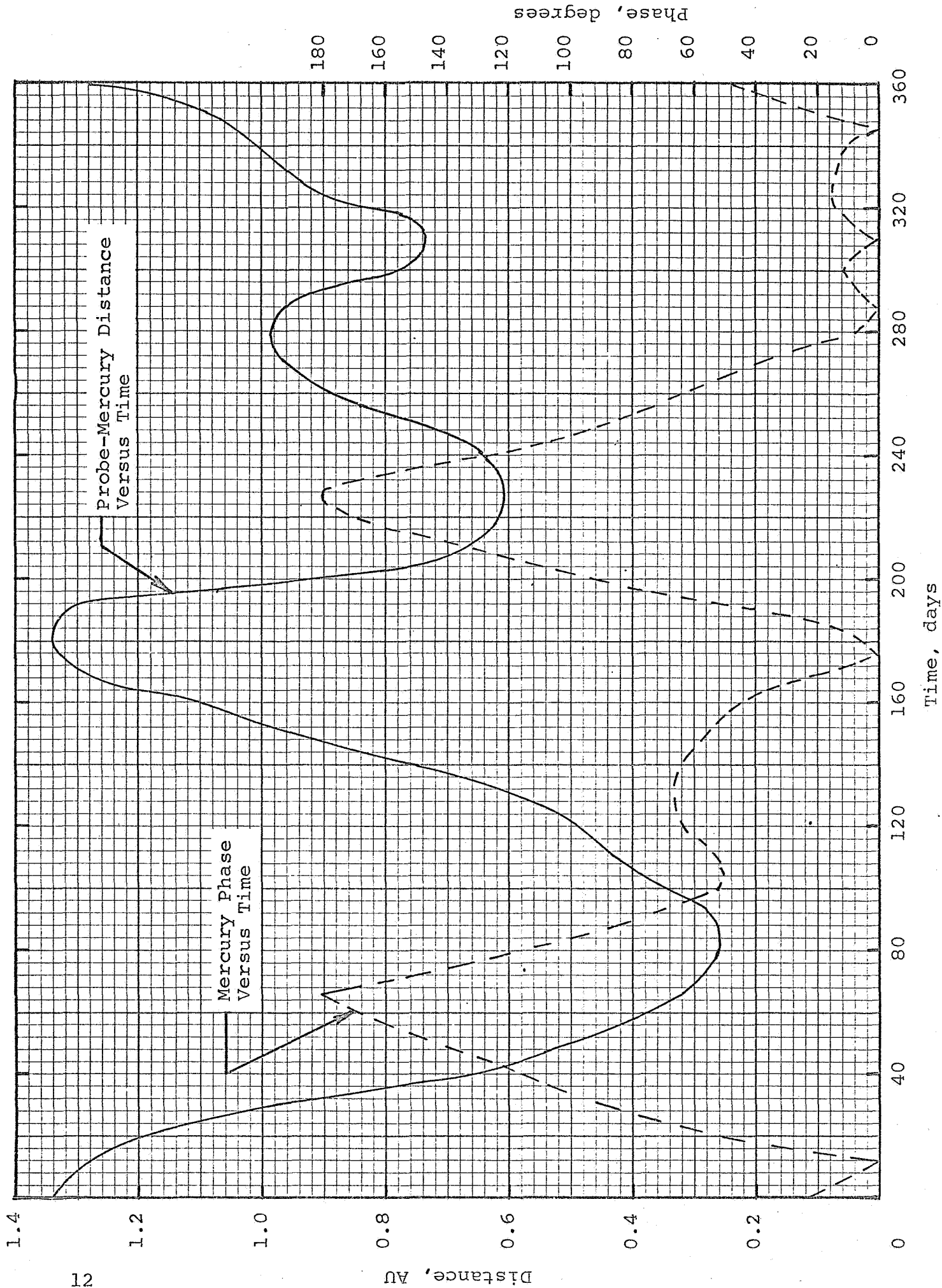
During the entire mission, the earth phase angle will always be 90 degrees or less, which is favorable. The period of minimum earth signal will be around 160 to 240 days, when the probe-earth distance approaches 2 astronomical units (AU).

At approximately 120 days after launch, the angle between the earth and Venus, as seen from the probe, will be very small, which could lead to sensing problems. A similar situation exists for the earth and Mercury just after 180 days. It recurs at approximately 210 days, but at this time the phase angle of Mercury is large.

At approximately 295 days, the earth and the sun are in conjunction and optical earth aspect sensing is not possible.







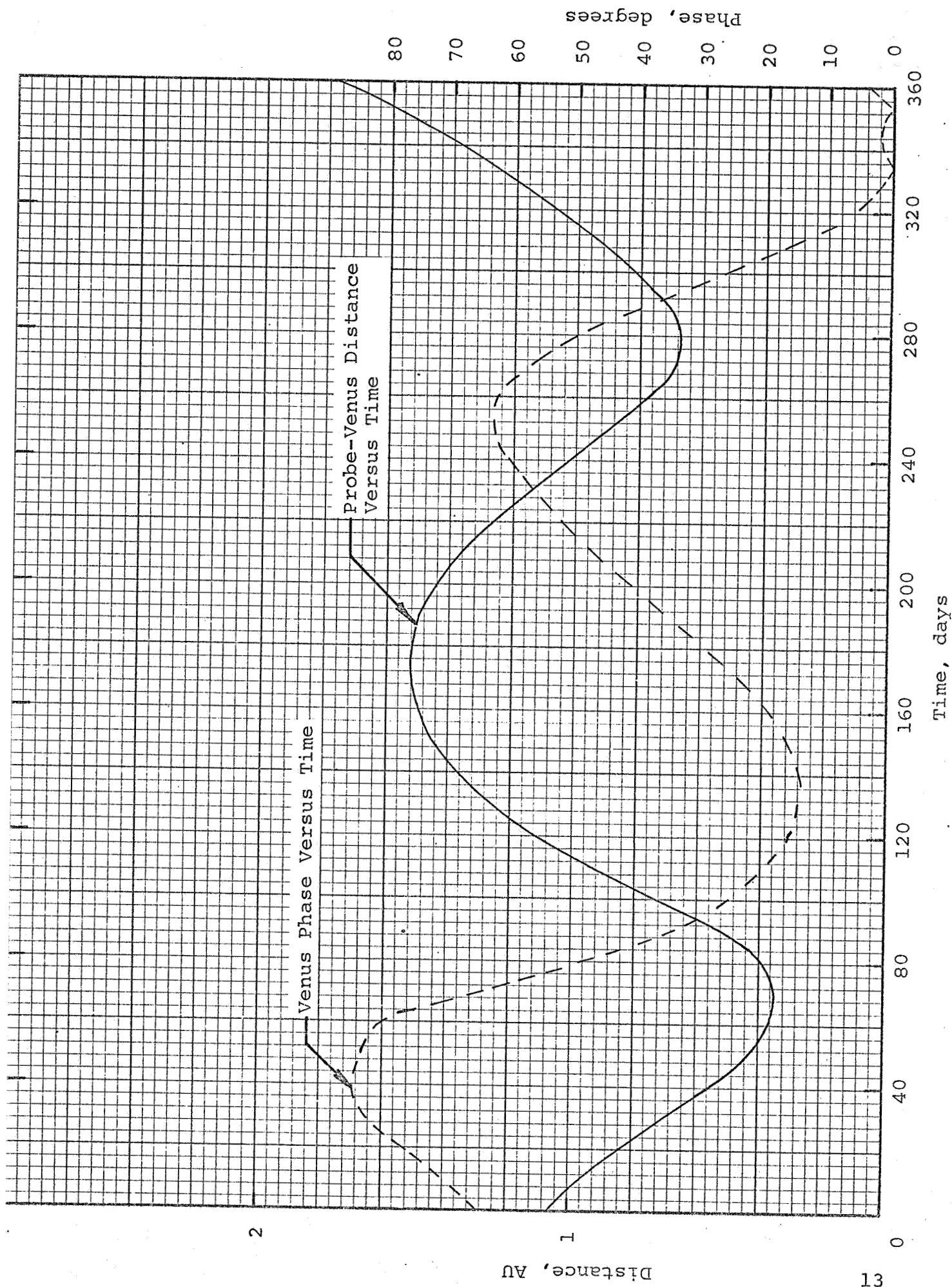


FIGURE 4. PROBE-VENUS DISTANCE AND VENUS PHASE

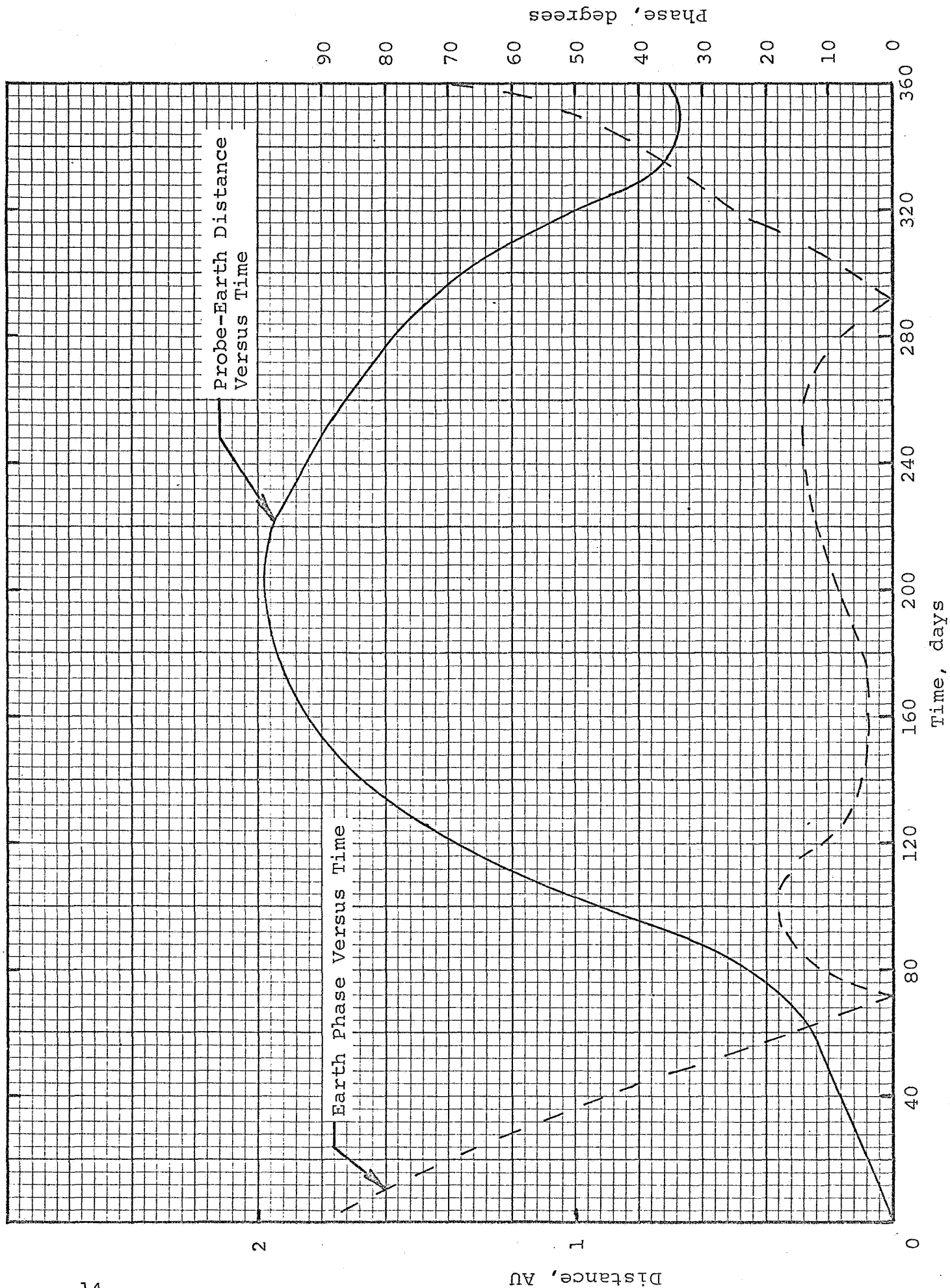


FIGURE 5. PROBE-EARTH DISTANCE AND EARTH PHASE

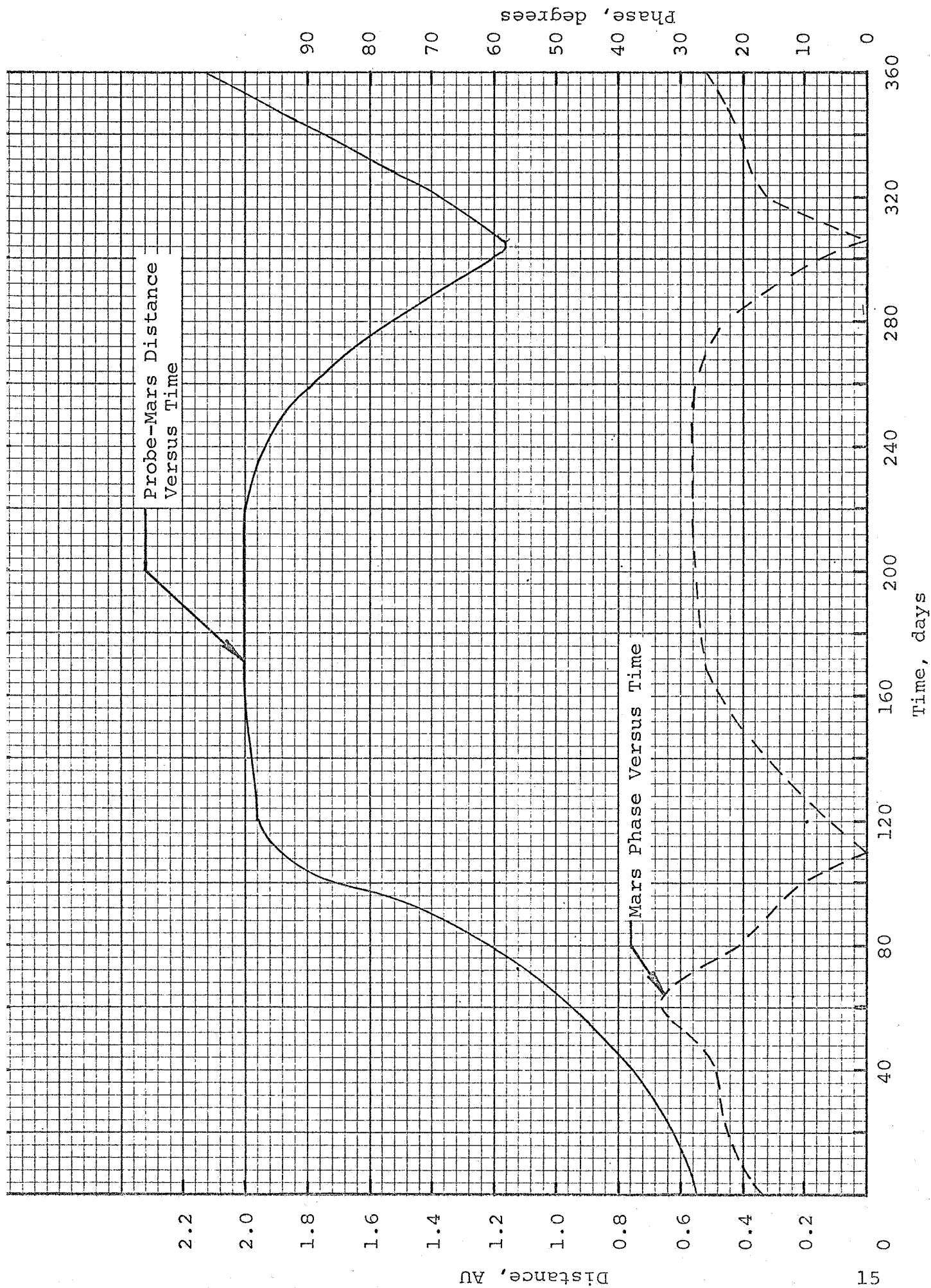
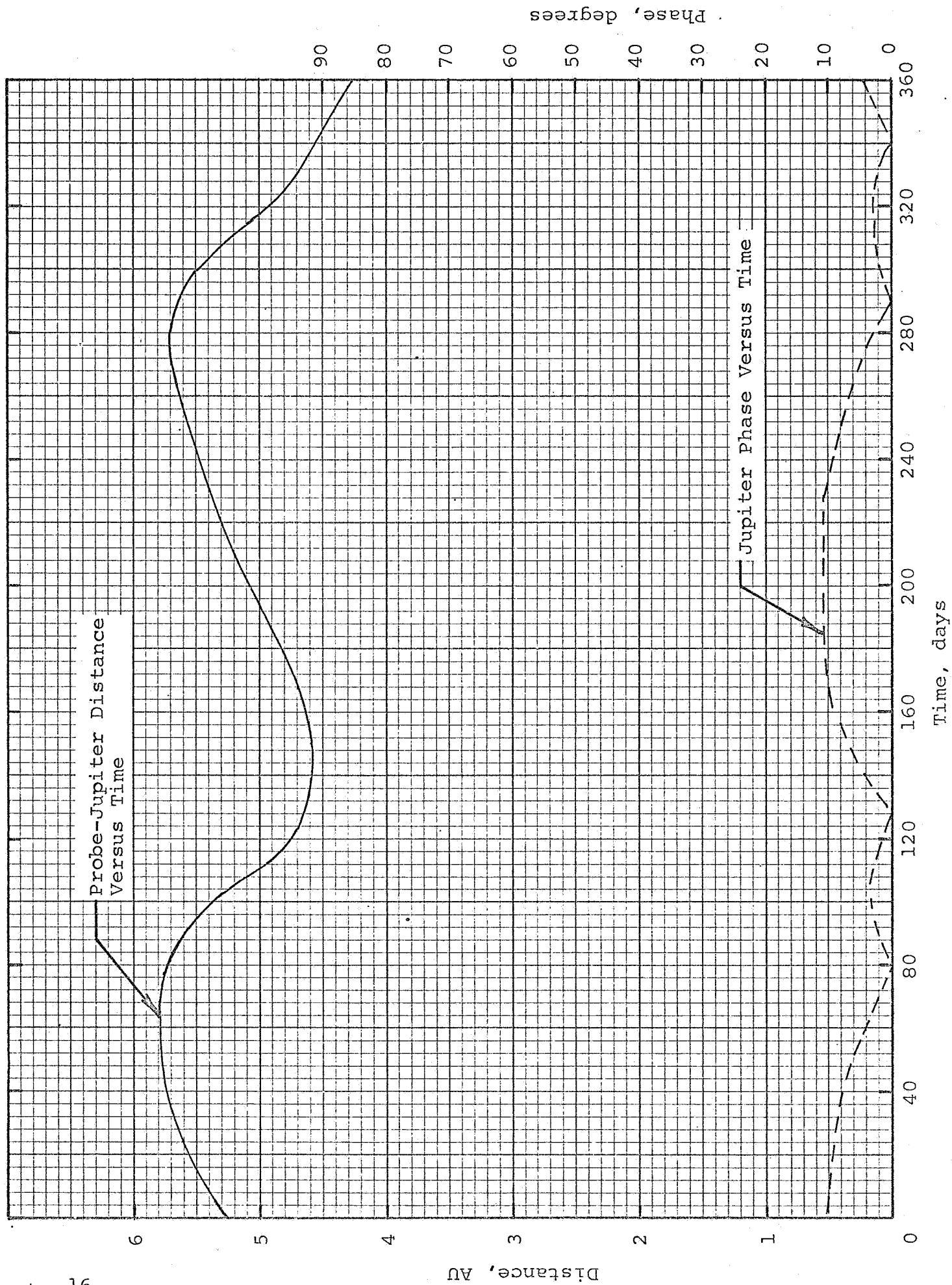
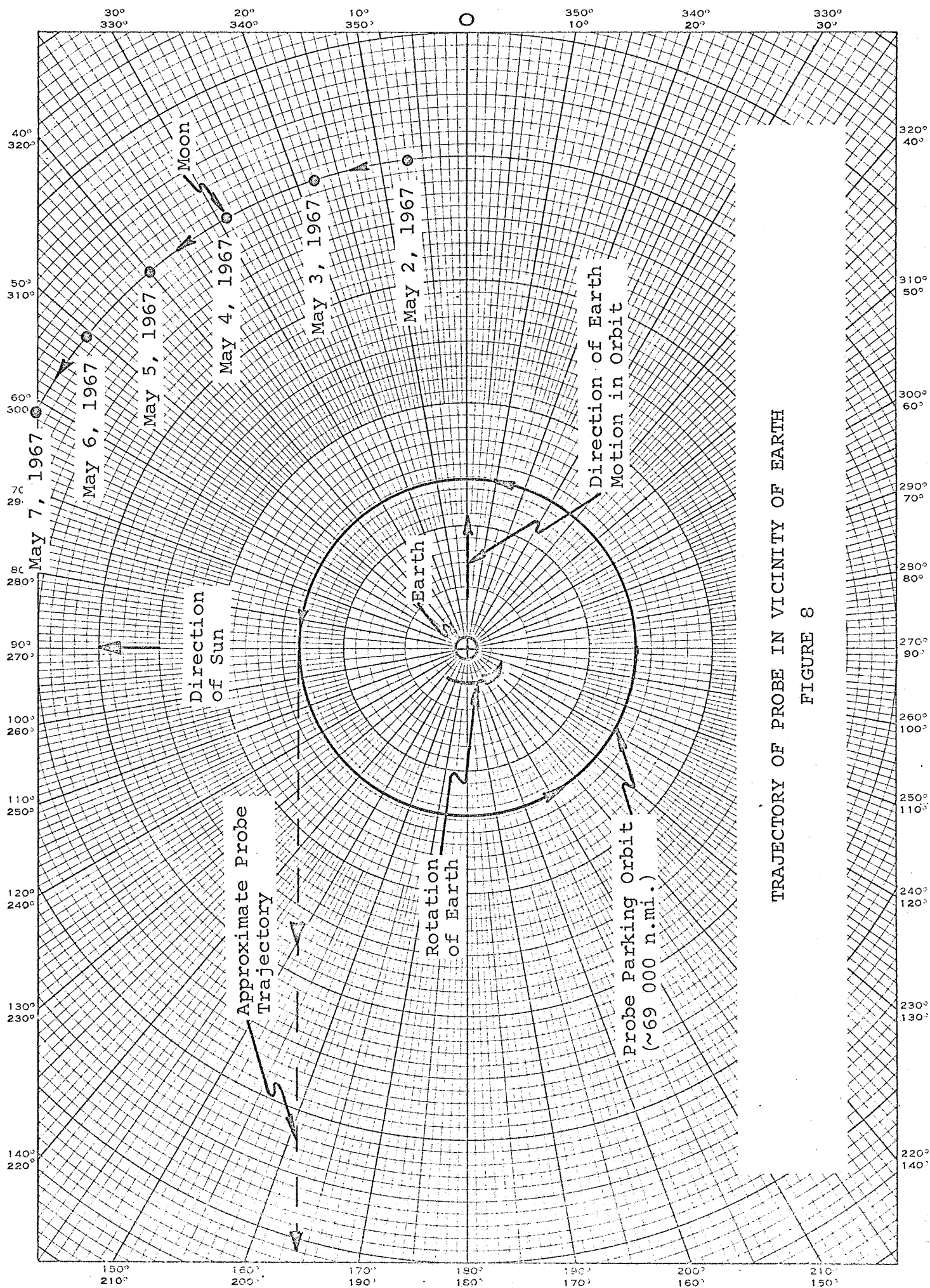


FIGURE 6. PROBE-MARS DISTANCE AND MARS PHASE





TRAJECTORY OF PROBE IN VICINITY OF EARTH
FIGURE 8

4. Conclusions of Mission Study

As a result of the study of the solar probe mission described above and other typical missions, the following conclusions were drawn concerning the EAS design.

1) For most missions, at certain times during the mission, the apparent brightness of some of the planets will greatly exceed the brightness of the earth. Also, because of phase and distance changes, the apparent brightness of all targets will vary widely. Thus, a sensing device based on apparent total brightness did not appear feasible.

2) Except during departure of the probe from the earth and during very close approaches to planets, all targets will have a small angular diameter and at most times can be considered point sources. At times when the probe is close to a target, the angular size of the target will be varying rapidly; for this reason, aspect sensing or discrimination based on angular size did not appear feasible.

3) There will be short periods, during missions going away from the sun, in which the phase angle will approach 180 degrees. For these short periods, successful EAS operation is very doubtful.

B. Target Radiation Study

A knowledge of the radiation characteristics of the earth was of course essential before the design of an optical EAS could be undertaken. In addition, since the EAS may have to distinguish between the earth and such possible interfering targets as the moon and the planets, the radiation characteristics of these bodies should also be known. In order to choose the most favorable operating wavelengths, a wide spectral range from ultraviolet to infrared was considered.

Planetary radiation falls into two categories: reflected sunlight and thermal self emission. For the earth, reflected sunlight is dominant in the ultraviolet, visible, and near-infrared regions to approximately 4 microns, while thermal emission becomes predominant in the infrared beyond 4 microns. Since radiation studies in the various wavelength regions were done by different researchers using different techniques, the regions are discussed separately below.

1. The Visible Region (0.353 to 1.0 Micron)

Of all the wavelength regions, the visible region is the most thoroughly studied and best known. The work in this field up through 1960 is well summarized in references 2, 3, and 4; unless otherwise noted, all information in this discussion is derived from these references.

Visible radiation will be discussed in terms of five standard bands, as follows:

<u>Band</u>	<u>Center Wavelength (micron)</u>
U	0.353
B	0.448
V	0.554
R	0.690
I	0.820

The optical bandwidth of each of these bands is relatively wide (of the order of 0.1μ). Of the five, the V band is the best known and corresponds very closely to the response of the average human eye.

a. Factors Affecting Planetary Magnitude

The magnitude of a planet (or the moon*) as seen from a particular point in space depends on many factors. This dependence is summarized quantitatively in the following equation:

$$V(d, \alpha) = V(1, 0) + 5 \log(rd) + \Delta m(\alpha), \quad (1)$$

where $V(d, \alpha)$ = magnitude of planet as a function of d and α ,

d = distance of planet from observation point (AU),

α = phase angle of planet (degrees),

$V(1, 0)$ = magnitude of the planet, with distance from the sun and the observation point reduced to unity and with a zero-degree phase angle,

* In general, the word "planets" as used in this document includes the moon.

r = distance of planet from sun (AU),
 $\Delta m(\alpha)$ = variation in magnitude of the planet
as a function of phase angle (also called
"phase law").

The value of $\Delta m(\alpha)$ is different for each planet. In the case of the major planets, it can be measured over only a limited range but can be extended by theory out to 180 degrees.

Referring to equation (1), it appears that with $V(1,0)$ and $\Delta m(\alpha)$ known; the magnitude of a planet as seen from any point in space can be defined. However, $V(1,0)$ is subject to variations due to such parameters as the rotation of the planet and seasonal variations in surface characteristics. Saturn is the most interesting case, since its value of $V(1,0)$ varies considerably with the inclinations of the observation line of sight to the plane of the rings.

Table I lists values of $V(1,0)$ and the phase laws of the planets. Again, planets beyond Saturn were not considered, since they are very faint as seen from all points closer to the sun than Saturn. Some of the phase laws are not expressed mathematically; these are given in Table II.

b. Calculation of Irradiance in the V Band

The relationship between the V-band magnitude of a planet and its spectral irradiance is given by the following equation from reference 5:

$$\log f_{\lambda}(V) = -0.4V - 8.42, \quad (2)$$

where $f_{\lambda}(V)$ = spectral flux outside atmosphere
near 5500 Å (erg/cm²-Å-sec).

It is often more convenient to express the irradiance in other units:

$$H_{\lambda}(V) = \left[f_{\lambda}(V) \times 10^{-3} \right] \text{watts/cm}^2\text{-}\mu.$$

It is now possible, using equations (1) and (2) and Tables I and II, to calculate the approximate spectral irradiance in the V band for any of the listed planets as functions of phase angle and distance from the observation point. This is useful information for two reasons. First, it makes possible the calculation of signal and signal-to-noise ratio in the V band. Second, nearly all information on magnitudes in the U, B, R, and I bands is stated in terms of differences from V-band magnitudes. It should be noted here that equations (1) and (2) apply to these four bands as well as to the V band.

TABLE I

PLANETARY MAGNITUDE AND PHASE LAWS

Planet	$V(1,0)$	$\Delta V(1,0)$	Phase Laws, $\Delta m(\alpha)$
Sun	-28.81	$\pm 1.5\%$	
Mercury	-0.36	Very small, if any	$3.80(\alpha/100) - 2.73(\alpha/100)^2$ $+2.00(\alpha/100)^3$ for $3^\circ \leq \alpha \leq 123^\circ$
Venus	-4.29	Very small	$0.09(\alpha/100) + 2.39(\alpha/100)^2$ $-0.65(\alpha/100)^3$ for $0.9^\circ \leq \alpha \leq 170.7^\circ$
Earth	-3.87	± 0.25 mag.	$1.30(\alpha/100) + 0.19(\alpha/100)^2$ $+0.48(\alpha/100)^3$ for $0^\circ \leq \alpha \leq 133^\circ$
Moon*	+0.21	$\sim \pm 0.04$ mag.	See Table II
Mars	-1.52	± 0.08 mag.	See Table II
Jupiter	-9.25	± 0.22 mag.	0.005 mag./degree for $0^\circ \leq \alpha \leq 12^\circ$ See Table II
Saturn (ball)	-8.88	± 0.06	0.044 mag./degree for $0^\circ \leq \alpha \leq 6^\circ$ See Table II
Saturn (system)**	$(-8.88 - \Delta V_r)$		

* Based on measurements of only that portion of the moon facing the earth.

** $\Delta V_r = 2.60 \sin B - 1.25(\sin B)^2$, where r refers to Saturn's rings and where B is the latitude of the observation point with respect to the plane of the rings. For observation from the earth, $B_{\max} = 27^\circ$.

TABLE II

ADDITIONAL PLANETARY PHASE LAWS

22

Phase Angle, α (degrees)	Moon $\Delta m(\alpha)$	Mars $\Delta m(\alpha)$		Jupiter $\Delta m(\alpha)$		Saturn $\Delta m(\alpha)$	
		Measured	Predicted	Measured	Predicted	Measured	Predicted
0	0.00	0.00		0.00		0.00	
5	0.08			0.025		0.22	
10	0.23	0.16		0.05			
20	0.51	0.32			0.063		
30	0.79	0.48					
40	1.06	0.64	0.65		0.241		0.241
50	1.35				0.371		0.371
60	1.62		0.96		0.534		0.534
70	1.91						
80	2.24		1.34		0.962		0.962
90	2.63						
100	3.04		1.63		1.55		1.55
110	3.48						
120	3.93		2.21		2.39		2.39
130	4.44						
140	5.07		3.04		3.64		3.64
150	5.9						
160	7.5		4.23		5.52		5.52
170							
180							

In calculating signals, the main concern of course is the earth. Figures 9 and 10 each show a family of curves of constant V-band earth magnitudes as functions of phase angle and distance from observation point. These curves also represent curves of equal magnitude in the other wavelength bands if the same phase law is assumed to hold for these bands. They also indicate lines of equal irradiance, equal signal, and equal signal-to-noise ratio and are therefore useful tools in EAS design.

c. Multi-Color Planetary Discrimination

One of the most obvious means of discriminating against interfering targets involves observing these targets at more than one wavelength. Color data on the planets are commonly given either as magnitude differences in the various wavelength bands (Table III) or as the ratio of reflectivity at a given band to reflectivity at the V band (Table IV). Based on the data in Table IV, the following equation can be used to compute irradiance ratios for a given planet:

$$\frac{H_{\lambda}(M)}{H_{\lambda}(V)} = \frac{\rho_{\lambda}(M)}{\rho_{\lambda}(V)} \times \frac{W_{\lambda}(M)}{W_{\lambda}(V)}, \quad (3)$$

where M represents the U, B, R, or I color bands,

V represents the V color band,

ρ_{λ} = spectral reflectivity of the planet,

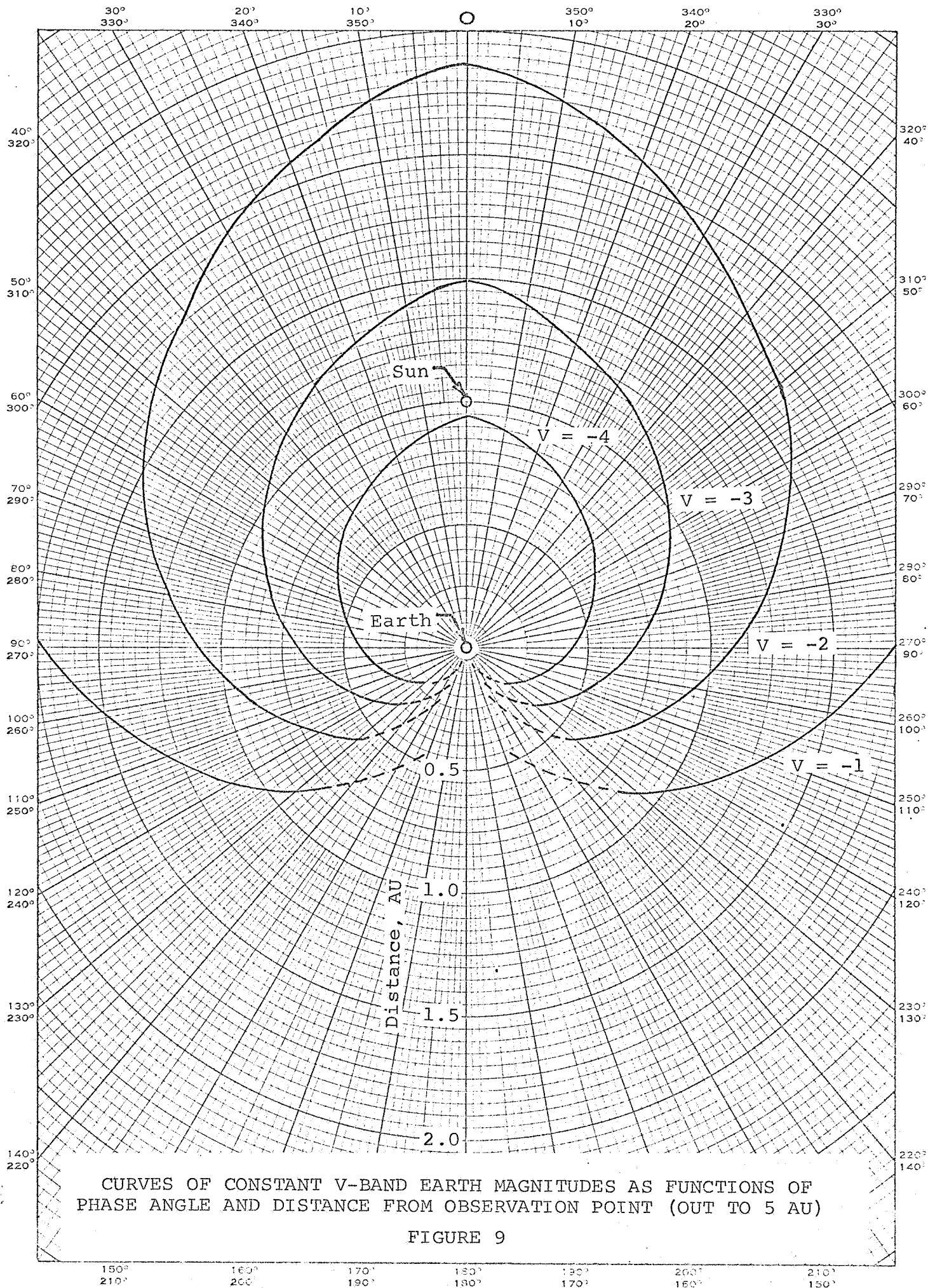
W_{λ} = spectral radiant emittance of the sun.

This relationship applies when relatively broadband filters are used (of the order of 0.1 μ).

$H_{\lambda}(M)/H_{\lambda}(V)$ is plotted as a function of wavelength for the earth, the moon, and the planets in Figures 11 and 12. Intermediate values are approximated by lines drawn between the plotted points, since the observation bandwidth is not less than about 0.1 μ ; this tends to be substantiated by measurements of Mars reflectivities at intermediate wavelengths. All of the data plotted in Figures 11 and 12 proved to be very useful in the selection of specific operating wavelengths for color discrimination against interfering targets. From inspection of the irradiance ratios, one fact that facilitated sensor design is quite apparent, i.e., that the earth is unique in being much "bluer" than other planets or the moon.

The reflectivity measurements of Saturn were made at a time when the inclination of the rings from the line of sight was very small, and the data were reduced to a "no inclination" condition. Therefore, Table IV and Figure 12 data refer to the planetary ball. As the inclination to the rings increases, the color of the planet as a whole will be somewhat bluer, but according to R. H. Hardie, who made some of the original measurements, this effect is small and is probably within the accuracy limits of the original measurements.^{6*}

* Superscripts indicate items in reference list.



CURVES OF CONSTANT V-BAND EARTH MAGNITUDES AS FUNCTIONS OF
PHASE ANGLE AND DISTANCE FROM OBSERVATION POINT (OUT TO 5 AU)

FIGURE 9

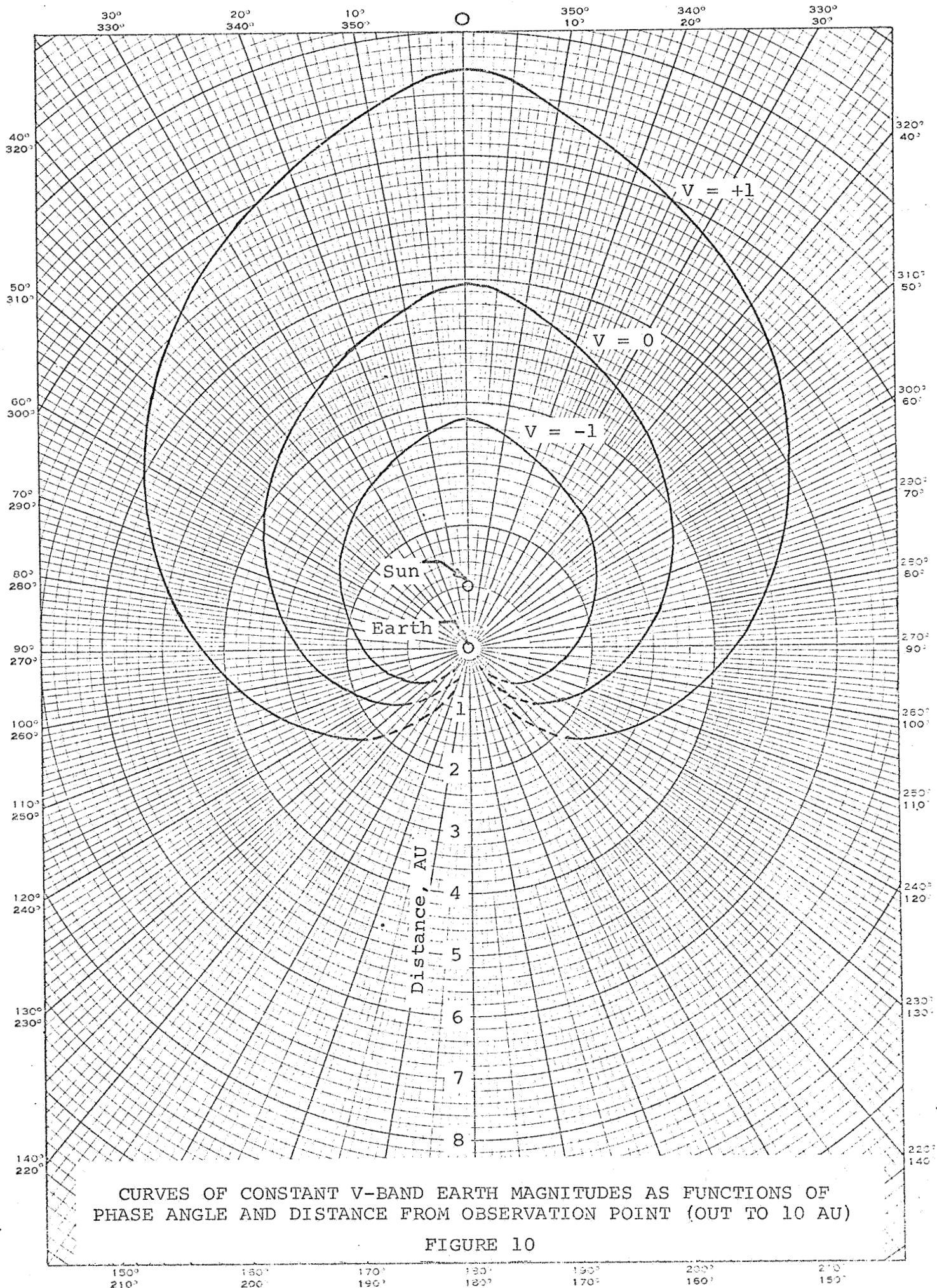


TABLE III

PLANETARY MEAN COLORS

Body	Mean Color (Magnitude Differences)				Uncertainty and Variability
	<u>U-B</u>	<u>B-V</u>	<u>V-R</u>	<u>R-I</u>	
Sun	0.14	0.63	0.45	0.29	"Accurate"
Mercury		0.93	0.85	0.52	Values uncertain because measurements must be made at twilight.
Venus	0.50	0.82			
Earth		0.21			$\Delta R = \pm 0.07$; $\Delta V = +0.25$; $\Delta B = \pm 0.18$
Moon*	0.46	0.92	0.80	0.46	$\Delta V \approx 0.08$
Mars	0.58	1.36	1.12	0.38	$\Delta R \approx \pm 0.07$; $\Delta V \approx \pm 0.07$
Jupiter	0.48	0.83	0.50	-0.03	Possibly a slight color variation with phase.
Saturn (ball)	0.58	1.04			Measurements made when inclination of rings to line of sight was small.
Saturn (system)					Will be "bluer" than ball alone. Will be a function of inclination of ring plane to line of sight (27° max.)

* Color data for back side of moon unknown.

TABLE. IV
PLANETARY REFLECTIVITY RATIOS

Note: Tolerances are not stated for most of the values because they are not known.

Body	$\overline{\rho_U}/\rho_V$	$\overline{\rho_B}/\rho_V$	$\overline{\rho_V}/\rho_V$	$\overline{\rho_R}/\rho_V$	$\overline{\rho_I}/\rho_V$
Mercury		0.76	1.00	1.45	1.78
Venus	0.60	0.84	1.00		
Earth		1.33 $\begin{smallmatrix} +0.24 \\ -0.20 \end{smallmatrix}$	1.00	0.79 ± 0.05	
Moon	0.54	0.76	1.00	1.38	1.62
Mars	0.34 $\begin{smallmatrix} +0.12* \\ -0 \end{smallmatrix}$	0.52 $\begin{smallmatrix} +0.14* \\ -0 \end{smallmatrix}$	1.00	1.86	2.04
Jupiter	0.61	0.83	1.00	1.05	0.78
Saturn (ball)	0.46	0.68	1.00		
Saturn (system)			1.00		

* Mars appears bluer than usual on so-called "abnormal nights."

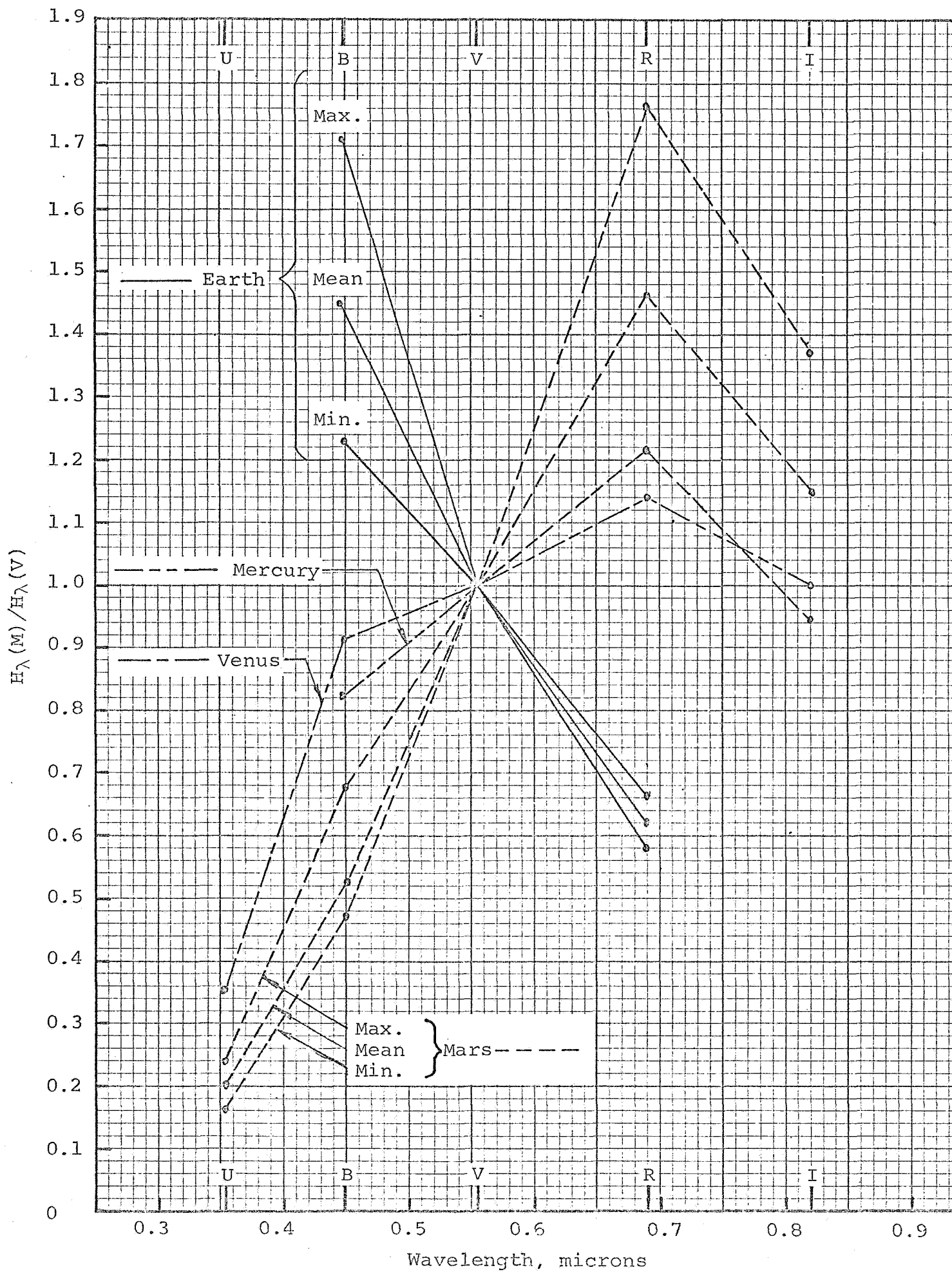


FIGURE 11. IRRADIANCE RATIOS VERSUS WAVELENGTH
(EARTH, MARS, VENUS, MERCURY)

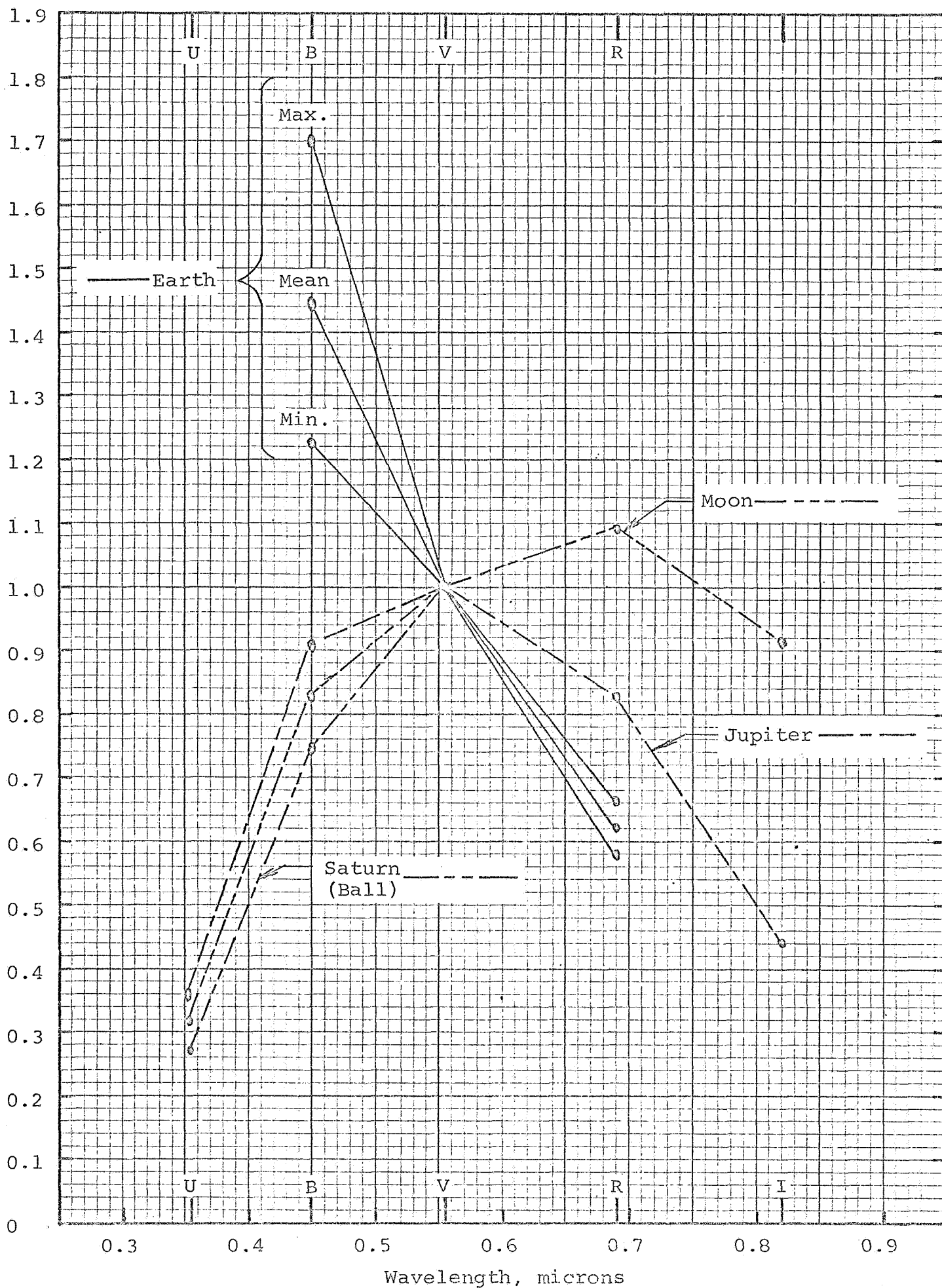


FIGURE 12. IRRADIANCE RATIOS VERSUS WAVELENGTH
(EARTH, MOON, JUPITER, SATURN)

TABLE V
BRIGHT STAR MAGNITUDES

Star	V	B-V	Celestial Latitude* (degrees)	Celestial Longitude* (degrees)
Sirius	-1.44	-0.01	41 S	105
Canopus	-0.72	+0.16	77 S	
Rigil Kentawus	-0.27	+0.71	43 S	240
Arcturus	-0.05	+1.24	32 N	201
Vega	+0.03	0.00	63 N	293
Capella	+0.09	+0.81	26 N	79
Rigel	+0.11	-0.05	31 S	75
Procyon	+0.36	+0.41	16 S	115
Betelgeuse	+0.40	+1.85	16-1/2 S	88
Achernar	+0.49	-0.17	60 S	350
Hadar	+0.63	-0.24	44 S	
Altair	+0.77	+0.22	28 N	302
Aldeberan	+0.80	+1.55	5 S	69
Acrux	+0.83	-0.26	57 S	207
Antares	+0.94	+1.83	4 S	249
Spica	+0.97	-0.23	2 S	208
Pollux	+1.15	+1.01	7 N	113
Fomalhaut	+1.16	+0.09	21-1/2 S	335
Deneb	+1.25	+0.08	63 N	320
Mimosa	+1.29	-0.25	53 S	210
Regulus	+1.34	-0.11	< 1 N	149
Adhara	+1.48	-0.17	52 S	113

* Approximate values only.

d. Multi-Color Stellar Discrimination

If an EAS is to be used on missions in which V-band magnitudes of the earth will reach -1 , possible interference from bright stars must be considered. For this reason, the V-band magnitudes of some of the brighter stars ($V = < 1.5$) are listed in Table V, along with values for B-V, celestial latitude, and celestial longitude. The stars that would require special attention are discussed below.

1) Canopus, Procyon, Altair, Fomalhaut, and Deneb have B-V color indices within ± 0.20 of that of the earth ($B-V = +0.21$); their spectral properties would thus have to be investigated more closely.

2) Procyon, Betelgeuse, Aldebaran, Antares, Spica, Pollux, Fomalhaut, and Regulus lie within 25 degrees of the ecliptic plane. Of these stars, only Procyon and Fomalhaut have a B-V color index close to that of the earth. In general, if the EAS is to operate in the $-1 < V < 0$ region, the effect of several of the brighter stars should be considered; if the EAS is to operate in the $0 < V < +1$ region, the effect of all the stars listed in Table V should be considered. If operation is required at $V > +1$, the number of possible interfering stars becomes much larger and considerable sophistication might be required unless the EAS field of view could be restricted to narrow limits about the ecliptic plane.

It should also be pointed out that star discrimination using color techniques will require sensing the earth and discriminating against targets both bluer (hotter) and redder (cooler) than the earth, while planetary discrimination alone requires only that the sensor discriminate against redder targets.

2. The Ultraviolet Region (0.2 to 0.3 Micron)

Measurements of the appearance of the earth and other planets in the ultraviolet wavelength region have been limited by the strong absorption of this band by the ozone layer of the earth's atmosphere at an altitude of approximately 80,000 feet. The information collected during the study is summarized below.

a. Earth

1) Measurements of the spectral radiance of the earth were made from an X-15 aircraft in the 0.2- to 0.28- μ wavelength (λ) region,⁷ with the following results for scattering angles of 102 to 130 degrees.*

λ (μ)	N (watt/cm ² -sr- μ)
0.24	2×10^{-7}
0.26	2.1×10^{-6}
0.28	1.2×10^{-5}

2) Theoretical predictions that are in fair agreement have been made of earth radiance in the ultraviolet wavelength region.^{8,9} These articles point out that any ultraviolet reflected by the earth is primarily due to scattering. The radiance values are derived in terms of radiance from a unit area on top of the earth's atmosphere and are functions of zenith angle, solar incidence angle, and scattering angle. The effective spectral radiance of the entire earth as seen from a relatively large distance has not been calculated but is of the same order of magnitude as the spectral radiance at the nadir with the sun at the zenith. These values vary somewhat, depending on the researcher and the assumed ozone distribution, but they are approximately as follows:

λ (μ)	N (watt/cm ² -sr- μ)
0.20	$1.6 \text{ to } 2.0 \times 10^{-5}$
0.22	$3 \text{ to } 6 \times 10^{-6}$
0.24	$1 \text{ to } 4 \times 10^{-6}$
0.26	$1 \text{ to } 5 \times 10^{-6}$
0.28	$0.6 \text{ to } 1 \times 10^{-5}$
0.30	10^{-4}

Spectral irradiance at any relatively large distance can be computed from these values of N by

$$H_{\lambda} = N_{\lambda} \pi \frac{R^2}{d^2}, \quad (4)$$

where R = planetary radius and d = distance of planet from observation point.

* The scattering angle is the supplement of the angle subtended at the target by the sun and the observation point.

b. Moon

A compilation of the lunar ultraviolet spectrum is presented by Heddle.¹⁰ Heddle has utilized results of work performed by Stan and Johnson and his own experimental observations, and has arrived at the values shown in the second column of Table VI for the spectral irradiance of the moon as received on the earth's surface. Based on the average distance from the earth to the moon and the moon's diameter, the effective spectral radiance of the moon in the ultraviolet region has been calculated and listed in the third column of Table VI.

c. Planets

Measurements of ultraviolet radiation from Mars and Jupiter were obtained from an Aerobee rocket at 140 kilometers over White Sands, New Mexico.¹¹ The irradiance at 2700 Å was measured, and since phase angles and distances at the time of measurement were known, reflectivities were calculated. These data are tabulated below.

	<u>Mars</u>	<u>Jupiter</u>
Flux at 2700 Å at earth ($\Delta\lambda \approx 300 \text{ Å}$), $\text{erg/cm}^2\text{-sec-100 Å}$	2.0×10^{-8}	1.5×10^{-7}
Phase Angle, deg	32.4	2.3
Reflectivity	0.24	0.26
Uncertainty in Measurement, %	$>\pm 15$	~ 15

Since the ultraviolet solar irradiance at both of these planets can be calculated, the approximate irradiance at 0.27 μ from these planets can be calculated as a function of distance and phase.

3. The Near-Infrared (IR) Region (1 to 4 Microns)

Although numerous studies have been made of planetary radiation in the near-IR region, much of the work has been directed toward high-resolution spectroscopic observations concerned with determining details of the planetary atmosphere or surface. Of more immediate applicability to EAS design, however, is radiation in relatively broad optical bands and especially ratios of radiation in one band to that in another. Kuiper² has measured relative intensities of some of the planets at 1 and 2 μ , using broadband filters and a lead sulfide detector. The ratio of intensities at these wavelengths should be relatively independent of phase angle and distance from the observation point. The intensity ratios were adjusted so that the solar ratio is 1.00; the resulting reflectivity ratios are listed below. Near-IR data concerning the earth should be available in the near future.

TABLE VI
LUNAR ULTRAVIOLET DATA

Wavelength		Spectral Irradiance of Moon on Earth's Surface	Effective Spectral Radiance of Moon
μ	\AA	$(\text{photons}/\text{cm}^2\text{-sec-}\text{\AA})$	$(\text{watts}/\text{cm}^2\text{-}\mu\text{-sr})$
0.22	2200	6.8×10^4	9.22×10^{-6}
0.23	2300	1.1×10^5	1.54×10^{-5}
0.24	2400	1.5×10^5	1.90×10^{-5}
0.25	2500	2.3×10^5	2.78×10^{-5}
0.26	2600	5.5×10^5	6.42×10^{-5}
0.27	2700	1.4×10^6	1.57×10^{-4}
0.28	2800	1.7×10^6	1.86×10^{-4}
0.29	2900	4.2×10^6	4.42×10^{-4}
0.30	3000	6.1×10^6	6.17×10^{-4}
0.31	3100	9.4×10^6	9.25×10^{-4}
0.32	3200	1.3×10^7	1.30×10^{-3}
0.33	3300	2.1×10^7	1.94×10^{-3}

<u>Planet</u>	<u>Reflectivity Ratio</u>
Mercury*	3.5
Venus	1.61
Mars	1.00
Jupiter	0.21
Saturn (ball)	0.47
Saturn's Rings .	0.45

In general, it does not appear that the near-IR region can compete with the visible region for either aspect sensing or color discrimination, because solar radiation is down in the near-IR region, and reflectivities would have to be considerably higher than in the visible region to compensate. Also, the normalized detectivity (D^*) of the lead sulfide detector is lower than that of the silicon detectors used in the visible region.**

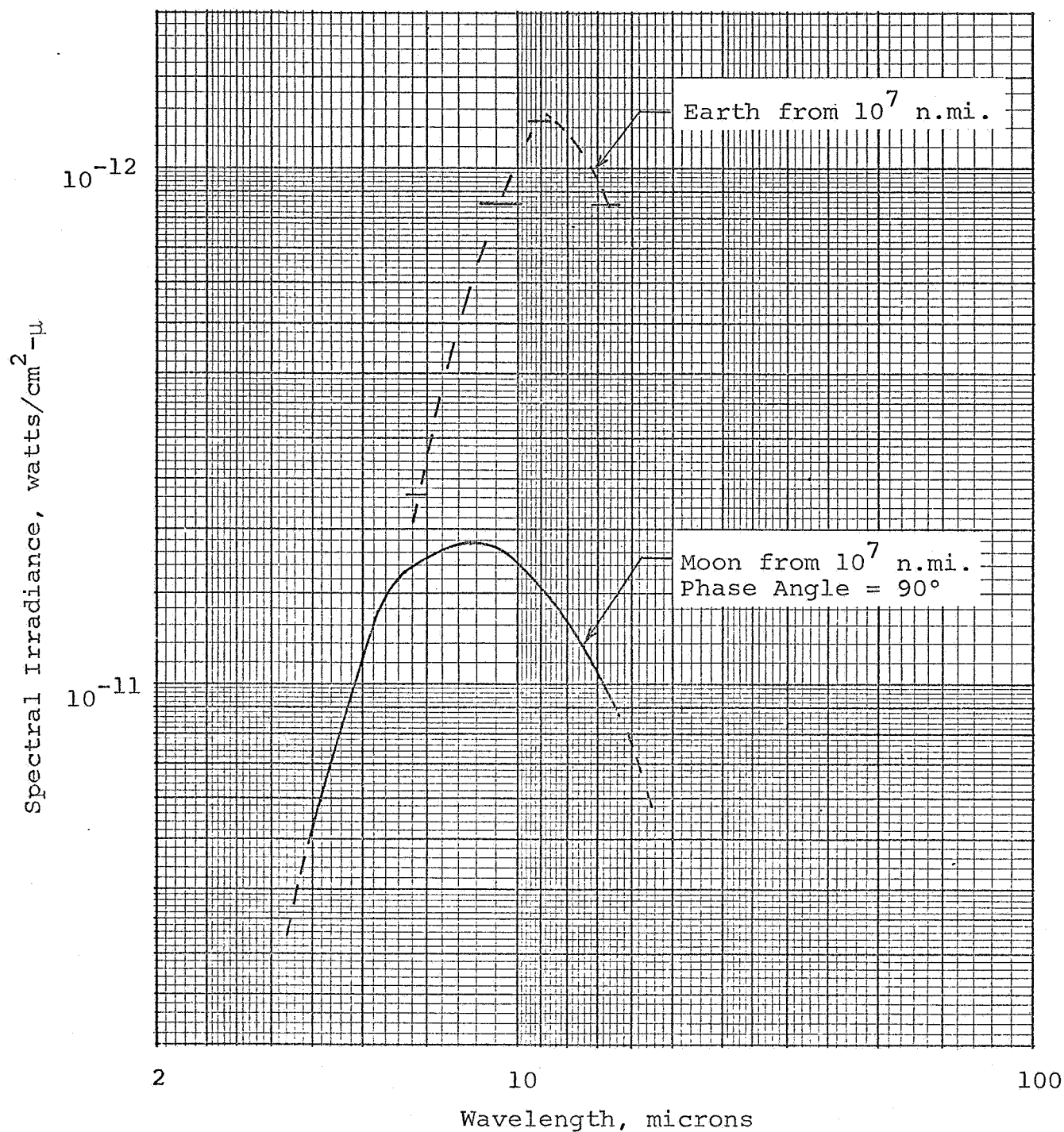
If a band in the near-IR region at 2μ or less could be correlated to the V band of the visible region as to relative reflectivities, it might in some cases be a valuable color discrimination band, but such information is apparently not available at present.

4. The Emitted-Infrared Region (> 4 Microns)

Figure 13 is a plot of spectral irradiance from the earth and from the moon in the infrared region beyond 4μ where thermal emission predominates over reflected IR. The conditions are a viewing distance of 10^7 nautical miles (n.mi.) and, in case of the moon, a phase angle of 90 degrees. For the earth, the emitted radiation is relatively independent of phase angle; for the moon, which has no atmosphere, the emitted radiation is strongly dependent on phase angle. The lunar-emission phase law is plotted in Figure 14.

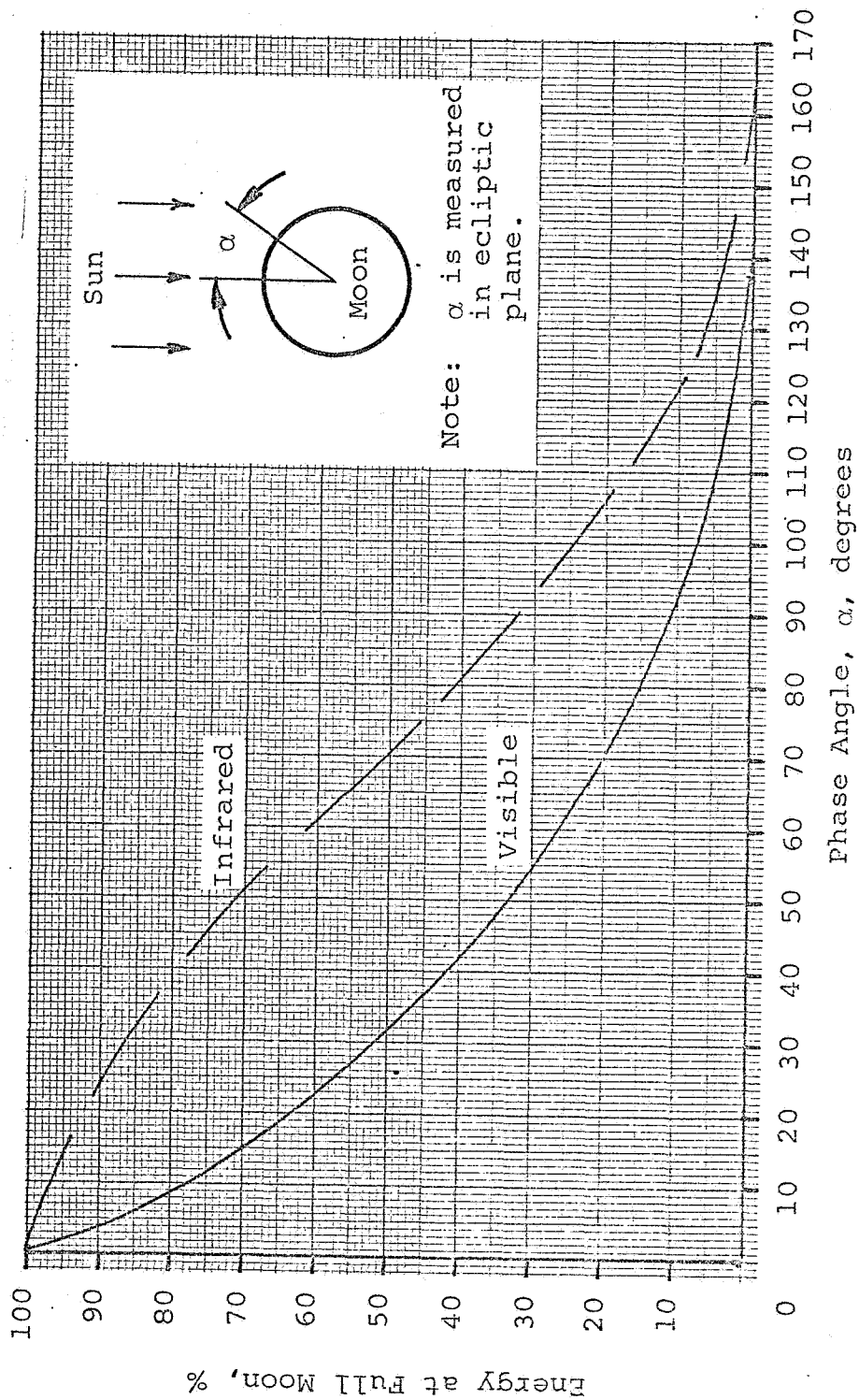
* The apparently high value for Mercury is due to a relatively high level of emitted IR at 2μ .

** See Appendix A for a definition and discussion of D^* .



SPECTRAL IRRADIANCE FROM EARTH AND MOON IN IR REGION

FIGURE 13



VISIBLE (REFLECTED) AND IR RADIANT ENERGY FROM THE MOON
AS A FUNCTION OF PHASE ANGLE

FIGURE 14

It appears that earth aspect sensing in the IR region beyond $4\ \mu$ would have only limited application. A calculation for a typical system using a 3-inch-diameter aperture and a thermistor bolometer detector results in a signal-to-noise ratio of less than 1 at a range of 10^7 n.mi. Since 10,000,000 n.mi. is equal to 12.4% of 1 AU, aspect sensing should be limited to a small fraction of most solar probe or interplanetary missions. The range could be extended in several ways, as discussed below.

a. Increase the Aperture

This approach does not appear practical, since 3 inches is probably already at or in excess of a practical size. Also, the signal-to-noise ratio will increase in proportion to the diameter; thus, doubling the aperture diameter will extend the range by a factor of only 1.41.

b. Use a Cooled Photodetector

This approach will require a cryogenic cooler and would require more power and complexity than is practical for a long-duration mission.

c. Use an Earth-Tracking System

The signal-to-noise calculations mentioned above assumed a 300-cps noise bandwidth for a sensor, on a spinning vehicle, that could sense the earth once every revolution. A tracker that continuously scans the earth could use a much narrower bandwidth (~ 1 cps), and thus the signal-to-noise ratio would improve by a factor of 17. However, consideration of such a device appears to be outside the scope of this effort.

An IR EAS might, however, be worth considering for specialized application where the required operating range is small. The advantage of IR over visible sensing is that IR is not subject to the phase-angle limitations of a reflected-sunlight sensor.

5. Comparison of Ultraviolet, Visible, Near-IR, and Emitted-IR Sensing

Table VII compares the various parameters of the four wavelength regions discussed above. It is obvious that the visible region is by far the best choice of operating wavelengths in nearly all respects. The possibility of using one band in the visible region for aspect sensing and another region for aiding in color discrimination has been considered, but this approach has some serious disadvantages. First, a different kind of detector would probably be required for each region, which could introduce serious drift problems. Second, different optical materials might have to be used for each region, which could complicate the design. Third, measurements outside the visible region are not well related to the

TABLE VII

COMPARISON OF ULTRAVIOLET, VISIBLE, NEAR-IR, AND EMITTED-IR SENSING AND DISCRIMINATION

Wavelength Region (μ)	Information Available	Relative Irradiance	Detectors	Relative S/N	Optics	Remarks*
Ultra-violet (0.2-0.3)	Little information available. No experiments could be done until recently because of ozone layer.	$(H_{UV}/H_{VIS})_{Earth}$ $\approx 10^{-5}$ to 10^{-3} H_{UV}/H_{VIS} Planets $\approx 10^{-2}$ to 10^{-1}	Photomultipliers Silicon photo-diodes Pbs	Good Fair Poor	Limited choice of refractive materials. Silica is commonly used.	When more is known, this wavelength region might be suitable if target data are well related to V-band data in the visible region. At $\lambda < 0.27 \mu$, signal levels will probably be too low.
Visible (0.3-1)	Extensive studies done; however, a few information gaps remain.	High. Solar flux peaks at $\sim 0.5 \mu$ with half power points at 0.31 and 0.93μ .	Silicon photo-voltaic Photomultipliers Cds or CdSe Pbs	Good Very good Fair	Large variety of refractive materials. Somewhat limited because non-browning glass must be used.	This region appears to be the best operating region in nearly all respects.
Near-IR (1.0-4.0)	Moon and earth probably fairly well known. Some measurements of planets.	$(H_{IR}/H_{VIS})_{Earth}$ $\approx 5 \times 10^{-3}$ to 5×10^{-1} The ratio is probably similar for the other planets.	Pbs	Poor	Most conventional materials OK out to about 2μ .	Potentially a good region out to about 1.6μ when measurements are made on targets that are well related to V-band data. An instrument capable of doing this has been built (ref. 12).
Emitted-IR (4.0-30)	Earth and moon well known. Probably some data on planets.	$(H_{IR}/H_{VIS})_{Earth}$ $\approx 10^{-2}$ 90° phase angles for visible.	Thermistor bolometer	Poor	Limited number of materials. Germanium, silicon, and Intran-4 are commonly used.	Suitable for close-in missions (\approx several million miles). Signal not a function of phase angle.

* Any pair of $\Delta\lambda$ bands used for sensing and discrimination should have target measurements made in each band by closely related techniques. This means, in general, that both chosen bands should be in the same wavelength category (first column above).

visible region either by common instruments or by researchers using the same techniques. Thus, there is additional uncertainty as to the color ratios. For this reason, it was decided to design an EAS that would operate in a wavelength region between 0.3 and 1 μ .

6. Comparison of Discrimination Techniques

There appear to be four parameters that could serve as a means of discriminating against possible interfering targets: brightness, angular size, position with respect to the vehicle spin phase (using solar references), and color. As was discussed earlier, the brightness and angular size of the earth and possible interfering targets vary widely; these two approaches must therefore be ruled out.

Spin-phase discrimination would consist of blanking the EAS output during most of each spin cycle and gating it open through a narrow phase-angle range. (Here the term phase angle refers to vehicle spin phase and is not to be confused with the term that refers to the angle subtended at the target by the sun and the vehicle.) The logical spin-phase zero reference is the sun, which of course is the most distinct and unambiguous of all the celestial targets. However, the earth phase angle changes continually with respect to the sun. If the spin-phase technique were used, therefore, a clock together with a programmed phase shifter that would be unique for every mission would be required. A further complexity is that the phase-shifting program is a function of the launch date and time. This factor would be particularly critical with a mission in which aspect sensing might be required while the vehicle is in a parking orbit about the earth.

The technique that appeared the most favorable and that was investigated in the greatest detail was color discrimination.

7. Decisions Reached as a Result of the Target Radiation Study

a) Further effort on the EAS was restricted to optical sensing in the wavelength region of 0.3 to 1 μ .

b) Further effort on the EAS target-discrimination function was restricted to color discrimination.

C. Detector Investigation

As was noted above, it was decided, as a result of the target radiation study, to restrict further EAS design effort to the 0.3- to 1.0- μ wavelength region. Fortunately, within this region, the technology of radiant-energy detectors is well advanced and a number of highly sensitive detector types are available. Part of the detector investigation effort consisted of a review of available detector data, followed by a comparative evaluation of various detector types with regard to their suitability for use in the EAS. Photodetectors considered were ones that respond well over some optical bandwidth within the chosen 0.3- to 1.0- μ region and that are available with extended-area photosurfaces ($\sim 1 \text{ cm}^2$). A brief survey of the detector field disclosed three types of detectors that merited serious consideration: silicon detectors (either photovoltaic or biased), photomultiplier tubes, and cadmium sulfide or cadmium selenide detectors. In addition to the usual performance parameters, performance under adverse environmental conditions was considered, particularly the effect on these detectors of periodic pulses of high light levels, a condition that may be encountered in the EAS because the sun enters the field of view once during each revolution of the vehicle. Since manufacturers' data were insufficient to answer this question, it was necessary to devise and conduct a special test on the representative detector types.

Section C.1 following presents the evaluation of the three types of detectors considered. Section C.2 describes the special testing to which two of the detectors were subjected.

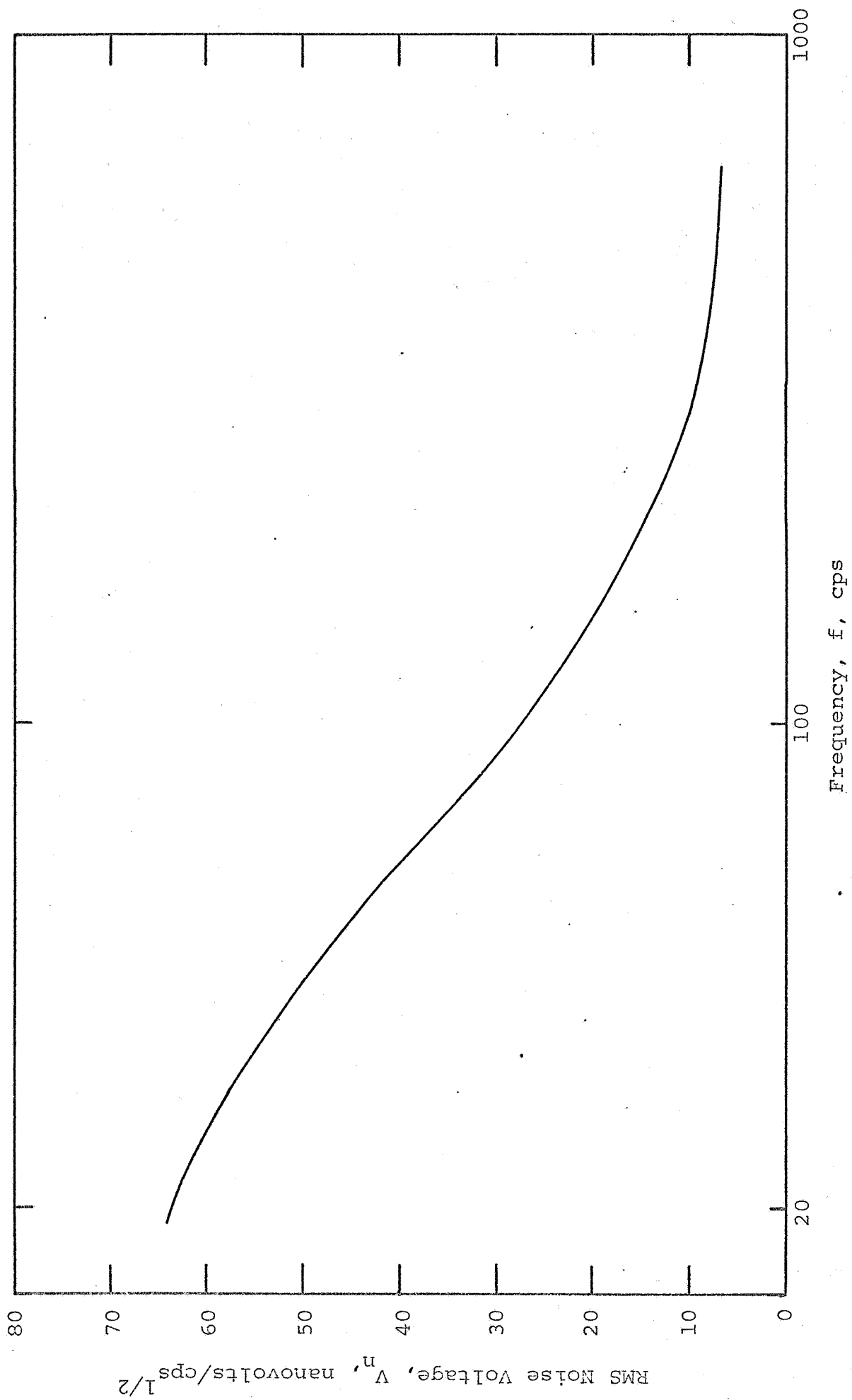
1. Detector Review and Evaluation

a. Silicon Detectors

Silicon detectors are characterized by high normalized detectivity (D^*), fast response time, and good stability when subjected to environmental extremes.** These detectors are p-n junction devices and thus can be considered photodiodes. Some types are designed for operation in the photovoltaic or low back-bias voltage mode, while others are designed for operation at bias levels of several hundred volts. Although the high-bias type exhibits a higher responsivity than the photovoltaic type, the $1/f$ noise characteristics at frequencies below 1 kc are probably excessive.

Over a limited range, the responsivity of the photovoltaic type of silicon detector can be controlled during manufacture. Unfortunately, detector noise increases with responsivity, but to some extent a detector "optimized" for operation with a given preamplifier can be specified. Noise characteristics of a typical photovoltaic detector are shown in Figure 15. The relative spectral response of

** Ref. Appendix A.



NOISE CHARACTERISTICS OF TYPICAL SILICON PHOTOVOLTAIC DETECTORS

FIGURE 15

most types of silicon detectors peaks at 0.85 micron, with half-power points at approximately 0.5 and 1.0 micron (see Figure 16). Silicon detectors perform satisfactorily from liquid air temperature up to approximately 70 or 80°C. At high light levels, the number of carriers are limited and signals tend to saturate. Thus, when the sun is within the field of view, the signal will certainly be saturated. However, upon removal of the light input, the signal should decay exponentially whether it is saturated or not. The decay is given approximately by the following equation:

$$V = V_0 e^{-t/\tau}, \quad (5)$$

where V = signal voltage at time t after removal of light input,

V_0 = peak signal voltage,

τ = time constant of detector (1 to 10 μ s for most photovoltaic silicon detectors).

Silicon detectors are very stable against long-term drift. Most performance characteristics will remain constant to within 5% over long periods of time. Electro-Nuclear Laboratories has measured long-term relative drift in responsivities for many multiple-array detectors and has found no relative drifts in excess of 5%.

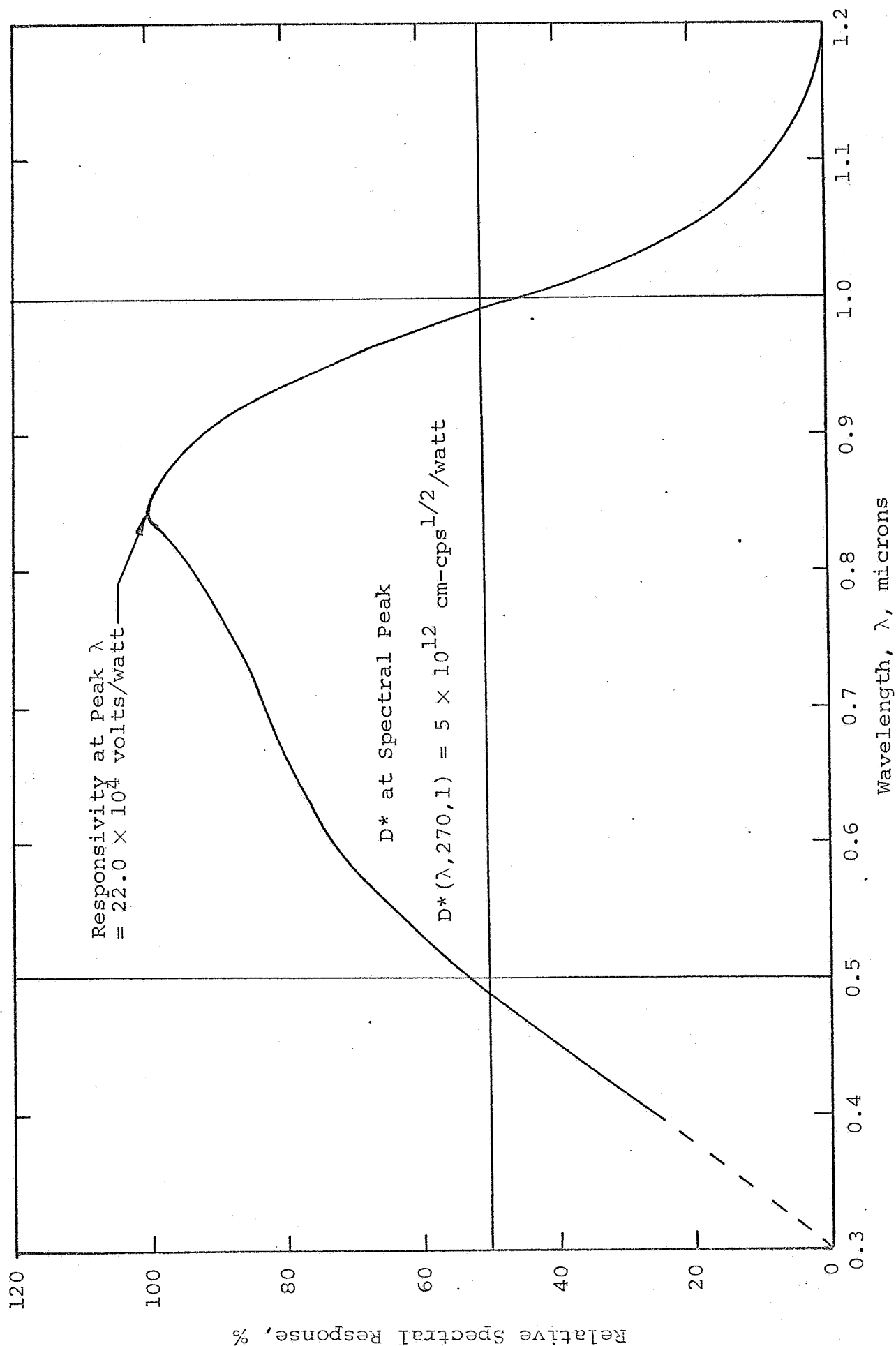
Silicon detectors are degraded to some extent by high-energy proton bombardment. The effect is very similar to that on silicon solar cells.

b. Photomultiplier Tubes

Photomultiplier tubes are more sensitive than solid-state detectors and therefore can provide the EAS with a considerably greater operating range. The D^* of a 1P21 photomultiplier is approximately two orders of magnitude higher than that of the best silicon detectors. Under operating conditions in an EAS, this high photomultiplier detectivity can be realized because tube noise will predominate over preamplifier noise, while in the case of silicon detectors preamplifier noise will usually predominate. There are some obvious disadvantages, however, to the use of photomultipliers. They require a well regulated high-voltage power supply (~ 1 to 2 kv) and occupy much more space than a solid-state detector. Reliability has also been a problem.

The spectral response of a photomultiplier depends on the photocathode material and glass envelope combination. Response curves for a number of representative types are shown in Figure 17.

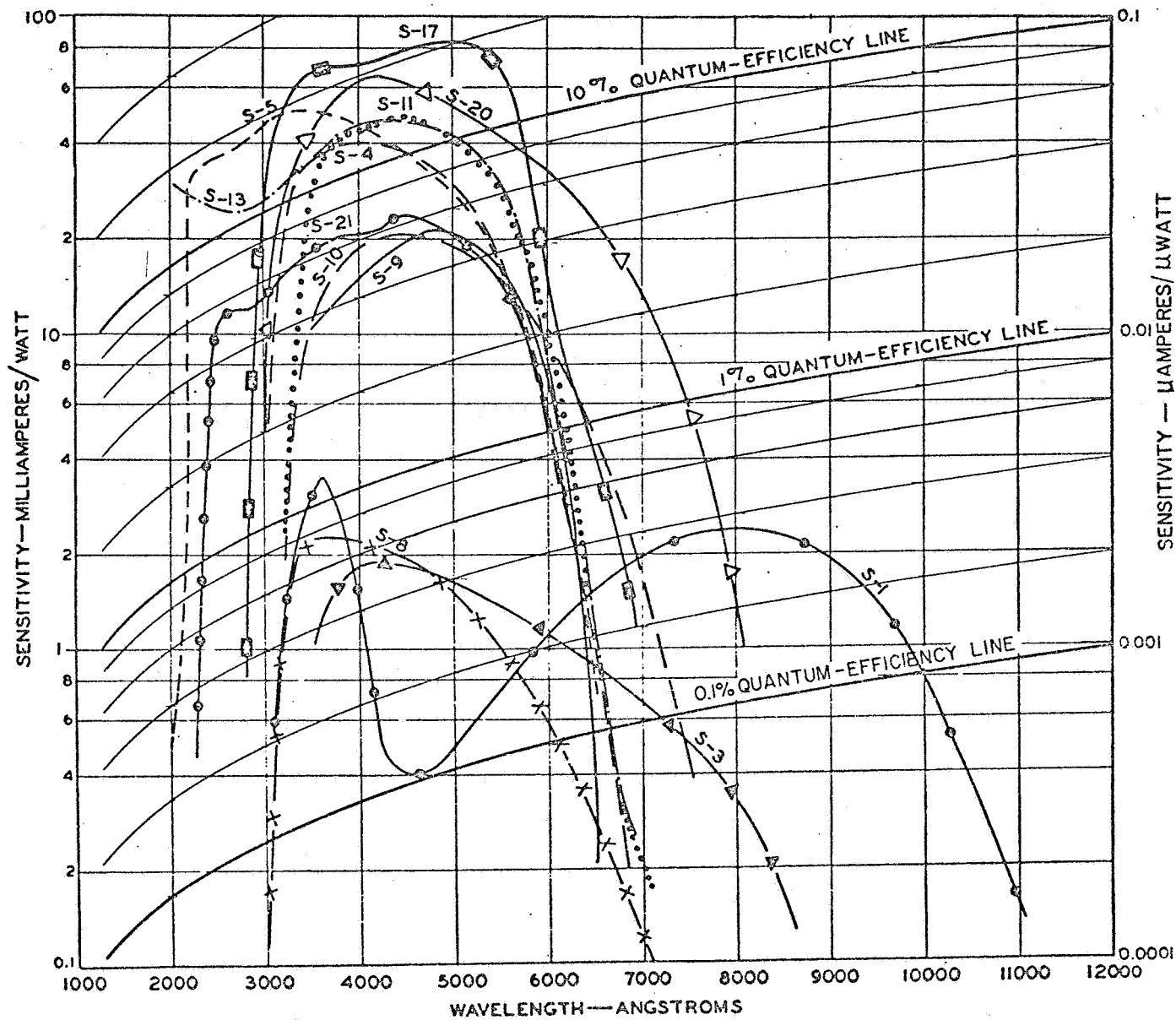
The following general conclusions were drawn about the performance of photomultiplier tubes under adverse environmental conditions:



Note: Abstracted from data on Electro-Nuclear Laboratories detector 602-10.

SPECTRAL-RESPONSE CHARACTERISTICS OF SILICON PHOTOVOLTAIC DETECTORS

FIGURE 16



Note: Reproduced from ITT Industrial Laboratories brochure.

SPECTRAL-RESPONSE CHARACTERISTICS OF REPRESENTATIVE PHOTOMULTIPLIER TUBES

FIGURE 17

1) Cathode sensitivity for most cathode-type photomultipliers does not decrease at elevated temperatures up to 75°C. However, there is a gain change in tubes with photocathodes containing cesium, including among others, many of the types that might commonly be considered for EAS application, such as S-4, S-11, and S-20. This gain change is caused by a migration of cesium ions from the cathodes to the dynodes. The net result is an effective sensitivity change caused by the high temperatures.

2) The dark current for most cathode-type photomultipliers approximately doubles for every 10°C rise in ambient temperature. In most high-quality tubes, thermionic emission is the predominant dark-noise source; in these tubes, the dark noise as a function of ambient temperature can be predicted in a given electronic bandwidth since it is proportional to the square root of the dark current.

3) The maximum ambient temperature most tubes can withstand (with bias on) before permanent damage occurs is approximately 75°C. Some tubes, however, are rated for 150°C.

4) Most manufacturers claim that their tubes can safely withstand vibration and shock levels well above those of typical launch levels.

With regard to the effect on photomultiplier tubes of high light levels (a problem of particular concern in the EAS design), it was found that a definite tube fatigue occurs at high light levels. This is a dynode effect caused by high currents. Some sort of protective technique would therefore be required in the EAS. One approach would be to shutter the optics periodically as the sun entered the field of view, an undesirable complication in a long-life space device. An alternative approach would be to switch the supply voltage off during the sun-exposure intervals, or to limit the anode current by biasing off the first two or three dynodes when the sun is in the field of view. This could be done by using a small sun sensor with a field of view coincident with and larger than that of the EAS. The sun sensor output could be used to reduce the photomultiplier dynode voltages. However, even if the tube were biased off during periods of high light input, the dark noise of the tube would still increase as the result of direct incidence of light on the first or second dynode, causing cathode fatigue. Since manufacturers could supply no information on this effect, a photomultiplier tube was purchased and subjected to special tests (see Section C.2).

Because of funding limitations, the most likely single candidate from among the various tubes available was selected for testing, an EMR 541D-05-14. The photocathode is a sodium-potassium bi-alkali that contains no cesium. It has extremely low dark noise, and even though the dark current (which is proportional to the square of the dark noise) triples for every 10°C temperature rise, it is still lower than that of most other tubes at elevated temperatures. The spectral response peaks at between 3000 and 4000 Å and is similar to the S-11 response. Complete manufacturer's specifications are given in Appendix B.

c. Cadmium Sulfide and Cadmium Selenide Type Detectors

Detectors of this class exhibit slow time constants, of the order of seconds. However, they are characterized by extremely high responsivity. In addition, cadmium sulfide cells have been made which have D^* values rivaling those of photomultiplier tubes when tested at chopping speeds of 90 cps. These detectors are photoconductive and must be biased.

Since most manufacturers do not make this type of detector expressly for low-light-level applications, information on performance at these levels was not easily obtained. However, several comments on characteristics having a bearing on their suitability for EAS use can be made:

- 1) The operating ambient-temperature range is usually 0 to 55°C, although special units that can operate at up to 85°C have been made.

- 2) The maximum temperature the detectors can withstand without permanent damage is about 85°C.

- 3) Long-term drift of performance characteristics is at least an order of magnitude worse than with silicon detectors. In general, cadmium sulfide detectors or detectors with a preponderance of cadmium sulfide are more unstable than cadmium selenide detectors.

- 4) The dark resistance of this type of detector is extremely high (of the order of hundreds of megohms), making pre-amplifier design difficult.

- 5) Recovery from a high light level, such as solar flux, requires a long time (probably of the order of minutes). However, certain types might respond well to a low-level signal, even while recovering from a high-level signal.

It was decided that detectors of the cadmium sulfide and cadmium selenide type compared unfavorably with silicon detectors and photomultiplier tubes with respect to their suitability for use in the EAS. Hence, no further consideration was given to cadmium sulfide-selenide detectors, and no testing was performed.

Some of the more significant properties of the various detector types considered are listed in Table VIII.

TABLE VIII
TABULATION OF DETECTOR PROPERTIES

**Properties Detector Type	Wavelength of Peak Response (micron)	Wavelengths at 50% Response (micron)	$D^*(\lambda_p, f, l)$ (cm-cps $^{1/2}$ /watt)	Responsivity	Limiting Noise Mechanism at $f < 1$ kc	Time Constant (sec)	Maximum Operating Temperature (°C)
Silicon Photovoltaic	~0.85	0.5-1.0	5×10^{12} at $f = 270$ cps (Electro-Nuclear 602-10)	4×10^4 V/W	$1/f$ noise at $f < 300$ cps. Johnson (thermal) noise at $f > 300$ cps.	$(1 \text{ to } 10) \times 10^{-6}$	~80
Silicon Back Biased	~0.9	0.5-1.1	1.8×10^{12} at $f = 1000$ cps (E.G. & G. SGD-444A)	$0.25 \mu\text{A}/\mu\text{W}$ at 0.9μ	$1/f$ noise at $f < 300$ cps. Johnson noise and shot noise at $f > 300$ cps.	$\sim 10^{-7}$	150
Cadmium Sulfide	~0.52†	0.5-0.6	$\sim 10^{14} \dagger\dagger$	Very high	Current noise	> 1 for low light levels	55-85
Cadmium Selenide	~0.73†	0.72-0.75	Usually less than CdS	Very high	Current noise	> 1 for low light levels	55-85
Photomultiplier	Function of photocathode material and glass enve- lope (see Figure 17)	See Fig. 17	$\sim 10^{16}$	0.015 to ~ 0.068 A/W at cathode, depend- ing on cathode type; usual gain is 10^6 to 10^7	Dark noise (shot noise) at very low light levels. Noise in signal at higher levels.	$\sim 10^{-8}$	75 for cathodes con- taining cesium up to 150 for bi-alkali types

** Properties are representative for sensitive areas of the order of 1 cm^2 .

† Cadmium sulfide-selenides are available with intermediate spectral-response properties.

†† This is representative of some of the higher values measured for a number of CdS detectors of area $< 1 \text{ cm}^2$ (ref. 13).

2. Detector Tests

a. Equipment

As mentioned previously, the primary purpose of the detector tests was to investigate the behavior of detectors when subjected to periodic pulses of sunlight. More specifically, it was desired to determine the ability of the detectors to detect a periodic low-level light input, such as might be received from the earth, in the presence of the periodic solar pulse. Of concern were detector recovery time from this solar pulse, the effect of the solar pulse on detector noise level, and, in the case of photomultipliers, cathode fatigue.

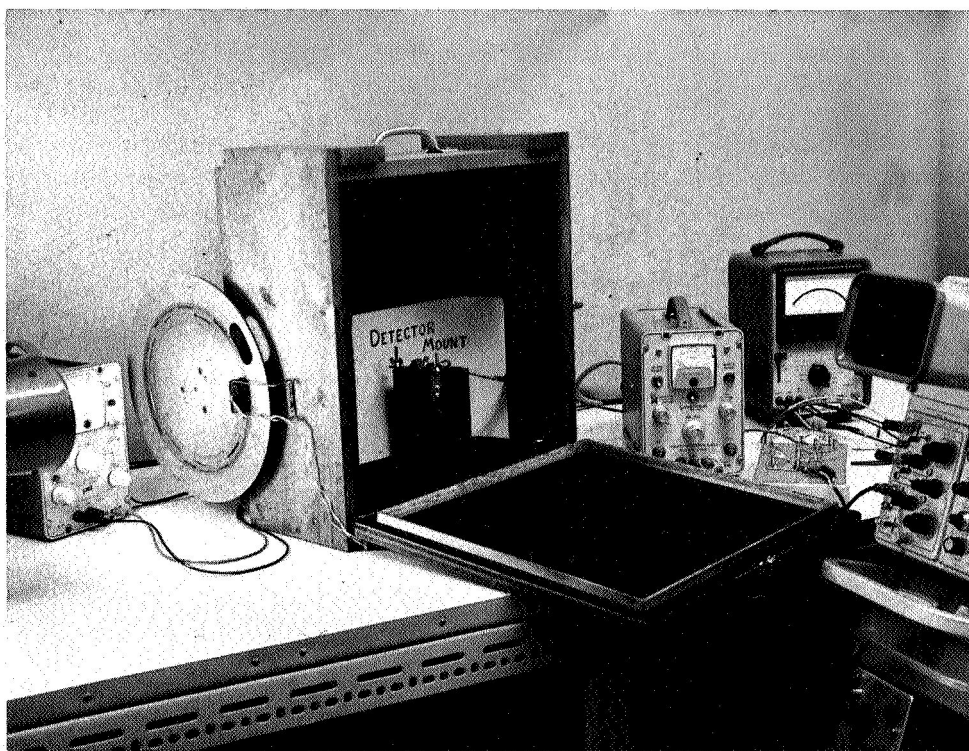
The equipment used to conduct the tests is shown in the photograph and schematic of Figures 18 and 19. The detectors were mounted in the box, which is light tight except for the two apertures closely adjacent to the chopper wheel. The chopper wheel provides a means of varying the phases of the solar and earth pulses relative to each other during the spin cycle. Near the periphery of the chopper wheel is a large opening that admits sunlight for about 25 degrees of spin phase. Inboard of this large opening are eight smaller openings or slits that admit low-level light from a light bulb to simulate the earth signal. In practice, all but one of these inboard slits were masked off, making possible the selection of any one of eight phasings of earth pulse relative to solar pulse. The wheel can be rotated at any speed within the anticipated range of probe spin rates (0.5 to 2 rps). A pickoff on the chopper-wheel shaft served to periodically bias off the photomultiplier during the solar pulse. A preamplifier for the silicon photovoltaic detector and a high-voltage power supply for the photomultiplier tube were designed and built. Standard laboratory electronic instruments completed the test equipment.

b. Detectors Tested

The following detectors were tested:

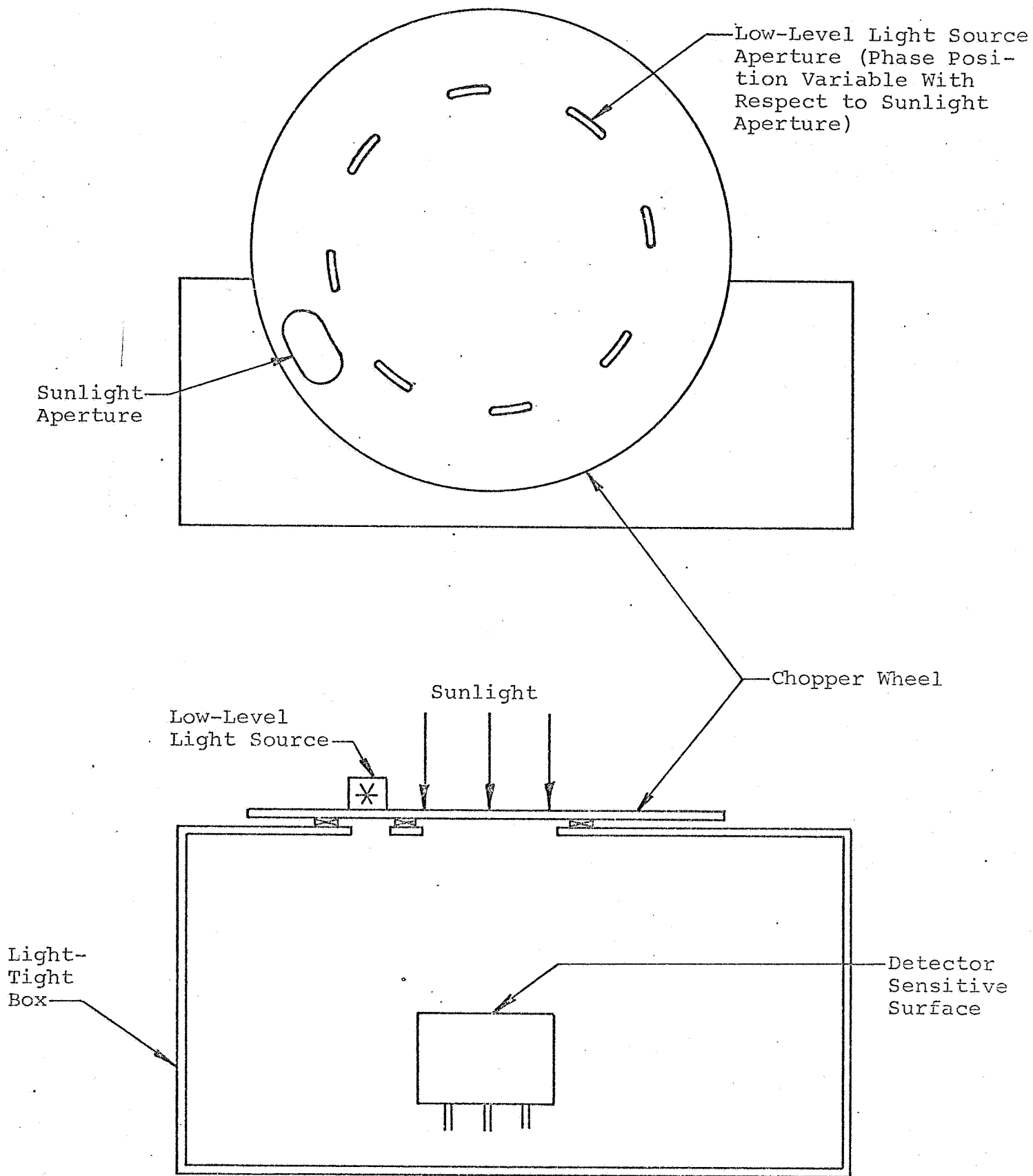
- a) 541D-05-14 photomultiplier tube with a bi-alkali cathode, manufactured by Electro-Mechanical Research, Inc.
- b) 601-10 silicon photovoltaic detector, manufactured by Electro-Nuclear Laboratories, Inc.

It was also intended to test a silicon detector designed to operate as a biased diode, but the vendor was unable to deliver this item. A cadmium sulfide detector and a cadmium selenide detector were also purchased, but their time constants upon exposure to high light levels proved so long as to completely eliminate them from consideration.



DETECTOR TEST EQUIPMENT

FIGURE 18



DETECTOR TEST EQUIPMENT SCHEMATIC

FIGURE 19

c. Photomultiplier Tube Test Results

During the testing, the tube was protected from the high light levels by switching off the high voltage during sun exposure by means of a high-voltage reed switch actuated by a cam attached to the chopper wheel. Figure 20 shows the photomultiplier output for one complete cycle of the chopper wheel (corresponding to one complete vehicle revolution). The intensity of the light bulb used to simulate the earth pulse was adjusted to produce a signal corresponding to that produced by a fully illuminated earth at a distance of 4 AU. As can be seen on Figure 20, the transients produced by switching the high-voltage supply off and on are rather severe. If this technique were used for a flight instrument, these transients would prevent the system from operating for approximately 20 ms after the sun leaves the field of view, corresponding to 7 degrees and 29 degrees for vehicle spin rates of 1 rps and 4 rps, respectively. It should be pointed out here that direct switching of the high voltage is also undesirable from a power standpoint, since several hundred milliwatts are required to operate the high-voltage reed switch.

As shown in Figure 20, the peak-to-peak noise riding on the earth pulse is 2 mV. This is a factor of two higher than the noise level of the tube when not periodically exposed to the sun.

In the EAS, the transient interference caused by switching the voltage off and on could probably be reduced by switching the low-level supply voltage in the primary of the dc-to-dc converter off and on. If this is done, however, the converter frequency must be 50 to 100 kc to prevent the filter time constant from being prohibitively long. (With a converter frequency of 2 kc, the filter time constant causes an angular dead zone on either side of the sun which is three to four times that produced by the high-voltage turn-on transient.)

An alternative approach would be to reverse-bias the cathode and the first dynode of the photomultiplier during periods of sunlight exposure instead of switching off the entire power supply. This technique has been investigated by workers at Electro-Mechanical Research, Inc.¹⁴ Unfortunately, the tube used for the detector tests at Quantac (procured before ref. 14 was received and reviewed) has the voltage-divider dynode resistors potted integrally with the tube; it was therefore impossible to investigate the cathode biasing technique with this particular unit.

To definitely establish whether either of the protective techniques noted above is acceptable, extensive photomultiplier life testing would have to be conducted. Even though the short-term transient effects might be acceptable, periodic exposure to the sun over a long period of time might degrade the performance of the tube to an unacceptable level.

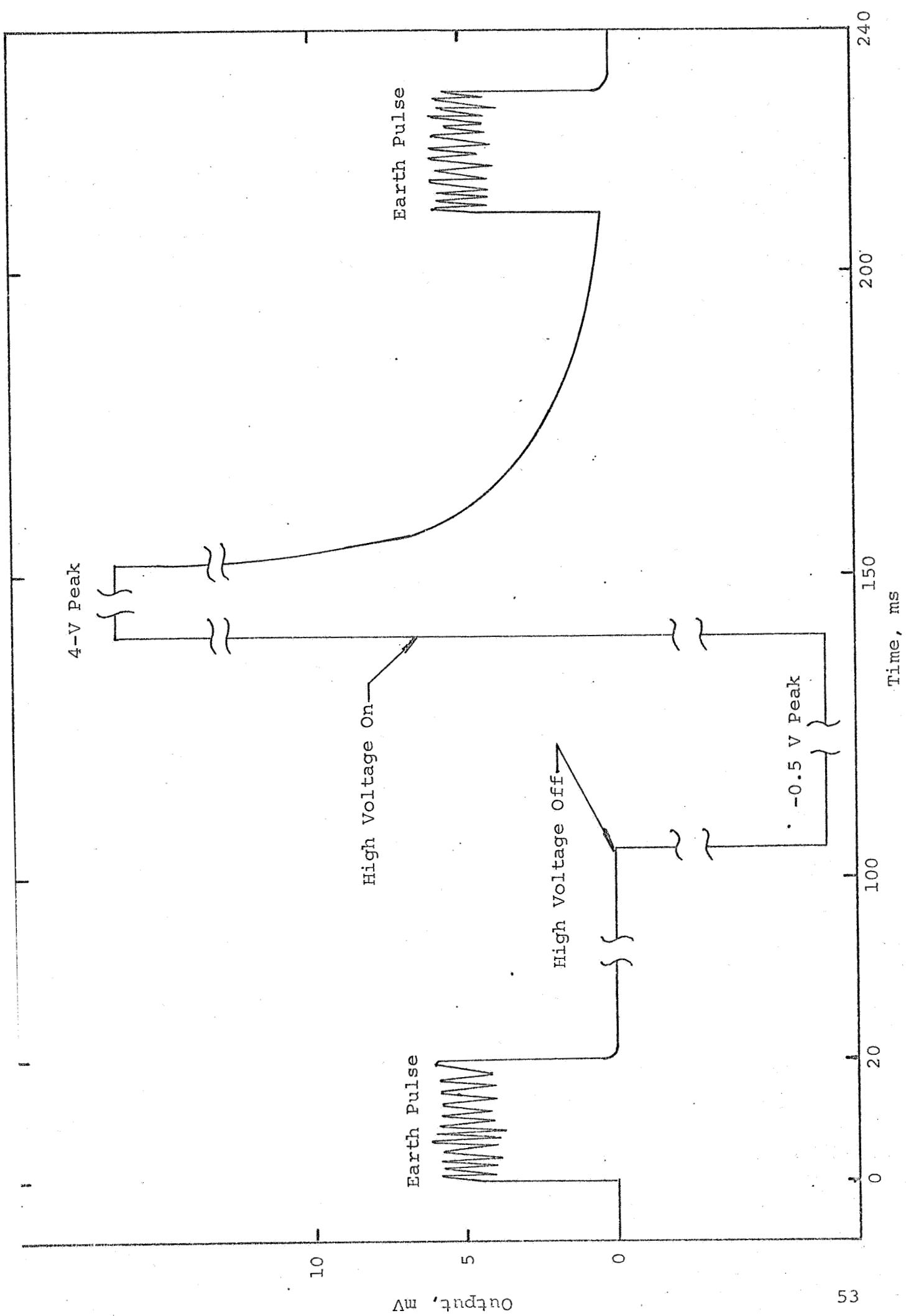


FIGURE 20. PHOTOMULTIPLIER OUTPUT FOR ONE COMPLETE CYCLE OF CHOPPER WHEEL.

Considerably more testing would be required to definitely establish the suitability of a photomultiplier tube for the EAS application. Preliminary tests indicate, however, that it could be used, although the long recovery time from the solar pulse would limit its performance.

d. Silicon Photovoltaic Detector Test Results

Figure 21 shows the photovoltaic diode output during exposure to sunlight (0 to 30 ms) and just after exposure to sunlight (30 to 35 ms). The method of testing was basically the same as for the photomultiplier tube in that the same test setup and sun exposure rates were used.

As can be seen in Figure 21, there is a noticeable output from the detector after the sun has passed from the field of view. This output is in the form of an exponential decay with a maximum value of 20.4 mV and a time constant of approximately 1 ms. A careful check of the instrumentation proved the effect to be a characteristic of the device rather than an electrical effect caused by the instrumentation. The effect of this exponential decay following the solar pulse on operating range of the EAS depends on the optical and signal-processing concepts used. This effect is discussed further in connection with signal-to-noise calculations and operating-range predictions (ref. Section IV.B).

Note: This measurement was made with the detector loaded with 5(10³) ohms. Therefore, the 150-mV point is equivalent to an open-circuit detector output of 20.4 mV.

350-mV Peak

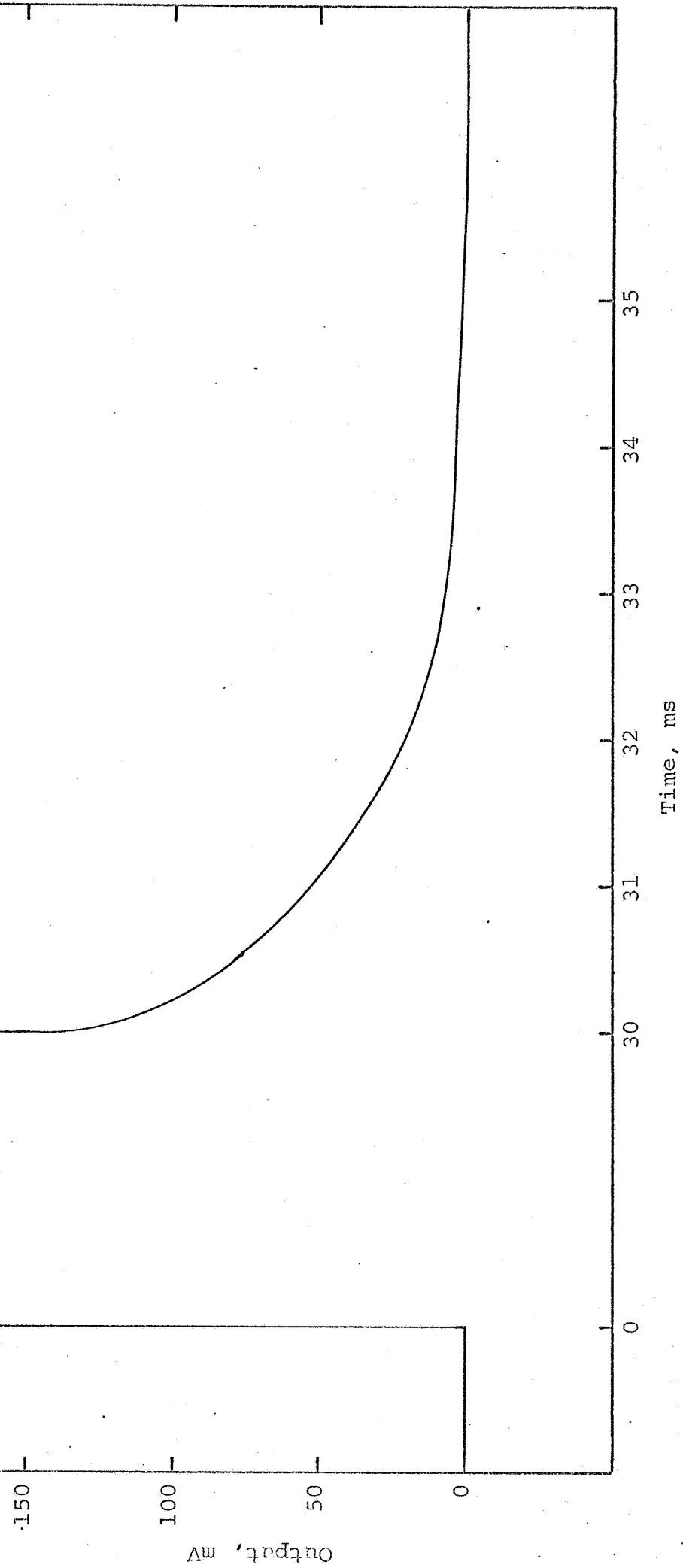
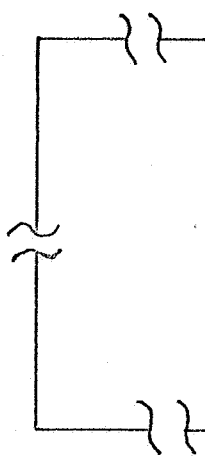


FIGURE 21. SILICON DETECTOR OUTPUT DURING AND JUST AFTER EXPOSURE TO SUN

PRECEDING PAGE BLANK NOT FILMED.

IV. EAS SYSTEM AND HARDWARE CONCEPTS

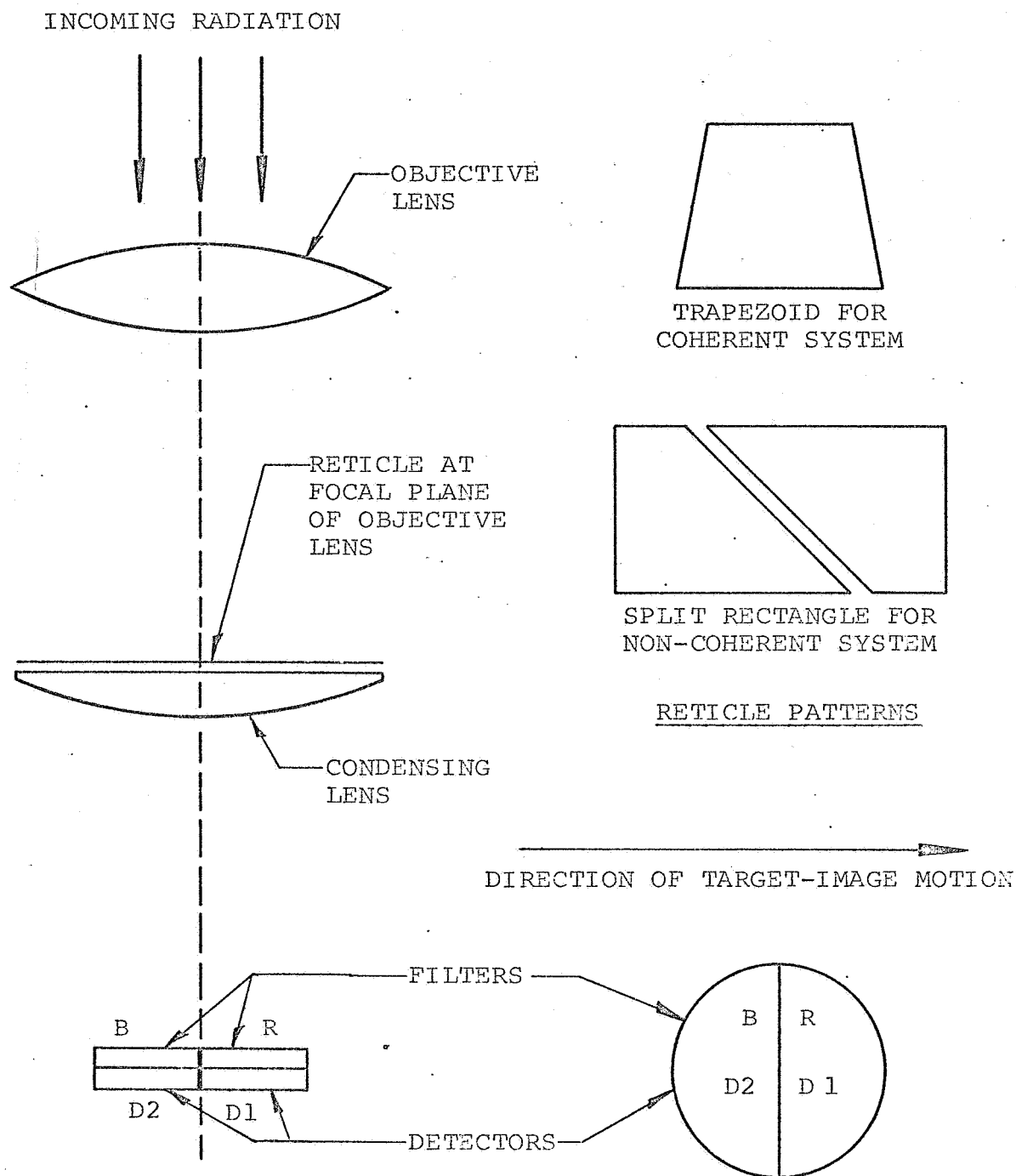
A. Optical Concepts

A variety of optical concepts were generated for presenting "earth look angle" information to the detectors and to the electronics for signal processing. In three of these concepts, the look angle is determined by sensing the earth directly, with one using the width of the earth pulse and the second using the amplitude of the pulse. The third is a direct digital system. A fourth concept based on star sensing is also described. Each concept is discussed below, followed by the evaluation that formed the basis for selection of the concept to be designed.

1. Pulse-Width Concept

The pulse-width concept can best be understood by referring to the optical schematic of Figure 22. Incoming radiation is imaged by the objective lens on a reticle at the focal plane, the reticle defining the field of view (FOV) by its pattern as indicated. This concept, with a minor variation in the reticle configuration (ref. Figure 22), is compatible with both of the signal-processing approaches considered (coherent and non-coherent). Signal-processing techniques are discussed in Section IV.B.

The direction of target motion across the FOV is from left to right. The objective lens is imaged on the detector by a condensing lens located immediately behind the reticle. Each detector has two semi-circular sensitive areas, immediately on top of which are placed semi-circular filters. These filters are designated as "blue" and "red" and are placed on detector halves D1 and D2 respectively. Since the radiation incident on this detector-filter array is completely defocused with respect to the system FOV, the spectral irradiance incident at the plane of the filters at any instant is constant over this plane. The spectral irradiance striking the detector surface, however, will be different for D1 and D2 because the filter characteristics are different. Remembering that the earth is "bluer" than the moon or the other planets, and assuming identical detectors, filters can be selected having spectral bandpasses such that the difference in detector outputs will always be positive for the earth and negative for the moon or the other planets. Thus a means of target discrimination by color is provided. In the coherent signal-processing system, a single positive pulse appears when the earth image sweeps across the FOV. The width of this pulse is a function of the height of the earth image as it sweeps across the trapezoidal reticle and is therefore a measure of the earth look angle. How this pulse is processed by the system electronics is described in detail in Section V.



OPTICAL SCHEMATIC
PULSE-WIDTH CONCEPT

FIGURE 22

In the non-coherent signal-processing system, the two detector outputs are fed to the two inputs of a differential pre-amplifier. As the target image sweeps across the split-rectangle FOV, the preamplifier output will appear as sketched below.



The relative width of the two pulses is a measure of aspect angle, with equal pulse widths indicating a null. The split-rectangle configuration is but one of a variety of shapes that can supply comparative pulse-width information to the non-coherent signal-processing electronics.

The pulse-width optical concept described above evolved from a number of similar concepts generated in the early part of the program. These concepts are described and evaluated in Appendix C.

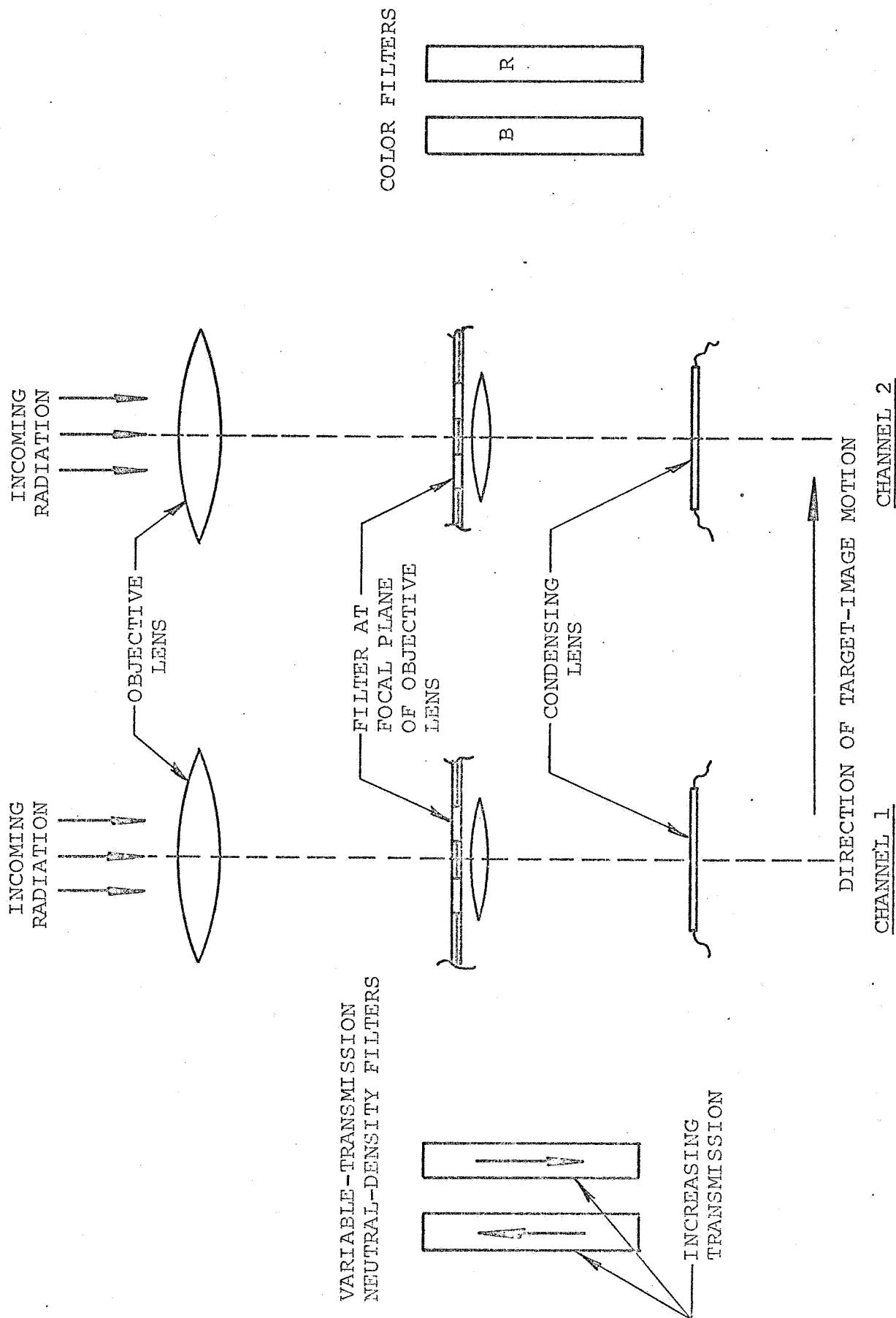
2. Pulse-Amplitude Concept

Another optical concept considered would obtain look-angle information by comparing the relative amplitude of the pulses rather than their width. It would probably be compatible only with a non-coherent type of signal processing.

For purposes of illustration, a two-channel version is described (see Figure 23), although with some additional complexity, a one-channel approach is feasible.

In channel 1, which senses the aspect angle, two neutral-density filters whose transmission values vary as a function of linear position are placed at the focal plane of the objective lens. One filter is placed so that its transmission versus spot position varies in the opposite sense as the other filter. The condensing lens serves to condense radiation passing through the filter onto the detector and also to image the objective lens on the detector. As the target image sweeps across the FOV, two sequential pulses are generated, and it can be seen that the relative amplitude of the two pulses is a function of aspect angle.

The arrangement in the color channel (channel 2) is almost identical, with two color filters (again "blue" and "red") replacing the neutral-density filters. In this channel, the relative pulse amplitude is a function of target color.



OPTICAL SCHEMATIC
PULSE-AMPLITUDE CONCEPT, TWO-CHANNEL VERSION

FIGURE 23

The system can be combined into one channel by using four filters in the focal plane, two color and two variable-transmission neutral density. However, since the filters must be separated to prevent image overlap at close distances from the target, the minimum angle of separation between the target and interfering targets is increased.

3. Direct-Digital Concept

An optical system based on the direct-digital concept would be very similar to that used on some digital sun sensors. A series of tracks carrying a coded mask is placed in the focal plane. As the target image passes over the masks, the presence or absence of a pulse from each track forms a digital word that indicates the vertical position at which the image crossed the mask.

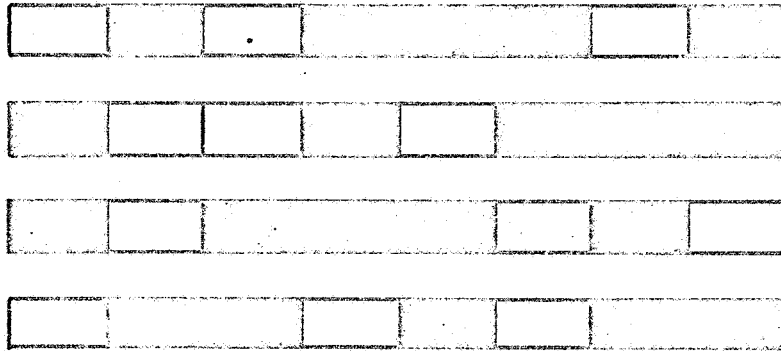
This type of system works well when the vehicle is far enough from the earth that the earth appears as a point source. However, when the vehicle is close and the earth subtends a significant angle, the output of the sensor becomes ambiguous. The ambiguity can be resolved by adding additional tracks to the basic mask, but the number of tracks required increases rapidly as the size of the earth to be sensed increases. Figure 24a is an example of a portion of such a mask that would provide unambiguous outputs with 1-degree resolution for earth diameters up to 2 degrees. More tracks would further extend the range of earth diameters that could be accommodated.

Another example of a coding mask that can be used in a direct-digital optical system is shown in Figure 24b. In this concept, the mask is arranged so that a target image crossing the mask from left to right will cross a varying number of bars depending on the vertical location of the image on the focal plane. The number of bars crossed determines the number of pulses produced. This pulse-counting system has the disadvantage of being unable to operate properly for large-diameter targets. Certain special sizes of the earth will produce a signal from the trailing edge that will cancel the signal from the leading edge; the result is no signal at all.

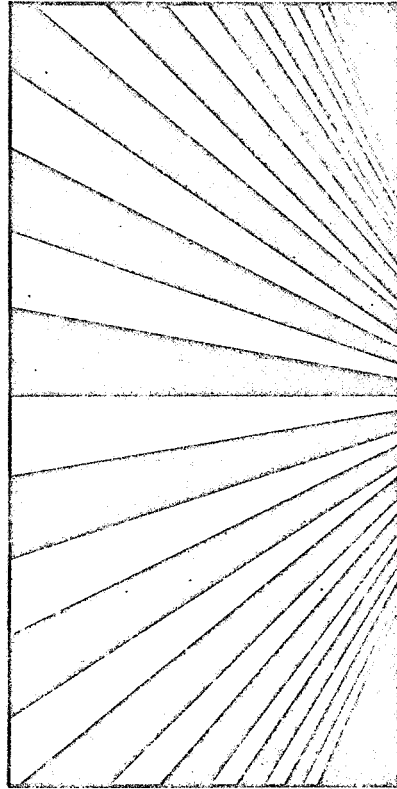
4. Star Sensor for Indirect Earth Aspect Sensing

The basic function of the earth aspect sensor is to provide a measurement of the angle between the vehicle spin axis and the ecliptic plane. This angle is indirectly sensed when the earth look angle is sensed, assuming that the vehicle is in the ecliptic plane. However, it is possible to sense the angle between the vehicle spin axis and the ecliptic plane by measuring star angles rather than earth angles. A method of sensing star angles was studied briefly during the EAS program. This method senses the star Canopus and measures the angle between the vehicle spin axis and the south ecliptic pole.

DIRECTION OF TARGET-IMAGE MOTION



a. Binary Coded Mask



b. Mask for Pulse-Counting System

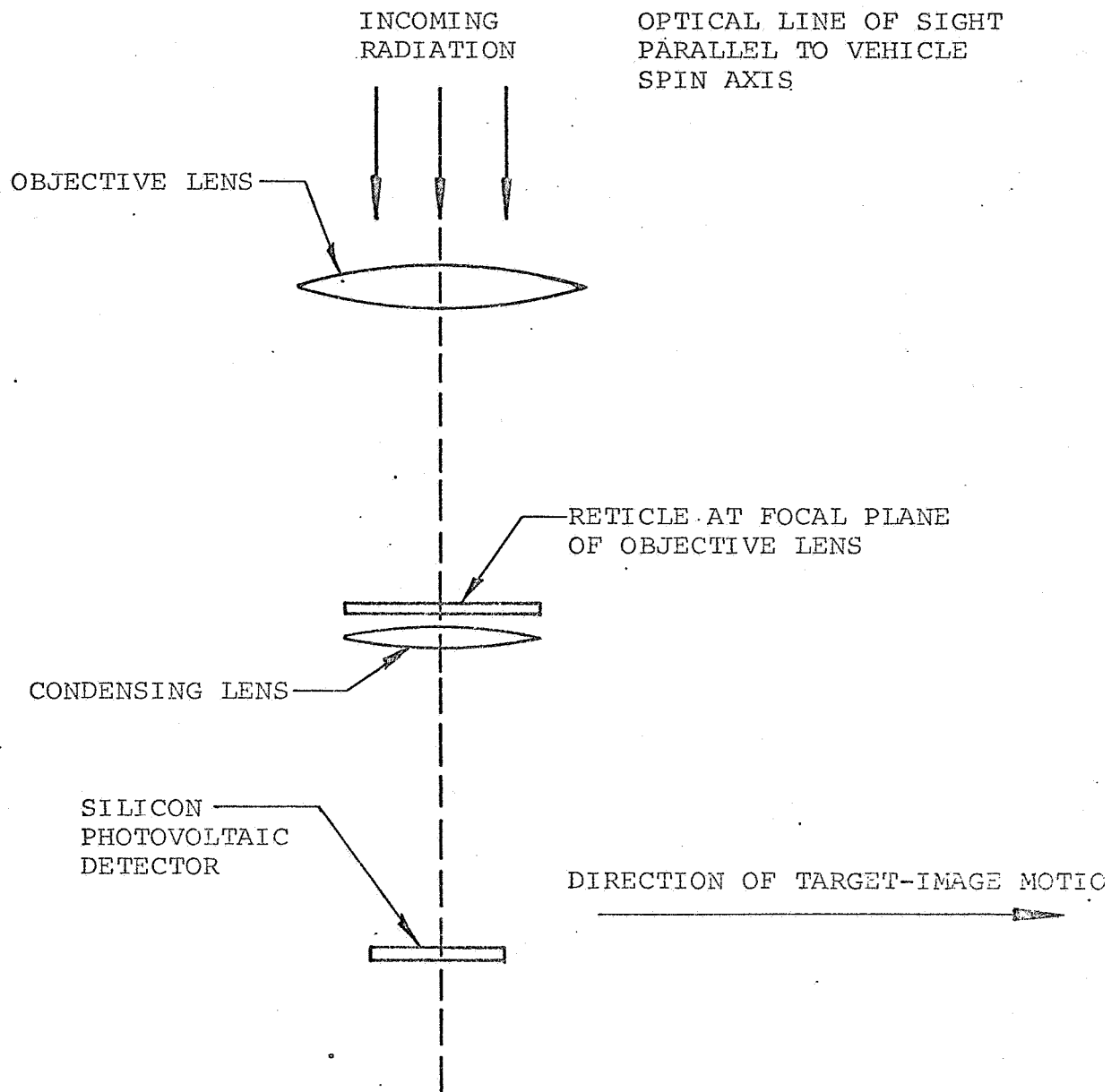
DIRECT-DIGITAL CONCEPT

FIGURE 24

The principle of operation can best be understood by referring to the optical and reticle schematics of Figures 25 and 26, which illustrate the Canopus tracking portion of the device. As indicated, the optical line of sight is parallel to the vehicle spin axis. When the vehicle is properly oriented, this telescope will sight in the direction of the south pole of the ecliptic, with the star Canopus approximately 14 degrees off axis. The reticle at the focal plane of the objective consists of a coded transmitting annular ring as indicated in Figure 26. As the vehicle spins, radiation from the Canopus image is modulated, as it passes through to the condensing lens, by the pattern of the reticle. The condensing lens images the objective lens on the surface of the detector. The reticle encoding would be such that information would be present in the signal on image phase about the spin axis with respect to a vehicle reference (pulse-width modulation), as well as on radial position of the image with respect to the spin axis (duty cycle). Various reticle patterns could be used.

Since Canopus is a bright star ($V = -0.72$), a reasonable aperture combined with a high-detectivity silicon photovoltaic detector should provide a satisfactory signal-to-noise ratio. Sensor outputs could be used to maintain the vehicle spin axis at 14 degrees from Canopus. One of the more attractive features of this device is that only a minimum of sun shielding will be required since Canopus will always be at least 75 degrees away from the sun. A brief discussion of sun shielding is presented in Appendix G.

Following is a brief description of the orientation of a spin-stabilized vehicle in an ecliptic-plane (or near-ecliptic-plane) mission and containing a sun sensor, an earth aspect sensor, and a Canopus sensor. First, the sun sensor will provide information to orient the vehicle spin axis perpendicular to the vehicle-sun line. Second, the vehicle will be caused to roll slowly about the vehicle-sun line while still maintaining spin about the nominal spin axis. As the spin axis becomes normal to the ecliptic plane, the earth aspect sensor will pick up the earth and the vehicle will be driven to null. At this point, the Canopus sensor should also be nulled. If not, the roll about the vehicle-sun line can be oscillated plus or minus several degrees until the Canopus sensor is nulled. With the vehicle oriented to null on the Canopus sensor, the vehicle can be maintained perpendicular to the ecliptic plane regardless of its position in the solar system. This type of aspect sensor will not be limited by phase angle or distance problems, as is the case with devices that sense the planets. However, if orientation is lost, acquisition of Canopus with only a sun sensor and the Canopus sensor is difficult for two reasons, as discussed below.

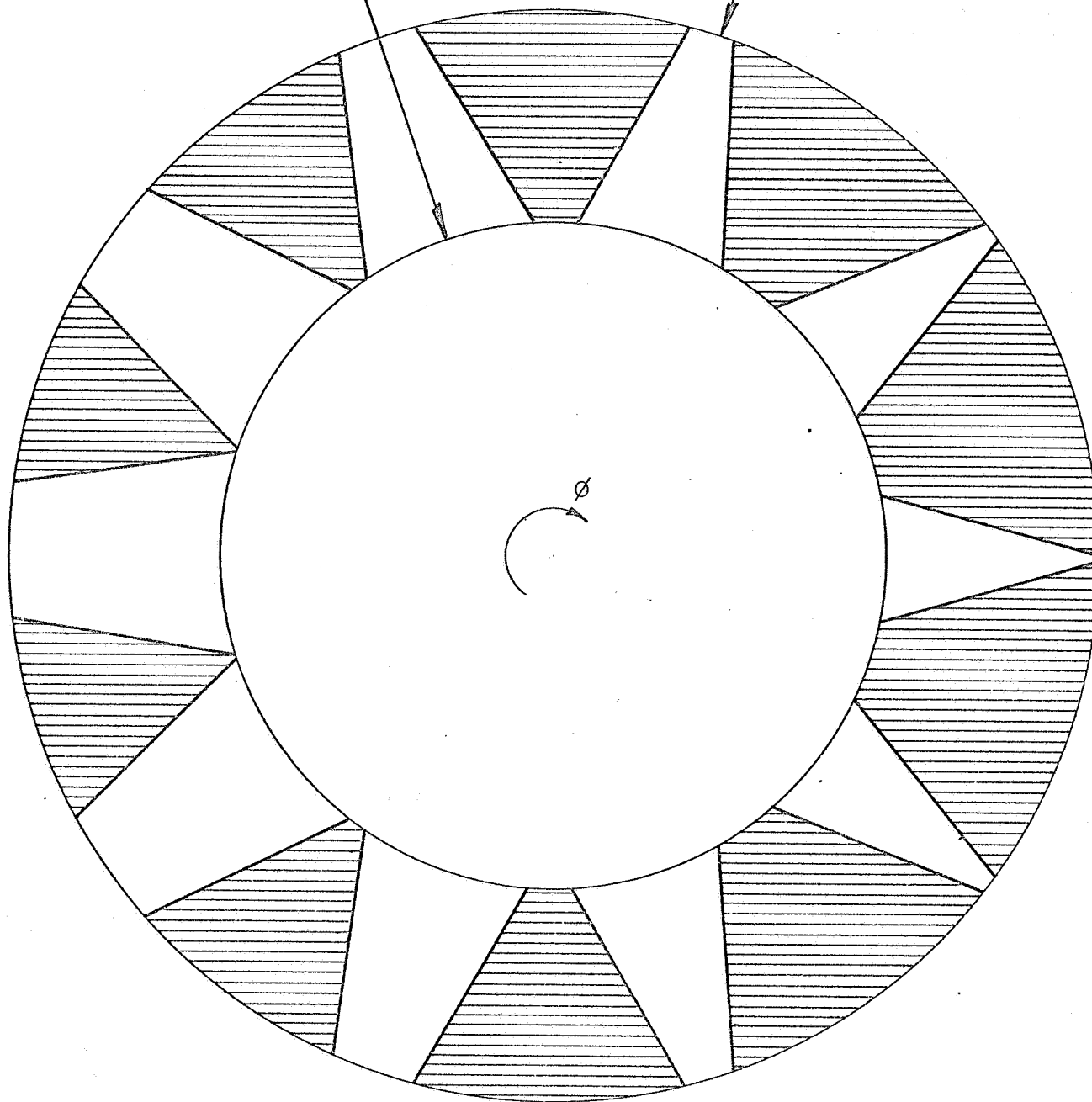


OPTICAL SCHEMATIC
CANOPUS TRACKER

FIGURE 25

INSIDE
OF RING
(Avg. duty
cycle = 80%)

OUTSIDE
OF RING
(Avg. duty
cycle = 20%)



NOTE: Schematic form only. Actual unit
would have ~100 cycles instead of 10.

RETICLE SCHEMATIC
CANOPUS TRACKER

FIGURE 26

First, there are two orientations in which the vehicle spin axis is perpendicular to the sun line and the Canopus sensor is nulled on Canopus. In only one of these orientations is the spin axis pointed at the south ecliptic pole. This difficulty can be overcome by observing the angle between the sun and Canopus, but considerable additional instrumentation would be required to make use of this information.

Second, after the sun is acquired and during the programmed rotation of the vehicle about the vehicle-sun line, other bright stars might move to a position 14 degrees from the spin axis (and hence from the Canopus-sensor optical line of sight). Unless the star sensor employs some type of discrimination technique (e.g., color discrimination), a star other than Canopus could be acquired. With the aid of the earth aspect sensor, however, the Canopus sensor can be driven to within a few degrees of Canopus, making acquisition easy. Hence, although the Canopus sensor range is unlimited for tracking Canopus, acquisition range is limited to those places in the ecliptic plane where the aspect sensor can sense the earth (or possibly another bright planet).

Both of these difficulties could be avoided by sensing one other bright star, for example, Sirius. Sirius ($V = -1.44$) is approximately 49 degrees from the south ecliptic pole. A Canopus-Sirius sensor could probably be combined in the same optical package. False acquisition would be avoided because simultaneous Canopus and Sirius signals would uniquely identify the south ecliptic pole.

No further effort was devoted to this concept since such effort was deemed to be outside the scope of the present contract.

5. Evaluation of Optical Concepts

As noted earlier, the various pulse-width optical concepts were evaluated (ref. Appendix C), and the version described in Section IV.A.1. above was selected as the best. This and the other three concepts described above were then compared and evaluated with a view to selecting the most suitable approach to implementing the EAS requirements. This evaluation effort is summarized in Table IX. As a result of this evaluation, the pulse-width system using color discrimination was selected for detailed design and fabrication. A further evaluation of this approach was also made; that is, the concept was compared and evaluated in four different versions, as is described in Section IV.B.

B. Signal-Processing Concepts

To establish a basic direction for the necessary signal-processing electronics, a decision had to be made between 1) complete aspect-angle and target-discrimination signal processing on board, and 2) telemetry of raw or incompletely processed data to ground

TABLE IX

COMPARISON OF OPTICAL CONCEPTS

Concept	Optical Complexity	Operating Range	Look Angle Proportional Range After Acquisition
1. Pulse Width	Relatively simple: One optical channel, radiation completely defocused on detectors, simple detector configuration.	Both approaches approximately equivalent in range when similar signal-processing techniques are used.	Can be made wide angle.
2. Pulse Amplitude	More complex than concept 1 in the one-channel version. Two-channel version would be no more complex than 1 but would increase system weight.		Can be made wide angle.
3. Direct-Digital	Coding-mask design becomes complex when earth diameters larger than $\frac{1}{2}^\circ$ must be accommodated.	Comparable to 1 and 2, but performance compromised at close approaches to earth without additional reticle complexity.	Probably less than ± 15 degrees.
4. Star Sensor * (Canopus-Sirius)	Non-conventional optics (e.g., light pipes) would be required to condense image of Sirius onto detector.	Unlimited. Unaffected by planetary phase. No interfering targets.	Of the order of 1 or 2 degrees. (Capable of very high accuracy.)

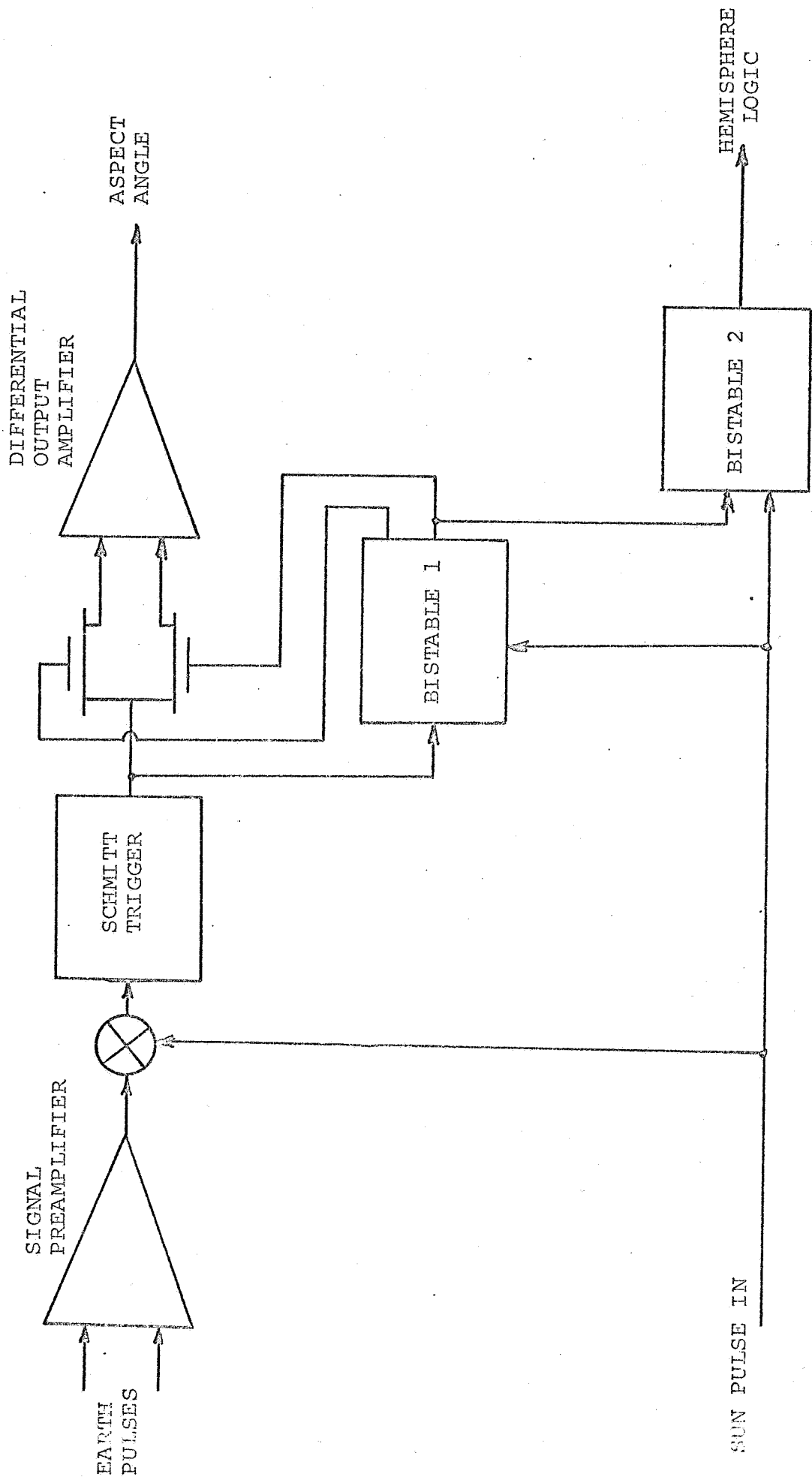
* Does not sense earth aspect angle directly.
Should be considered an ecliptic plane sensor.

stations. The communication and data-handling system of the Pioneer spacecraft (as a representative spin-stabilized, heliocentric orbiting, deep-space vehicle) was therefore investigated. The conclusion was that on-board signal processing was the more desirable approach. This decision was based on two major factors: 1) the relatively wide bandwidth required for transmission of the raw signals from the various optical concepts under consideration is not compatible with the A-D converter on Pioneer which provides six-bit resolution; 2) the commutation of the existing Pioneer telemetry system is not synchronized with the spin of the vehicle. The signal conditioning and storage required by these two factors would increase rather than decrease the complexity of the EAS over that required for on-board computation of aspect angle.

Electronic block diagrams were then generated for the various optical concepts; this work is summarized in Appendix D for reference. The following account traces the evolution of the electronic design that is described in detail in Section V, starting with the non-coherent signal-processing concept generated for use with the split-rectangle version of the pulse-width optical concept (ref. Section IV.A). As can be seen from the block diagram of Figure 27, the system is relatively simple in that only four functional blocks are required to compute aspect angle. This computation is accomplished by comparing the widths of the two consecutive pulses generated as the earth image sweeps across the split-rectangle reticle. The actual comparison is made by the differential output amplifier, in conjunction with the field effect transistor switches and bistable 1. The switches and bistable direct the first of the two pulses into the positive input of the output amplifier and the second pulse into the negative input. As a result, the filtered output from the amplifier is a dc level corresponding to the difference in pulse width and is therefore an analog indication of aspect angle.

The purpose of the Schmitt trigger is to provide the final step in the target-discrimination process. As was pointed out in Section IV.A., filters can be selected so that the blue-minus-red signal is positive for the earth and negative for the moon or other planets. The Schmitt, since it triggers only on positive signal-preamplifier outputs, prevents the negative signals from reaching the comparison circuits. The Schmitt also performs the important secondary function of providing constant-amplitude pulses to the comparison circuits. If this were not done, the output from the output amplifier would be a function of signal strength as well as pulse-width difference.

Hemisphere determination is derived by indirectly measuring the time between the sun and earth pulses for a particular pulse sequence. This function is performed by bistable 2.



NON-COHERENT SIGNAL PROCESSING FOR
SPLIT-RECTANGLE PULSE-WIDTH OPTICS

FIGURE 27

The sun input also insures that bistable 1 is always in the proper state in the event that it should be falsely triggered by noise or should fail to trigger on one of the negative Schmitt transitions. In addition, the sun input gates out the signal-preamplifier output when the sun is in the FOV.

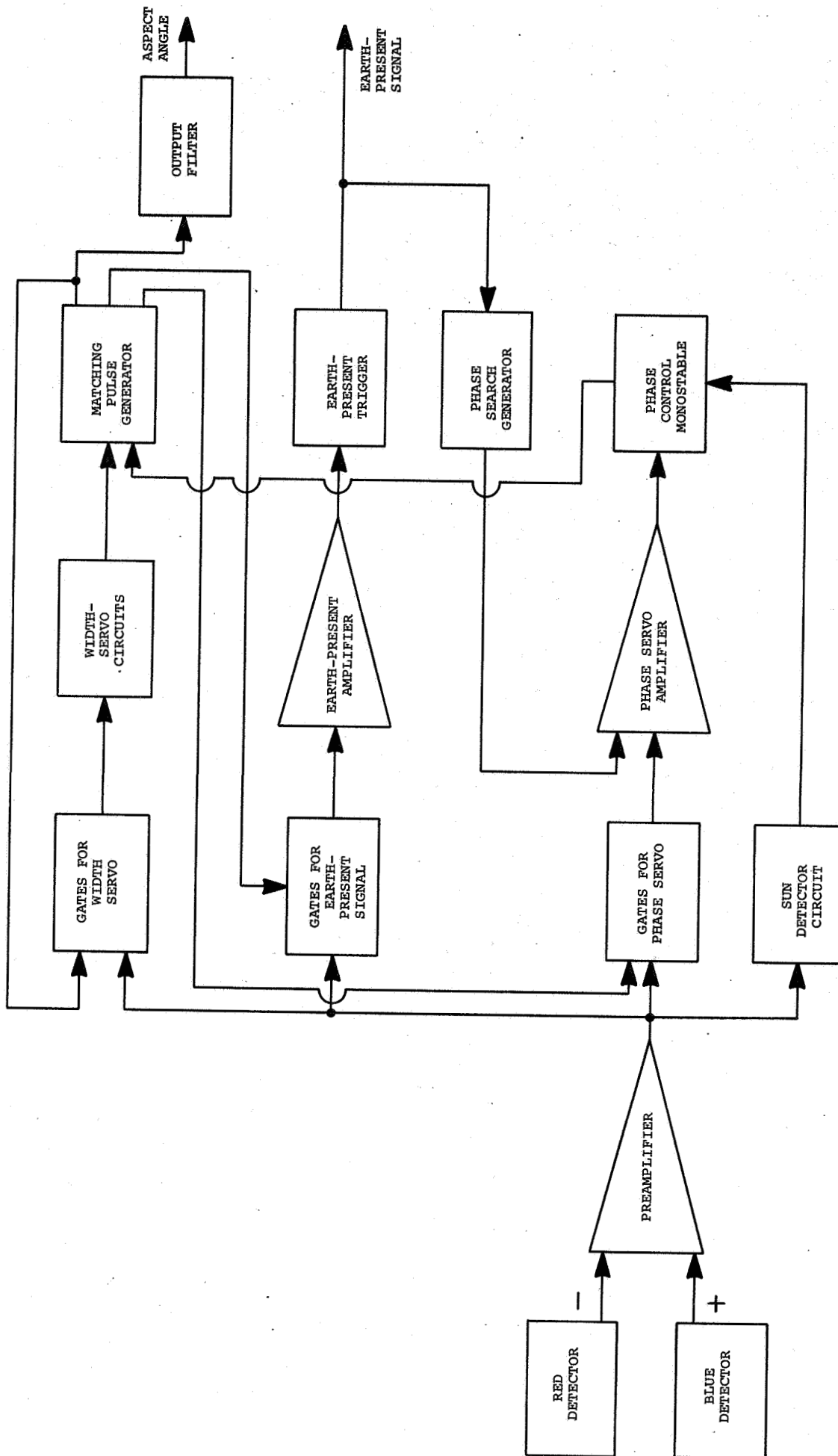
Simultaneously with conception of the non-coherent signal-processing system just described, a coherent system for use with the trapezoidal-reticle optical concept was also worked out (see Figure 28). Although considerably more complex than the non-coherent system, the coherent system has the advantage of being able to operate at a substantially greater distance from the earth than the non-coherent system, basically because the noise bandwidth in the coherent system is not determined by the signal-preamplifier bandwidth as with the non-coherent system. Instead, when the coherent system is "locked on" the earth pulse, the noise bandwidth is a function only of the closed-loop servo bandwidth. This servo bandwidth can be as narrow as the expected tilt rates will allow. The narrow-bandwidth system can perform satisfactorily, even though the earth signal is below the noise level in the wideband-preamplifier output.

Briefly, the operation of the coherent system is as follows. After the system has locked on the earth pulse, signals from the red and blue detectors are matched, in both width and phase, by means of a spin-coherent electronic signal-processing system. The matching is accomplished with two servo loops, one controlling time of pulse occurrence and the other duration of the pulses. A third channel provides an earth-present indication. Hemisphere determination can be derived by indirectly measuring the time between the sun and earth pulses for a particular sequence. This function would be performed by the phase control monostable.

Both of the signal-processing concepts described above were planned for use with solid-state silicon detectors. Either could be adapted for use with a bi-cell photomultiplier-tube detector by addition of circuitry to provide alternate sampling of the two photomultiplier sections. Also, the preamplifier for use with a photomultiplier would be somewhat different in that less gain would be needed because the tube itself amplifies the signal considerably. In any event, use of the photomultiplier tube would increase the complexity of the electronics.

At this point in the program, a decision was made, at a joint meeting of NASA/Ames Research Center and Quantic Industries (January 1966), to subject the following concepts to more detailed study and analysis:

- 1) Optics: Split-rectangle reticle and trapezoidal reticle.
- 2) Electronics: Non-coherent and coherent signal processing.
- 3) Detectors: Solid-state detector and photomultiplier tube.
- 4) Field of View: Narrow and wide.



COHERENT SIGNAL PROCESSING FOR
TRAPEZOIDAL PULSE-WIDTH OPTICS

FIGURE 28

A detailed evaluation of the two types of detectors is presented in Section III.C. Signal-to-noise calculations and operating-range predictions were made for four possible combinations: coherent signal processing (trapezoidal reticle) with solid-state detector, coherent signal processing (trapezoidal reticle) with photomultiplier tube, non-coherent signal processing (split-rectangle reticle) with solid-state detectors, and non-coherent signal processing (split-rectangle reticle) with photomultiplier tube. Details of this work are presented in Appendix E. (In each case, narrow-FOV optics were used. Wide-angle optics are discussed below.)

The results of the evaluation of these four systems are summarized qualitatively in Table X, where other parameters that must be considered are also rated comparatively. As can be seen, no one of the four versions would be superior to the others for all missions. For example, if long range is of paramount importance, a system using a photomultiplier tube should be used. On the other hand, if the required range is limited, a version using a solid-state detector could meet operating requirements without the additional weight, size, and high-voltage requirements of the photomultiplier-tube versions.

Since the EAS program was not confined to a specific mission, selection of the approach for detailed design and fabrication was made at a joint meeting between NASA/Ames and Quantic (May 1966). It was decided at this meeting to proceed with design of a non-coherent signal-processing system with solid-state detectors and a wide-angle FOV (>50 degrees in the direction perpendicular to direction of target motion). It had already been determined, however, that the optical configuration selected earlier would not be suitable for wide-angle FOV applications. Some optical modifications were suggested (see Appendix F for details), but their general complexity led NASA/Ames to redirect the effort toward design of a narrow-angle FOV optical system. This redirection included the decision to proceed with a spin-coherent electronic system for use with solid-state detectors* (and correspondingly the optical system with trapezoidal reticle).

The basic consideration leading to this decision was that, for greatest utility, an EAS of the type being studied should be capable of operation at distances of at least $1/2$ AU from the earth (5×10^7 n.mi.).

* Before the redirection of effort, two basic amplifier configurations were evaluated to determine which one would give the best noise performance for different values of detector shunt capacitance. In the signal-processing electronics, initial design and breadboarding of the Schmitt trigger, bistable multivibrator, and output amplifier were completed. In addition, a test generator to supply simulated, variable-width earth pulses to the Schmitt trigger was built and tested.

TABLE X

COMPARATIVE RATING OF DIFFERENT VERSIONS OF A PULSE-WIDTH OPTICAL APPROACH USING COLOR DISCRIMINATION

Note: Numbers 1, 2, 3, and 4 rate the systems, with 1 being the best.

Version	S/N	Operating Range*	Degree of Electronic Complexity	Power Consumption	Degree of Optical Complexity	Wt.	Remarks
a) Coherent Signal Processing, Solid-State Detector	3	3	3	2	All approaches approximately equivalent.	2	
b) Coherent Signal Processing, Photomultiplier Tube	1	1	4	4		4	Sun shutter or bias cut-off required.
c) Non-coherent Signal Processing, Solid-State Detector	4	4	1	1		1	
d) Non-coherent Signal Processing, Photomultiplier Tube	2	2	2	3		3	Sun shutter or bias cut-off required.

* For equal apertures.

At these great distances, a photomultiplier detector is normally used in order to provide high signal-to-noise ratios when viewing the dim earth. However, as already discussed in Section III.C. a photomultiplier was considered unsuitable for several reasons. To recapitulate: First, most of the applications of the EAS will be on vehicles operating in the ecliptic plane; hence, the sun will pass through the sensor FOV once each revolution of the vehicle. Since typical vehicle spin rates were expected to range from 1 to 4 rps, the sensor would be subjected to many thousands of sun pulses during its lifetime. Continual high-intensity pulses will cause deterioration in photomultiplier sensitivity. Although a mechanical shutter could be provided, the thousands of operations required of such a shutter would pose a reliability hazard in space. (See Appendix G for a discussion of sun shielding.) A second reason the photomultiplier is unsuitable is that this device, with its associated high-voltage power supply, is relatively bulky and heavy. Finally, it was believed that reliability for a long period in orbit would be higher with a solid-state detector since it requires no high voltages.

Selection of the solid-state detector led directly to selection of spin-coherent electronics. The detectivity of a solid-state detector is only a fraction of the detectivity of a photomultiplier. The resulting low signal-to-noise ratio requires a very long averaging time at the instrument output if usable measurements are to be achieved at great ranges. However, the coherent signal-processing system could provide a much better signal-to-noise ratio than the non-coherent system and, at the stage then developed, was capable of operation with signals simulating a range of 10×10^6 n.mi. compared to 5×10^6 for the non-coherent system. The range limit of 10×10^6 n.mi., however, was still short of the 5×10^7 system goal.* The design effort revealed that the limiting effect as far as long-range operation and specified system accuracy are concerned was not noise, but rather unavoidable dc offsets at the integrating-amplifier inputs. Investigations into possible methods of circumventing the offset problem led to design of the system described in Section V. This system uses digital rather than analog integration circuitry and as a result is far less sensitive to dc offsets.

* The operating range of 5×10^6 n.mi. would be adequate for the orientation requirements of the Pioneer series spacecraft; however, since the orientation procedure used on the Pioneer mission performed satisfactorily, the EAS development effort was re-directed toward a sensor system of greater range and capability.

V. EAS DETAILED DESIGN

A. Optics

The following description of the EAS optics applies to the optical head that was fabricated and assembled under Contract NAS2-3281. The one piece of checkout equipment needed to evaluate the optical head is described in Section VI.

1. System Operation

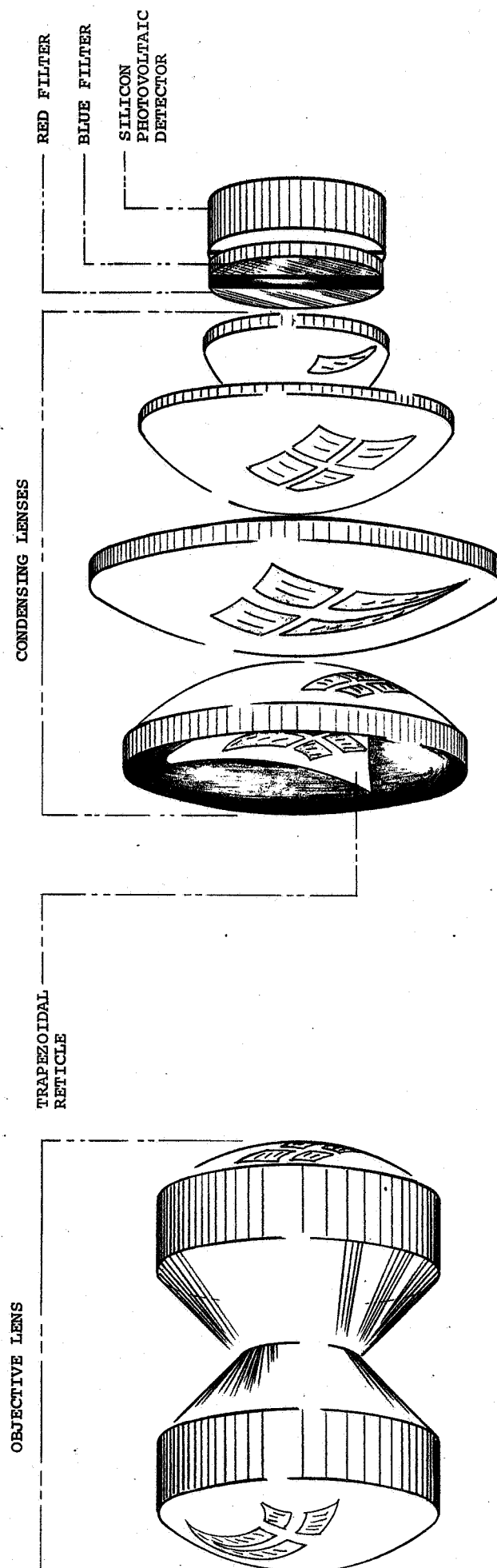
The principle of operation (discussed in some detail in Section IV.A) is re-stated briefly here. An optical schematic is shown in Figure 29. The objective lens images the earth onto a trapezoidal-shaped reticle. A condensing-lens system behind the reticle forms an image of the objective-lens aperture stop onto a circular, silicon photovoltaic detector. The detector is split along its diameter, and separate outputs are available from each half. One half of the detector is covered with a red filter, while the other half is covered with a blue filter. The condensing lens insures complete defocusing of the earth image so that light from the earth will be spread equally over both the red and blue halves of the detector.

The earth-aspect angle is measured as follows. The sensor is mounted on the vehicle with the optical axis perpendicular to the vehicle spin axis. As the vehicle spins, images of the stars, the earth, and other planets pass across the trapezoidal reticle, producing approximately square output pulses from the two detector halves. The width of these pulses is a measure of the angle between the vehicle spin axis and the line of sight to the targets. When the earth passes the FOV, the earth-pulse width is proportional to the earth-aspect angle to be measured.

The system is prevented from locking on a target other than the earth by incorporation in the optics of the means of color discrimination (the red and blue filters) mentioned above. The color discrimination is implemented by operating the electronic servos from the difference between the outputs of the blue and red detectors. The spectral bandpasses of the filters are selected such that the output from the blue detector half is larger than the output from the red detector half only for the earth. For the moon or other planets, the difference is of opposite polarity.

2. Packaging

The packaged optical head is shown in Figure 30. It is approximately 4.4 inches in length by 2 inches in maximum diameter and weighs approximately 0.8 pound. The head includes the objective lens, the condensing lenses with focal-plane reticle, the filters, the bi-cell detector, and the sun sensor. The sun sensor is the small projection mounted at the forward end of the telescope (near the objective lens). The housing is of black anodized Al 7075-T6.



EAS OPTICAL SCHEMATIC

FIGURE 29



EAS OPTICAL HEAD

FIGURE 30

3. Objective Lens

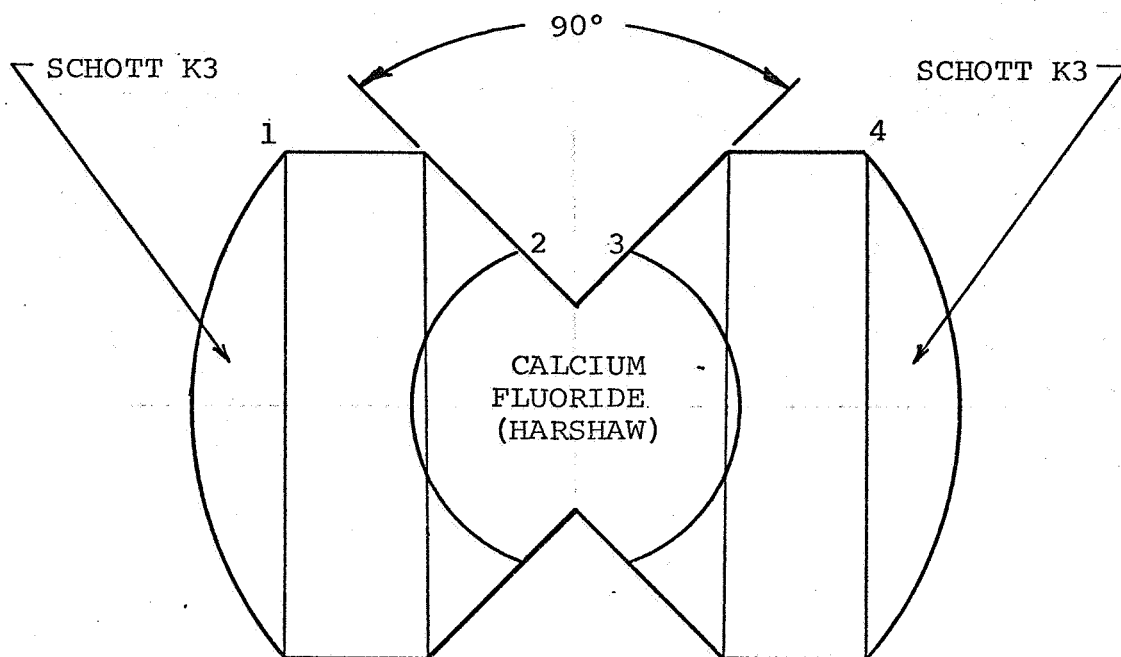
The objective lens is a concentric triplett (see Figure 31 for prescription). The lens was designed with the following criteria imposed:

- a) Aperture Diameter 0.75 in.
- b) Optical Bandpass 0.3 to 1.0 μ
- c) Focal Length Pertinent only to the extent the weight of the objective lens itself and the weight of the condensing lenses would be affected.
- d) Field 36 deg
- e) Resolution Point-source resolution
 <0.5 deg over entire field.

Since there was no requirement for a flat image surface (because it was found that the reticle could be deposited on a spherical surface), a concentric lens approach appeared suitable.

Ray-trace data for the objective lens are tabulated below for three wavelengths encompassing the optical bandpass. It should be noted that item g) gives the angular size of the disk of confusion for the three wavelengths. Since a concentric lens can have no lateral chromatic aberration, the blur circles at each of these wavelengths exactly superimpose and the over-all blur circle over the entire optical bandpass will be well within the 0.5-degree maximum. Also, since a concentric lens exhibits no extra-axial aberrations (i.e., no coma or astigmatism), the magnitude of the blur will be constant over the FOV.

	Wavelength		
	(u)		
	0.3650	0.5461	1.014
a) Effective focal length, in.	1.9999	1.9999	1.9999
b) Paraxial back focal length, in.	0.999	0.999	0.999
c) Marginal back focal length, in.	1.056	1.047	1.040
d) Spherical aberration, in.	-0.057	-0.048	-0.041
e) Diameter of disk of confusion, in.	0.00538	0.00447	0.00383
f) Distance of disk of confusion from aperture stop, in.	2.043	2.036	2.031
g) Angle subtended by disk of confusion at aperture stop, deg	0.15	0.13	0.11



PRESCRIPTION

			<u>Diameters</u>
r_1	1.001"	K3	1.300"
d_1	0.575"		
r_2	0.426"	CaF ₂	*
d_2	0.853"		
r_3	-0.426"	K3	1.300"
d_3	0.575"		
r_4	-1.001"		

* Since this is a notched sphere, the diameter is dependent simply on the radius and its tolerance.

OBJECTIVE LENS

FIGURE 31

4. Reticle

As mentioned above, the reticle is deposited on the first surface of the condensing-lens system, which is concave with a radius of curvature of 2.055 inches. This surface also corresponds to the focal surface of the concentric objective lens. The specification for the reticle pattern is shown in Figure 32.

The shape of the reticle has a significant effect on system operation. As can be seen in Figure 32, the scale factor (pulse width versus look angle) is a function of the slope of the two sides of the trapezoid. However, this scale factor can be increased only at the expense of bandwidth. The actual trapezoid size and shape were dictated by system size and optical considerations. The trapezoid height was chosen to allow for aspect sensing over a ± 15 degree range. The top of the trapezoid provides for a pulse width equivalent to 4 degrees of vehicle spin phase, which is about the lower practical limit of pulse width that can be processed to indicate aspect angle. The trapezoid base was made as large as possible without increasing the maximum off-axis field angle beyond 18 degrees. A wider base would have imposed a requirement for more or larger condensing-lens elements.

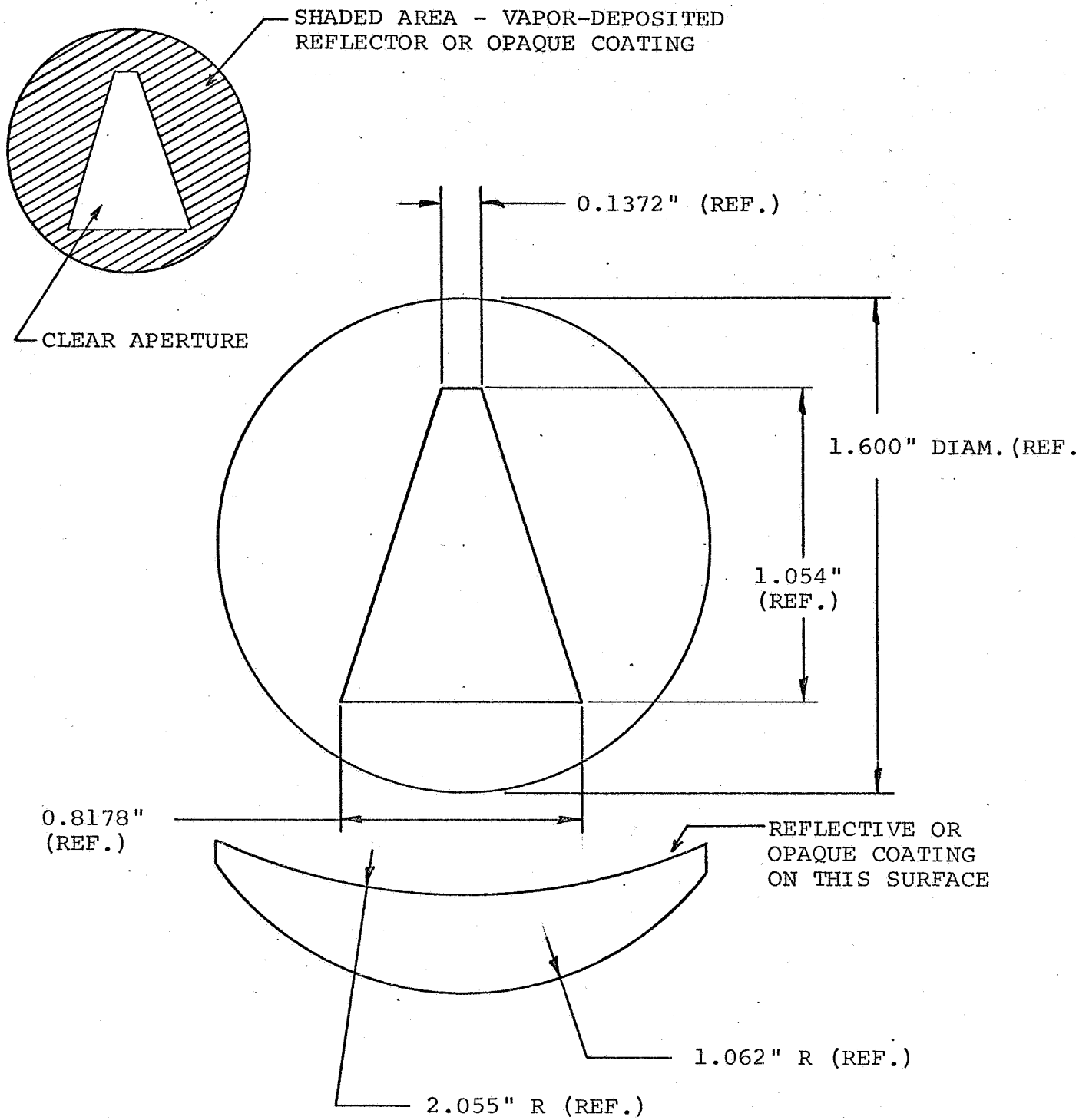
5. Condensing Lenses

The function of the condensing lenses is to image the objective-lens aperture stop onto the detector surface. Since higher detectivities and faster time constants can be achieved as detector size is reduced, this image should be as small as possible. The condensing-lens prescription is shown in Figure 33. As indicated, all four elements are made of fused silica. This lens system, with its first surface located at the focal surface of the objective lens, forms a 0.274-inch-diameter image of the 0.75-inch-diameter aperture approximately 0.25 inch from the rear surface of the last element.

6. Filters

Selection of the red and blue color-discrimination filters was one of the more critical problems encountered in the EAS design. The filters must be chosen such that the following two conditions are met:

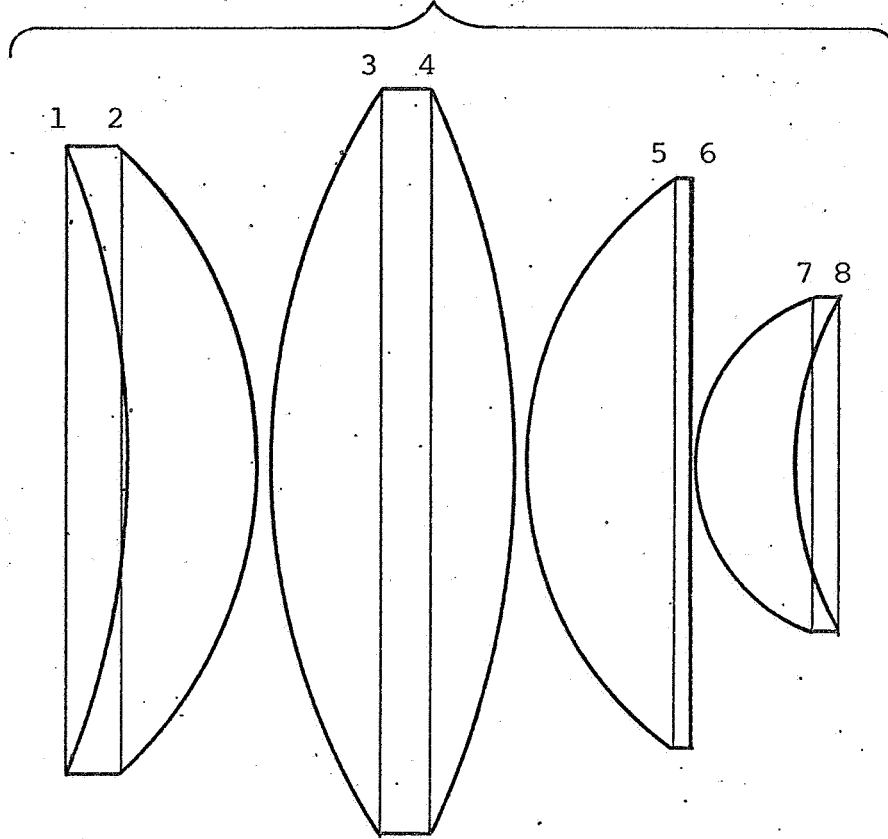
- a) $S_b - S_r \leq 0$ when viewing the moon or those planets that might be within detection range of the EAS.
- b) $S_b - S_r > 0$ when viewing the earth, and as large as possible without violating the constraints imposed by requirement a).



RETICLE

FIGURE 32

OPTICAL-GRADE SILICA



PRESCRIPTION

				<u>Diameters</u>
r_1	- 2.036"	}	Silica	1.600"
d_1	0.330"			
r_2	- 1.062"	}	(Air)	
d_2	0.020"			
r_3	1.719"	}	Silica	1.900"
d_3	0.650"			
r_4	- 2.149"	}	(Air)	
d_4	0.020"			
r_5	0.888"	}	Silica	1.450"
d_5	0.400"			
r_6	17.096"	}	(Air)	
d_6	0.020"			
r_7	0.457"	}	Silica	0.900"
d_7	0.250"			
r_8	0.851"	}		

CONDENSING LENSES

Here, S_b = signal developed by the half of the detector beneath the blue filter, and

S_r = signal developed by the half of the detector beneath the red filter.

The following five-step plan was outlined for selection of the filters:

a) Calculate and plot the relative response of the silicon detector to the earth, the moon, and the other planets as a function of wavelength, using the planetary color data presented in Section III.B, Table III.

b) Find the wavelength (λ_c) that will divide the area under each response curve (except that of the earth) into two equal areas. This step locates the cut-off and cut-on wavelengths for ideal blue and red filters, respectively, that will result in $S_b - S_r = 0$ for each target (condition a above). (The term "ideal" is interpreted to mean that the filter has 100% transmission within its optical bandpass and a step function cut-off or cut-on with zero-degree transmission outside the bandpass.)

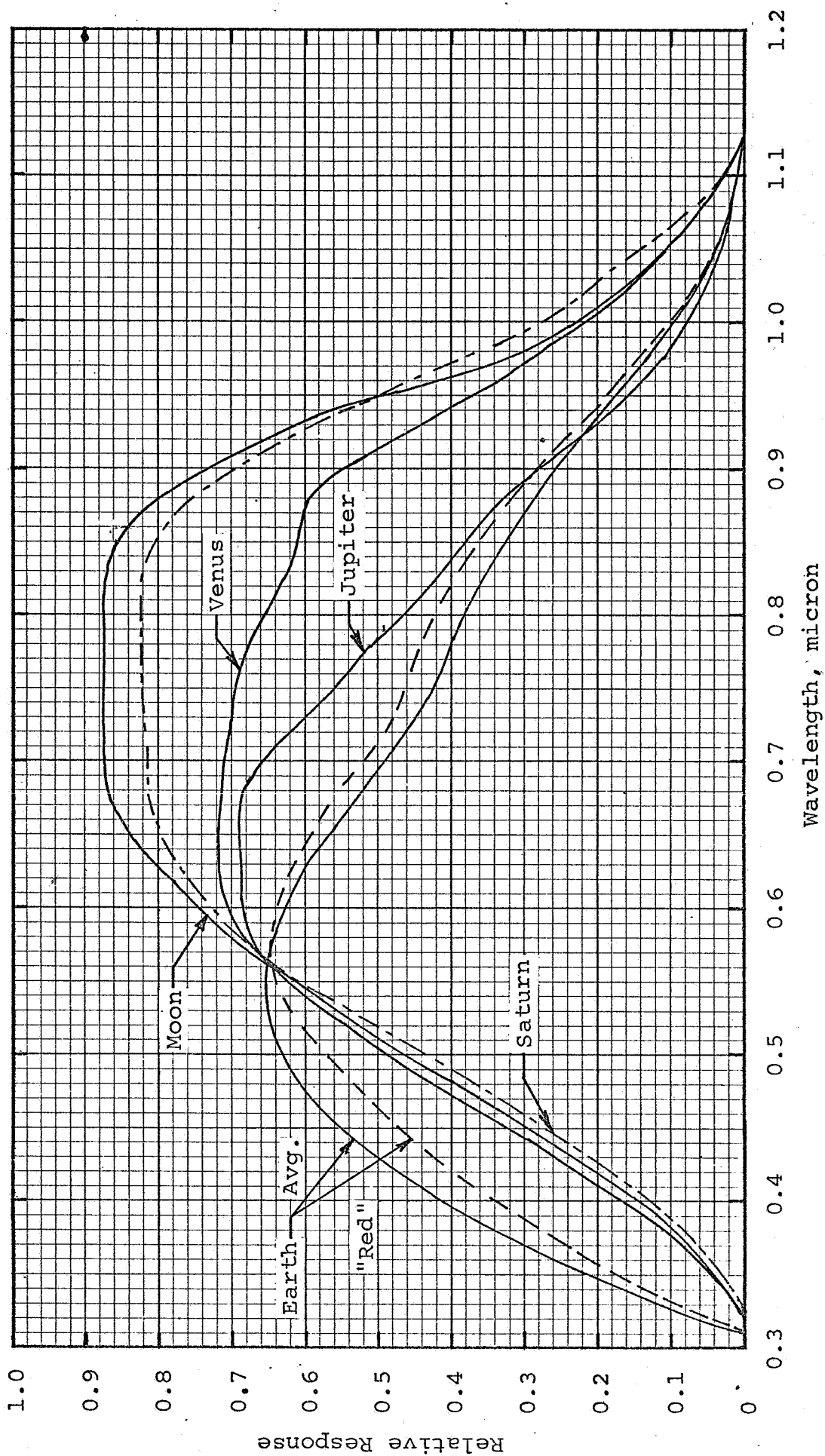
c) Shift the values of λ_c to the left (to slightly shorter wavelengths) to allow for a safety factor and thus provide for a slightly negative $S_b - S_r$ level.

d) Select the smallest value of λ_c , ignoring the curves for the targets that would be definitely out of range for a specific mission.

e) Select filters having characteristics as close as possible to those of the ideal filters (or have such filters designed and custom fabricated).

f) Use the smallest value of λ_c , in conjunction with the spectral-response curve of the earth (from Figure 34) to determine the magnitude of $S_b - S_r$ when viewing the earth (condition b above).

The above steps were taken (see Figure 34 for the spectral-response curves resulting from step a), and the ideal filters as determined by the smallest value of λ_c were specified. The original plan was to procure a series of cut-on and cut-off filters with an incremental series of cut-on and cut-off wavelengths. However, although cut-on filters of this type are readily available,



RELATIVE RESPONSE OF SILICON DETECTOR TO VARIOUS TARGETS

FIGURE 34

such cut-off filters are not. Obtaining a satisfactory set would have required a design effort as well as custom fabrication. For schedule and budget reasons, it was decided to purchase the series of cut-on filters but not to proceed with procurement of cut-off filter design and fabrication. Instead, the above approach was varied to use a red cut-on filter over the one detector half and to leave the other detector half unfiltered. An arrangement was to be provided to electrically attenuate the unfiltered detector half. Thus, by viewing actual planets and artificial targets, it would be possible to obtain the information necessary to specify a blue cut-off filter for a specific mission. However, the program ended before these tests could be conducted.

7. Detector

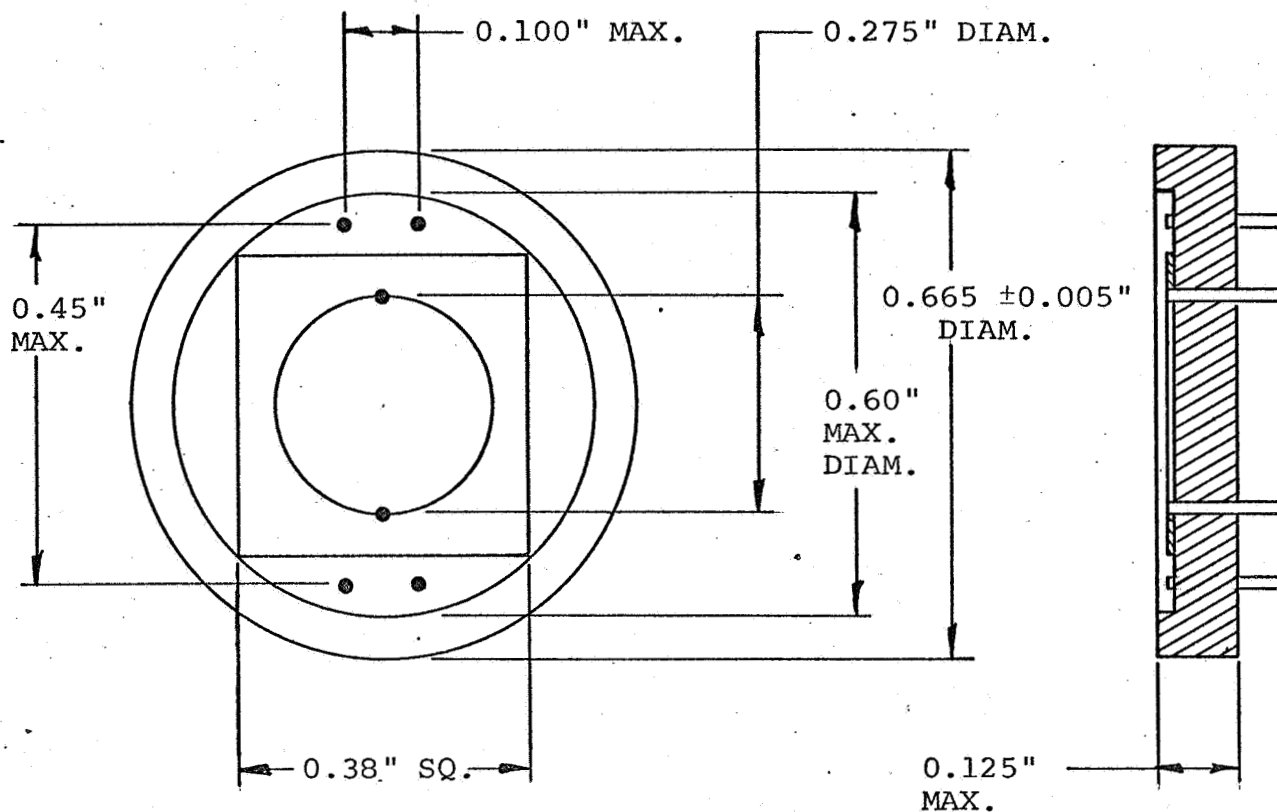
The detector is a silicon photovoltaic quadrant-cell unit. Detailed specifications are given in Figure 35. The unit is basically the Electro-Nuclear Laboratories detector model 640B in a special housing, with slightly modified electrical requirements. In use, two pairs of adjacent quadrants were connected in parallel to convert the detector into a bi-cell unit. The only reason for procuring the quadrant-cell unit was its availability as a stock item, which is not the case with bi-cell units.

8. Sun Sensor

As described in Section V.B, the purpose of the sun sensor is to provide the main timing pulse for monostable 1, which is triggered by delay of the solar pulse.

The sun sensor consists of a rectangular aperture that serves as a shadow caster to define a rectangular FOV and a silicon phototransistor with a small sensitive area as the detector. The specific detector used is a Siliconex phototransistor with the lens cap removed.

The rectangular FOV is $32^{\circ} \times 26^{\circ}$ and coincides with the EAS field of view, as shown in Figure 36, which also indicates some other pertinent dimensions.



Sensitive area: 0.7 cm diameter, consisting of four quadrants

Separation between quadrants: 0.005 in.

Wavelength of peak response (λ_p): $< 0.8 \mu$

(It is desired to shift the detector response to as short a wavelength as possible without compromising other performance characteristics.)

Dark impedance per quadrant: $< 1 M\Omega$

Capacitance per quadrant: $< 800 \text{ pF}$

Responsivity per quadrant: $\geq 0.4 \text{ A/W}$

$D^*(\lambda_p, 270, 1)$ per quadrant: $10^{12} \text{ cm-cps}^{1/2}/\text{W}$ at λ_p

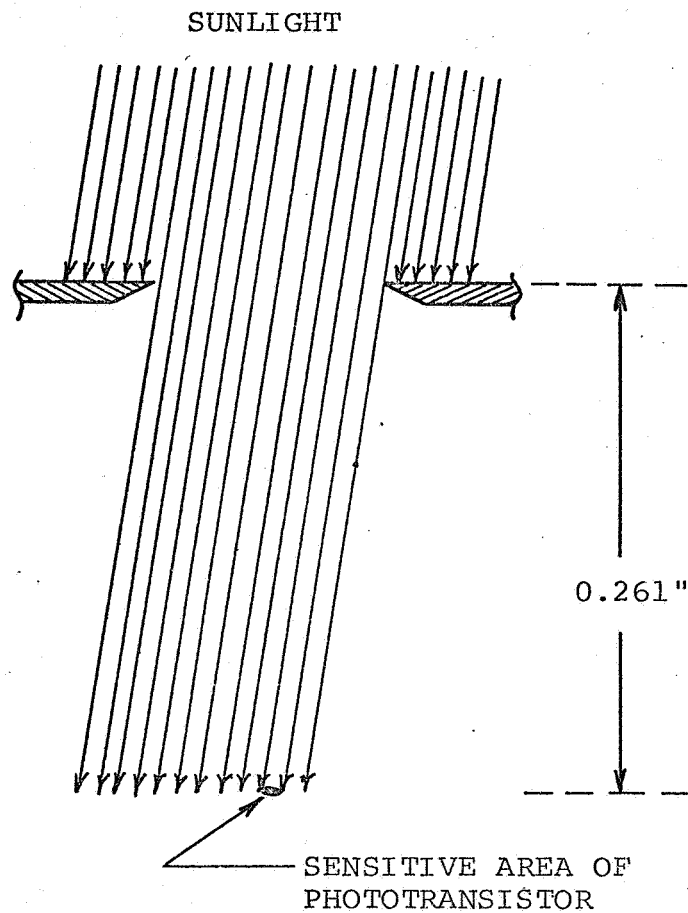
Matching between quadrants: 5% or better

SILICON PHOTOVOLTAIC DETECTOR

FIGURE 35

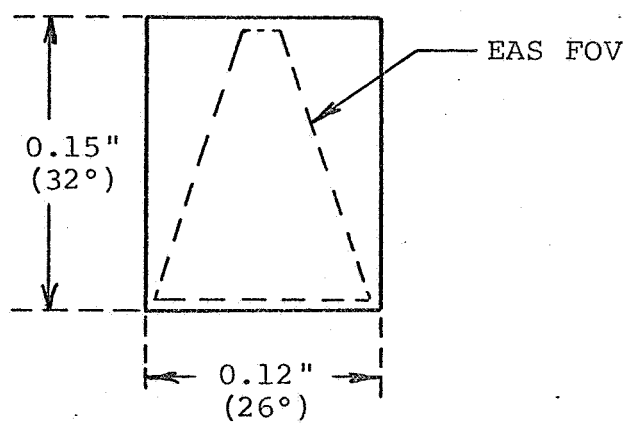
a. Schematic

Scale: 10×



b. Field of View

Scale: 10×



c. Actual Size



SUN SENSOR

FIGURE 36

B. Electronics

The following description of the EAS electronics applies to the final breadboard system that was assembled and partially tested under Contract NAS2-3281. The breadboarding and testing phase is discussed in Section VI. The operation of the system is described first, followed by derivations of the servo error signal and the servo transfer function. The concluding section describes the digital integrator used to achieve the desired transfer function.

1. System Operation

After earth acquisition (i.e., system locked on earth pulse), pulses generated locally are matched, in both width and phase (or position), to the weak earth pulses from the signal preamplifier by means of two all-electronic servo loops. The first loop, called the phase (or position) servo, controls the time (measured from sun passage) at which the locally generated pulses occur. The second loop, called the width servo, controls the duration of the locally generated pulses. A third channel provides an earth-present (i.e., track-check) indication. Hemisphere-determination logic can be obtained readily just by looking at the output of monostable 1, since its duty cycle is a direct indication of the angular separation between sun and earth for a given sun-earth pulse sequence.

With this kind of processing, the effective system time constant is equal to the time constant of the various servo loops involved. The digital integration techniques used permit time constants of almost any desired length. To clarify how the acquisition and pulse matching are accomplished, reference is made to the sequence of events listed below, the block diagram (Figure 37a), the schematic (Figure 37b), and the waveforms at key points in the system (Figures 38, 39, and 40). Figure 38 shows the waveforms before the system has locked on the earth pulse; Figure 39 shows the waveforms after the system has locked on the earth pulse in phase; Figure 40 shows the waveforms after the system has servoed on the pulse width. The conditions listed below prevail, whether the system is tracking or not.

- a) Monostable 1 is turned on by the negative transition of the sun pulse.
- b) Monostables 2, 3, 4, and 5 are turned on by the positive transition of the preceding monostable output.
- c) The on-time of monostable 1 is controlled by the output from amplifier A9.
- d) The on-time of monostables 2, 3, 4, and 5 is controlled by the output from amplifier A4.
- e) The on-time of monostables 2 and 5 are a few milliseconds longer than the on-times of monostables 3 and 4.

Sequence of Events

First Vehicle Revolution (immediately after sensor power is and before earth acquisition - ref. Figure 38)

- t_1 : Negative sun-pulse transition occurs; monostable 1 output goes negative.
- t_2 : Monostable 1 output goes positive (voltage from A9 is such that positive transition occurs 10 degrees from negative sun-pulse transition); monostable 2 output goes negative.
- t_3 : Monostable 2 output goes positive (voltage from A4 is such that on-time is at its minimum value); monostable 3 output goes negative.
- t_4 : Monostable 3 output goes positive; monostable 4 output goes negative.
- t_5 : Monostable 4 output goes positive; monostable 5 output goes negative.
- t_6 : Monostable 5 output goes positive.

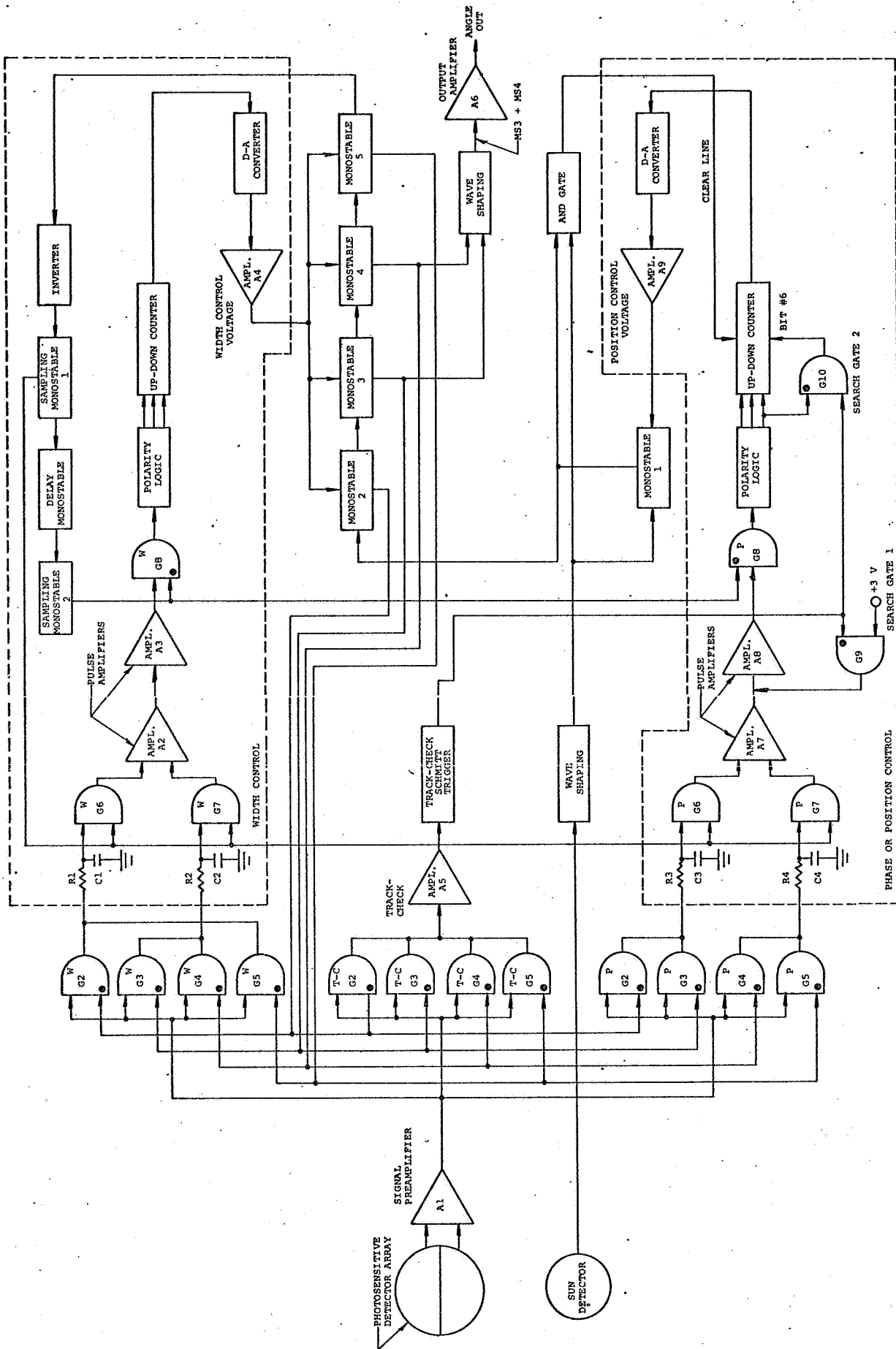
Second Vehicle Revolution

Same as first revolution, except that voltage from A9 is now such that the on-time of monostable 1 has increased slightly (on-time corresponds to a change of 0.2 degree in location of the negative transition relative to the sun pulse).

Third Vehicle Revolution

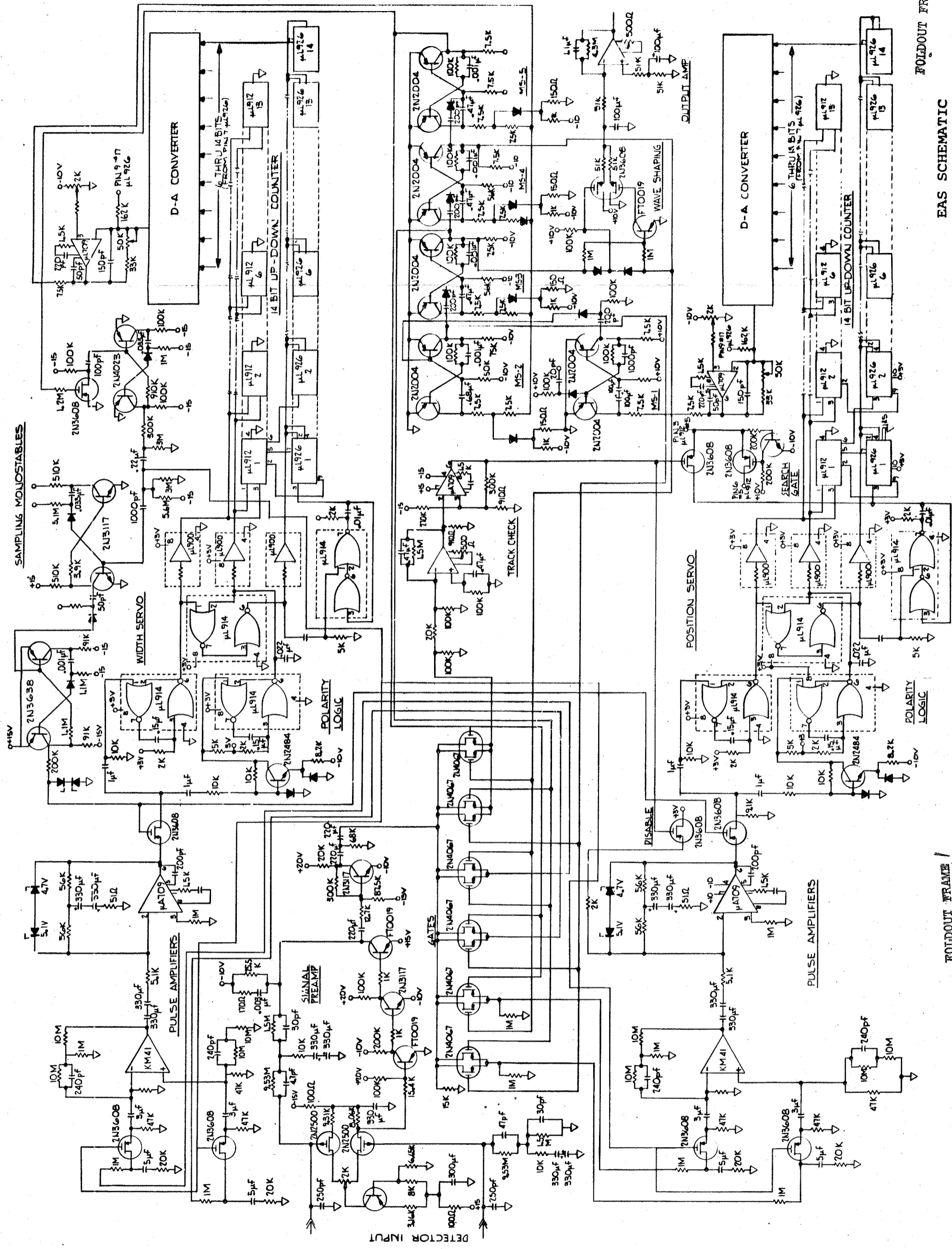
Same as second vehicle revolution.

This sequence continues until the earth pulse starts to appear at the outputs of track-check gates 2, 3, 4, and 5 (controlled, respectively, by monostables 2, 3, 4, and 5). When the sum of these four outputs is of sufficient amplitude, track-check amplifier A5 activates the track-check Schmitt trigger, turning control of monostable 1 on-time over to the digital integrator and amplifier A9. Servo action now takes over and the on-time of monostable 1 is corrected until all four monostable pulses fall within the earth pulse (ref. Figure 39); electrically, this happens when the output of position gates G2 + G3 equals the output of position gates G4 + G5.

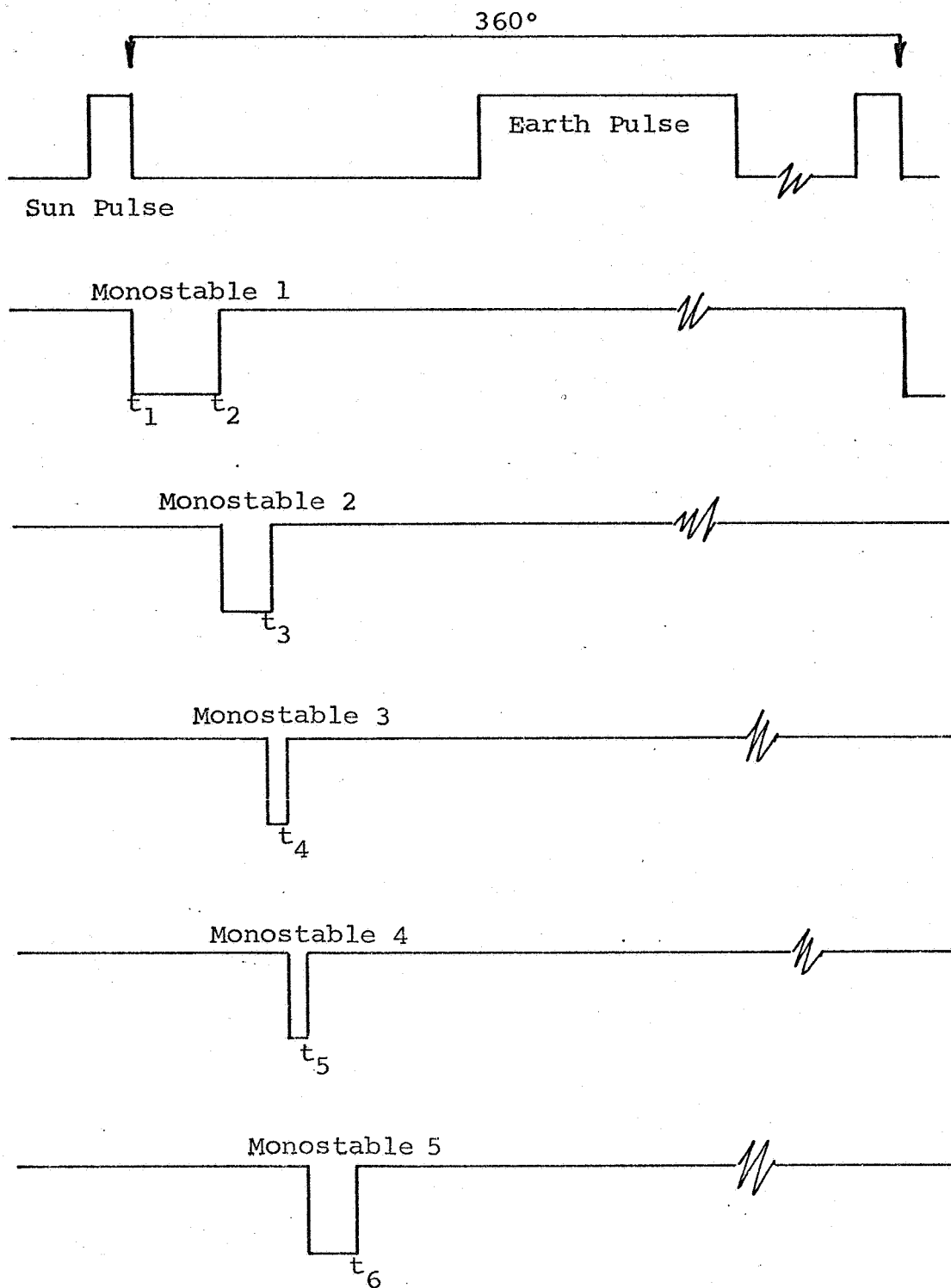


EAS BLOCK DIAGRAM

FIGURE 37a

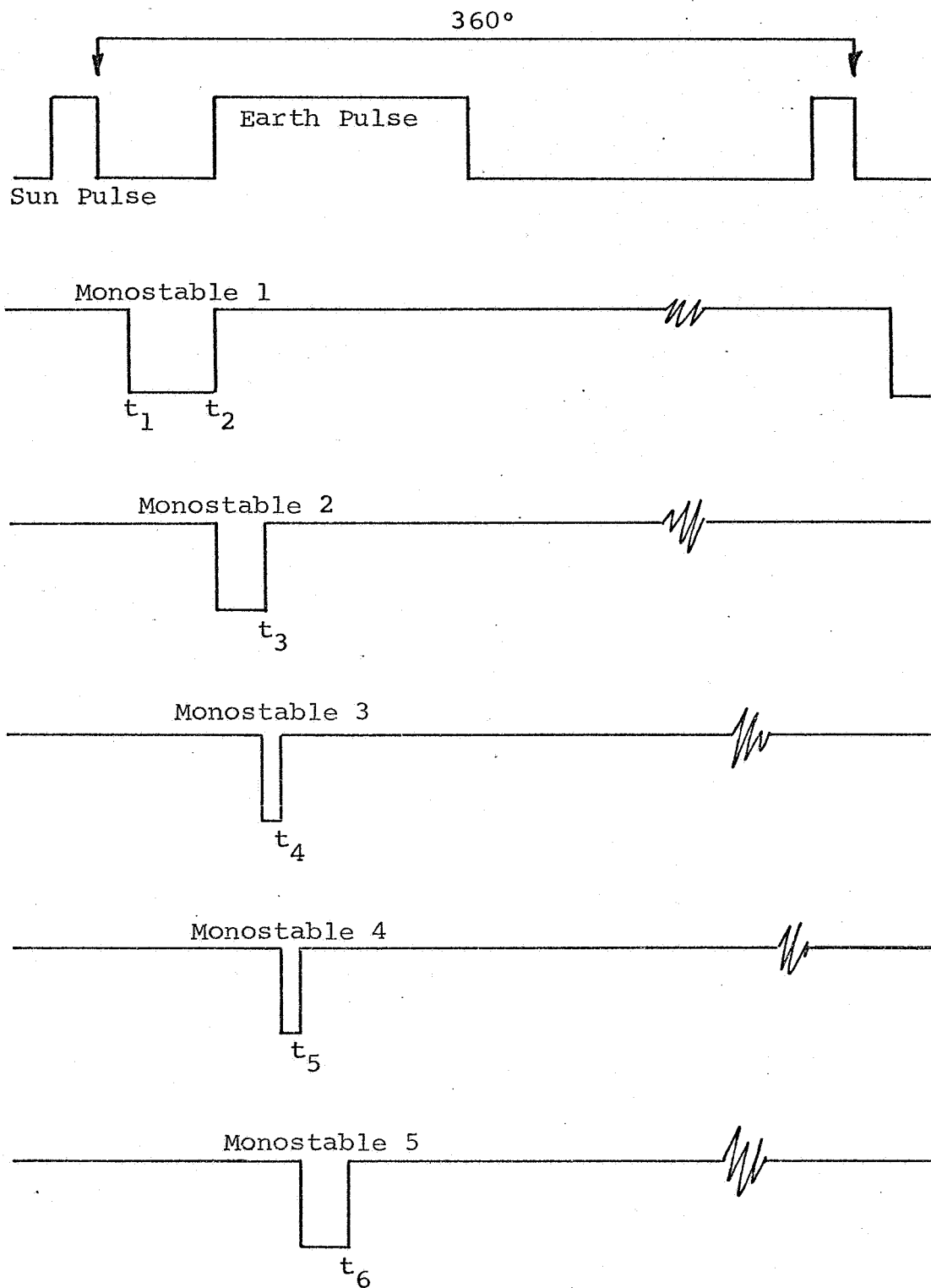


PRECEDING PAGE BLANK NOT FILMED.



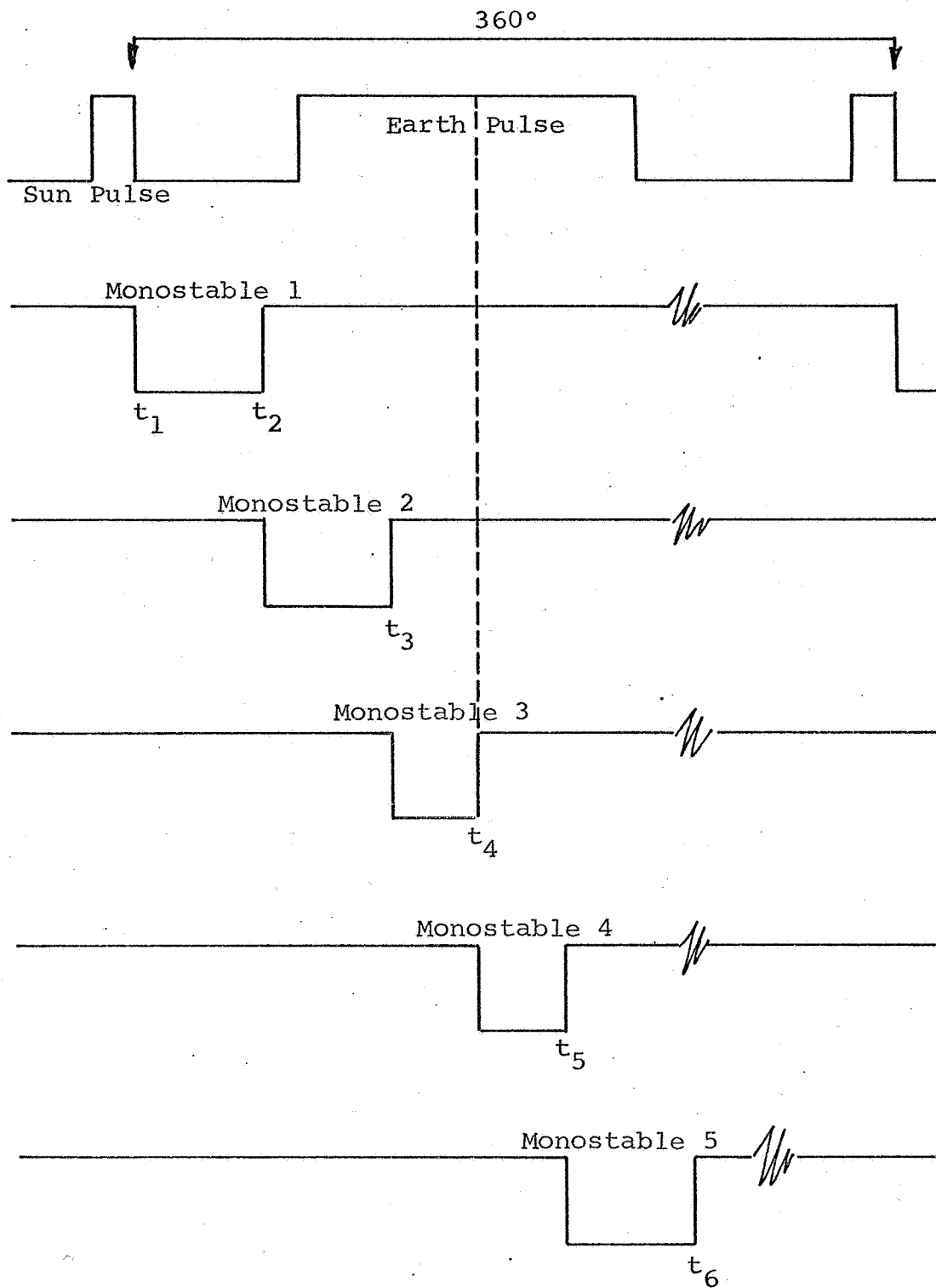
PULSE SEQUENCE BEFORE EARTH ACQUISITION

FIGURE 38



PULSE SEQUENCE AFTER EARTH ACQUISITION IN PHASE

FIGURE 39



PULSE SEQUENCE AFTER SERVOING ON PULSE WIDTH

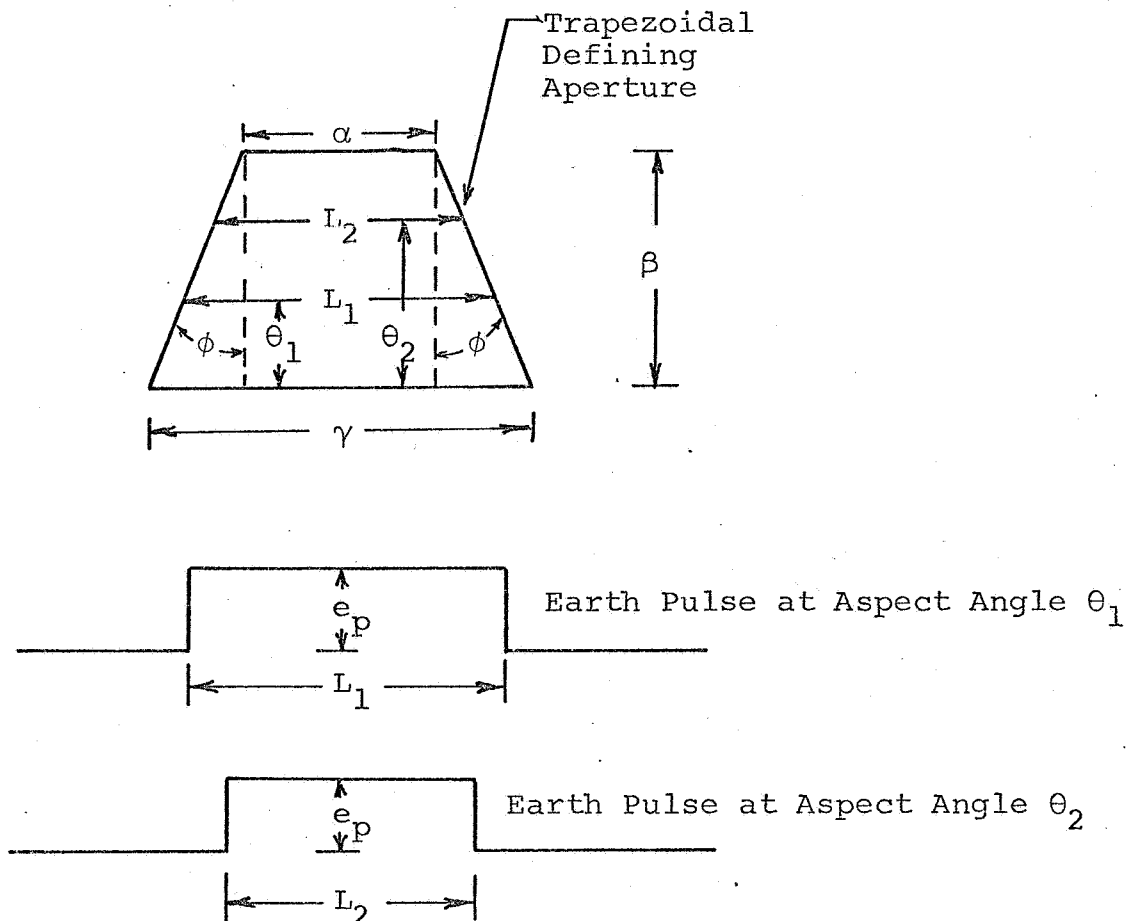
FIGURE 40

Once the "centering" described above is complete, the servo control of monostables 2, 3, 4, and 5 begins. Since the combined on-time of the four monostables is shorter than the earth-pulse duration (ref. Figure 39), the output of width gates G2 + G5 is greater than the output of width gates G3 + G4. This difference in voltage is the error signal that is processed in the digital integrator and amplified in amplifier A4; the amplified error signal is then used to servo the monostables until the output of G2 + G5 equals the output of G3 + G4 (ref. Figure 40). When this occurs, the combined pulse width of monostables 3 and 4 is equal to one-half the earth-pulse width.

To obtain aspect angle, all that is necessary now is to filter and amplify the monostable 3 and 4 waveforms (after appropriate shaping). This filtering and amplifying is done in output amplifier A6, whose output is an analog indication of aspect angle.

2. Derivation of Servo Error Signal

a. Width Servo



Definitions of Terms

α = angle subtended by narrow end of field of view = 4 degrees.

γ = angle subtended by wide end of field of view = 24 degrees.

β = angular height of field of view = 30 degrees.

θ = aspect angle, i.e., earth-crossing position.

$\phi = \tan^{-1} \left(\frac{\gamma - \alpha}{2} \right)$.

L_1 = length of earth pulse at $\theta_1 = \alpha + 2(\beta - \theta_1) \tan \phi$ (degrees).

L_2 = length of earth pulse at $\theta_2 = \alpha + 2(\beta - \theta_2) \tan \phi$ (degrees).

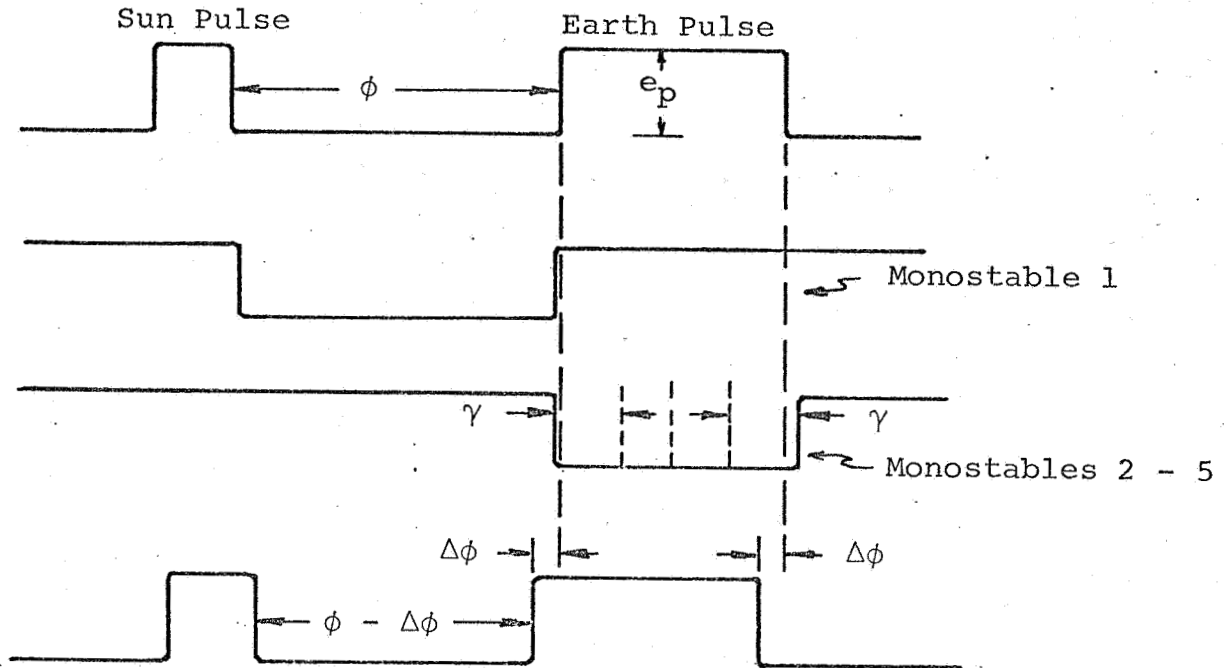
e_p = peak earth signal from detectors (after amplification by signal preamplifier).

$e_p \left(\frac{L}{360^\circ} \right)$ = earth signal averaged over one cycle.

In this derivation, it is assumed that the width servo has servoed onto an earth pulse of length L_1 . For a small change in aspect angle θ , the width servo must then correct itself to the new pulse length L_2 . Referring back to the description of system operation, the width-servo error signal (e_{we}) is obtained by subtracting the output of width gates G2 + G5 from the output of width gates G3 + G4. Since G3 and G4 "see" the center half of the earth pulse (reference Figure 40), where monostables 3 and 4 are each "on" for one-fourth of the earth pulse), the total change appears in the outputs of G2 and G5. This change, or error signal, is directly proportional to $L_1 - L_2$ and is derived as follows:

$$\begin{aligned}
 e_{we} &= e_p \left(\frac{\Delta L}{360^\circ} \right) = e_p \left(\frac{L_1 - L_2}{360^\circ} \right) \\
 &= \frac{e_p}{360^\circ} \left\{ \left[\alpha + 2(\beta - \theta_1) \tan \phi \right] - \left[\alpha + 2(\beta - \theta_2) \tan \phi \right] \right\} \\
 &= \frac{e_p}{360^\circ} \left[(\beta - \theta_1) - (\beta - \theta_2) \right] 2 \tan \phi \\
 &= \frac{e_p}{360^\circ} (\theta_2 - \theta_1) 2 \tan \phi \\
 &= e_p \left(\frac{\Delta \theta 2 \tan \phi}{360^\circ} \right) \\
 &= e_p \left(\frac{\Delta \theta \tan \phi}{180^\circ} \right) .
 \end{aligned} \tag{6}$$

b. Position Servo



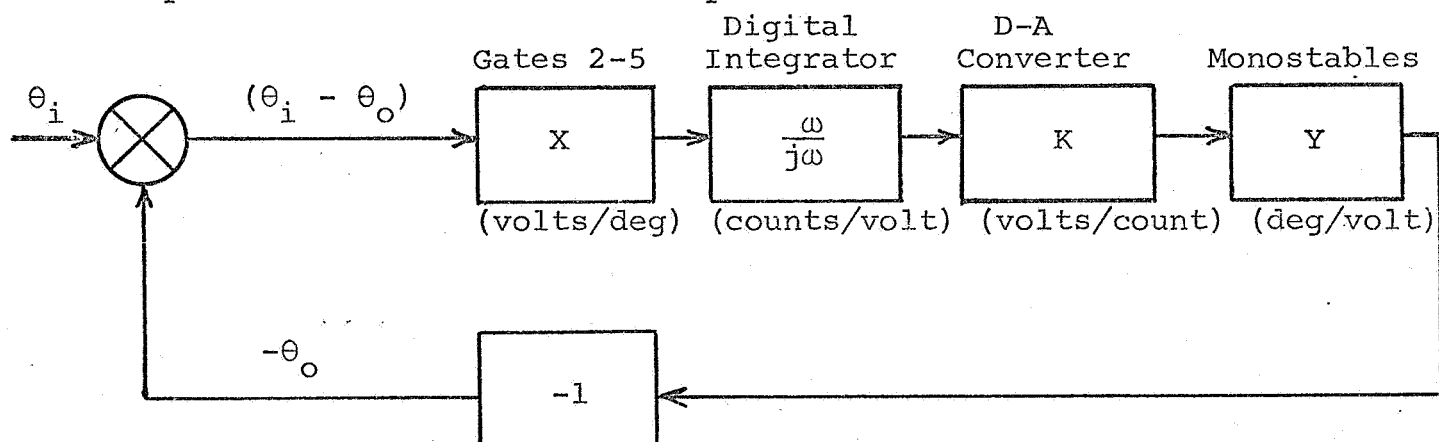
The derivation of the position-servo error signal is different from the derivation of the width-servo error signal in that operation of the position servo is essentially independent of aspect angle and FOV angular dimensions. For this derivation, it is assumed that both the width and position servos have locked onto some arbitrary pulse width at an angle ϕ between the sun-pulse trailing edge and the earth-pulse leading edge. Now consider a small change, $\Delta\phi$, in this angular position. Referring once again to the description of system operation, the position-servo error signal is obtained by subtracting the output of position gates G2 + G3 from the output of position gates G4 + G5. As in the case of the width servo, the outputs of G3 and G4 remain constant and equal; therefore the position-servo error is simply G2 - G5, or in equation form:

$$\begin{aligned}
 e_{pe} &= \frac{e_p}{360^\circ} \left[(\gamma - \Delta\phi) - (\gamma + \Delta\phi) \right] \\
 &= \frac{e_p}{360^\circ} (-2\Delta\phi) \\
 &= -e_p \left(\frac{\Delta\phi}{180^\circ} \right) \quad (7)
 \end{aligned}$$

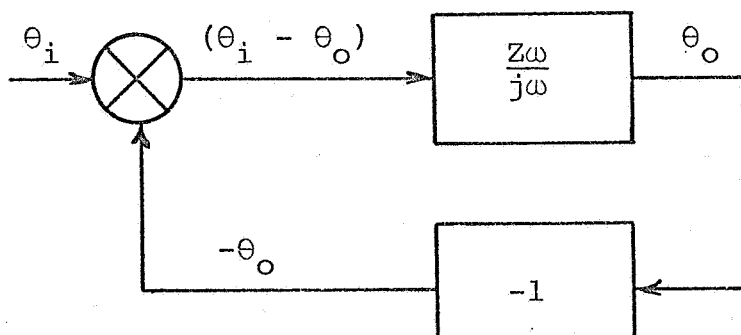
Note: As has been seen, the magnitudes of both the position-servo and width-servo error signals are a function of duty cycle only and are therefore independent of spin rate. However, since the monostables controlling the gates are on-time variable as a function of servo control voltage, they are affected by spin rate. This means that even though the derivations are correct for any given spin rate, a change in spin rate will change both the earth-pulse width and the timing between the sun and earth pulses and will therefore create error signals that will be driven out by the respective servos.

3. Derivation of Servo Transfer Function

The position-servo and width-servo block diagrams and transfer functions are identical in form, although, as was seen in the derivation of error signals, some of the scale factors in the various blocks are different. The following derivation deals with the transfer function in general form. Here the digital integrator is assumed to be an ideal integrator whose transfer function is represented by $\omega/j\omega$, where ω is the effective bandwidth of the integrator. The following sketch shows a block diagram model of the position and width servo loops.



This is equivalent to:



Here $Z = XYK$.

From this, the closed-loop transfer function is:

$$\frac{\theta_o}{\theta_i} = \frac{Z\omega/j\omega}{1 + Z\omega/j\omega} = \frac{Z\omega}{j\omega + Z\omega} \quad (8)$$

Note: The scale factors X and Y for the gates and monostables are shown as variables, since X is range dependent and Y is spin-rate dependent. This means of course that the transfer function itself varies as a function of both range and spin rate. If, however, the controllable parameters of the transfer function can be designed for worst-case conditions (target range of 5×10^7 n.mi. and 2 rps), the system will perform as well or better at closer ranges and/or lower spin rates.

The system accuracy specification is 0.5 degree. To achieve this accuracy, the combined rms-noise equivalent angle and other error sources cannot exceed 0.5 degree. Therefore, in the system design, the goal was to hold individual errors below 0.2 degree. To determine what the parameters of the system transfer function must be to achieve an rms-noise equivalent angle of less than 0.2 degree, the following equation was used (for the width servo only):

$$e_{e(0.2^\circ)} = e_{n(\omega_1)} \left(\sqrt{\frac{\omega_2}{\omega_1}} \right) \left(\sqrt{\frac{\sigma}{360^\circ}} \right), \quad (9)$$

$$\text{where } e_{e(0.2^\circ)} = e_p \left[\frac{(0.2^\circ) \tan \phi}{180^\circ} \right], \quad (10)$$

$e_{n(\omega_1)}$ = rms-noise voltage from signal preamplifier in a 1-cps bandwidth ($\omega_1 = 6.28$) at 30 cps,*

ω_2 = frequency, where the closed-loop transfer function,

$$\frac{Z\omega}{j\omega + Z\omega} = 0.707 = \text{closed-loop system bandwidth,}$$

σ = nominal earth-pulse width = 14 degrees.

* The 30-cps spot noise was used as a basis for computing noise equivalent angle because of the effect gating has on the output of the wideband signal preamplifier. A Fourier analysis of the gating waveform, for a nominal spin rate and pulse width, indicated that the frequencies of maximum transmission are around 30 cps (see Figure 41).

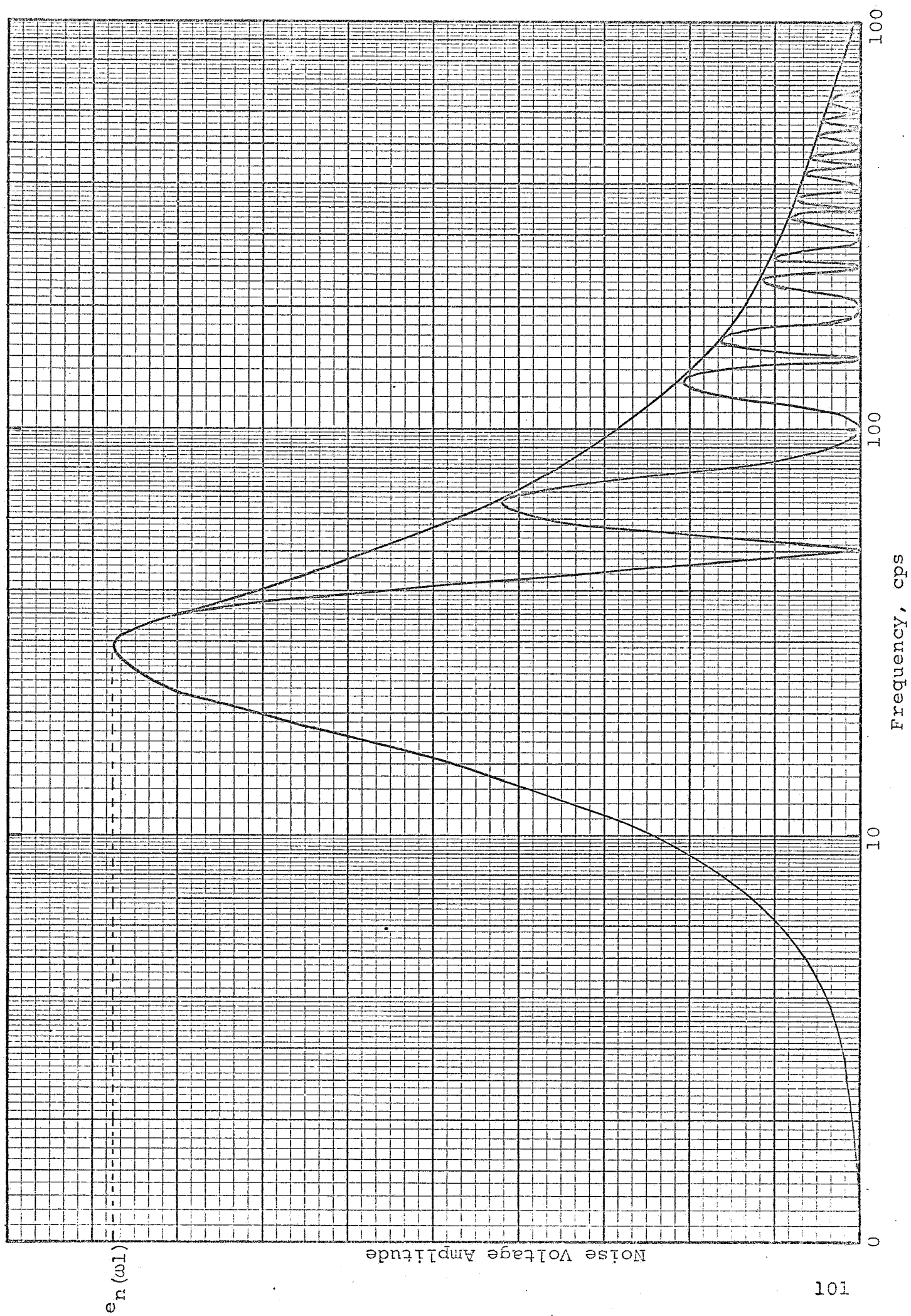


FIGURE 41. SPECTRAL CHARACTERISTICS OF GATING WAVEFORM AT NOMINAL SPIN RATE

Values for $e_{n(\omega_1)}$ were determined by laboratory measurements. Thus, in equation (9), for a given range, the only unknown is ω_2 , which is, rearranging equation (9):

$$\omega_2 = \left[\frac{e_e(0.2^\circ)}{e_{n(\omega_1)}} \right]^2 \omega_1 \left(\frac{360^\circ}{\sigma} \right). \quad (11)$$

Substituting ω_2 into equation (8), the closed-loop transfer function, gives

$$\frac{Z\omega}{j\omega_2 + Z\omega} = 0.707 ,$$

or $|j\omega_2| = Z\omega . \quad (12)$

For a given range and spin rate, X, Y, and K are known. Therefore, since $Z = XYK$,

$$\omega = \frac{\omega_2}{Z} = \frac{1}{\tau} . \quad (13)$$

After equation (11) is solved for ω_2 , equation (13) determines what the effective time constant, τ , of the digital integrator must be to satisfy the rms-noise equivalent angle requirement of 0.2 degree or less.

The measured value for $e_{n(\omega_1)}$ and the predicted signal level at 5×10^7 n.mi. were substituted into the preceding equations, resulting in a value of approximately 1000 seconds for the required closed-loop system time constant. From the standpoint of noise, therefore, if the long system time constant can be tolerated, operation at ranges out to 5×10^7 n.mi. and beyond appears feasible.

4. Digital Integrator

It was mentioned earlier that digital rather than analog integrating techniques are used in achieving the desired transfer function. The preliminary design of the coherent signal-processing system did use analog integrators, but, as already discussed in Section IV.B., the dc offsets at the integrating-amplifier inputs were so large compared to the predicted error signals at 5×10^7 n.mi. that the sensor accuracy requirement could not be met. The most promising solution to the problem appeared to be operation of the width and position servo circuitry in an ac or pulse mode until the error signal level is sufficiently high to be unaffected by dc offsets. Based on preliminary testing (see Section VI), the design shown in Figure 37 appears to satisfy the system design goal of operation at 5×10^7 n.mi.

The fundamental difference between the analog and digital integrator systems is the way in which the integration, or system time constant, is realized. In the analog design, the outputs of the position and width gates 2 through 5 (controlled by monostables 2 through 5) would be fed directly into integrating amplifiers; thus the error signals appearing at the outputs of the gates would have to be strong enough to overcome the dc offsets appearing at the input terminals of the integrating amplifiers. However, the dc offsets were large enough to prevent sensor operation out to the system range goal of 5×10^7 n.mi.

In the digital system, the integration function is performed by high-gain pulse amplifiers A2 and A3 in the width servo; amplifiers A7 and A8 in the position servo; sampling gates G6, G7, and G8; the polarity logic circuits; and the up-down counters (ref. Figure 37). Since operation of both the width servo and the position servo is essentially the same, the following discussion deals with the width servo only.

The outputs of gates G2 through G5, instead of being fed directly into a dc amplifier, are stored on capacitors C1 and C2. Once each revolution (after monostable 5 returns to its stable state), G6 and G7 sample the voltage stored on C1 and C2 (e_{C1} and e_{C2}). Amplifiers A2 and A3 amplify the difference between e_{C1} and e_{C2} . The resultant pulse is fed to the digital circuits, i.e., the polarity logic and the up-down counter. (Since the system is ac- or capacitive-coupled through both pulse amplifiers, amplifier dc offsets have no effect on pulse polarity.) The counter counts down if the pulse is positive and up if the pulse is negative.

The actual integrating is performed by the first 5 bits (buffer section) in the 14-bit up-down counter in that any counting or changes of state in the first 5 bits are not coupled into the digital-to-analog converter and therefore do not affect the on-times of monostables 2 through 5. In other words, 2^5 net positive or negative counts are required before a change or correction is made to the monostable pulse widths.

There are two inputs to capacitors C1 and C2: the noise output from the signal preamplifier and the earth pulse. The noise alone, since it is random in nature, has a probability of 0.5 of producing either a positive or a negative pulse. The error signal derived from the earth pulse, if there were no noise, has a probability of 1 of producing a negative or a positive pulse, depending on whether or not the monostable on-times are too long or too short. Combining the two effects, the probability of counting in the proper direction to null-out the error signal is $0.5 + A(S/N)$, while the probability of counting in the opposite direction is $0.5 - A(S/N)$, where S/N is the signal-to-noise ratio after integrating by R1 and C1 and R2 and C2, and A is a function of S/N .

Calculations for a 1-degree step change in aspect angle at 5×10^7 n.mi. resulted in the following:

Probability of counting in direction to null-out error = $0.5 + (0.38)(0.354)$.

Probability of counting in opposite direction = $0.5 - (0.38)(0.354)$.

If the sample rate is one sample per second, the total number of samples needed to null-out the 1-degree error in 1000 seconds is 1000 samples. Therefore, with a count granularity in the last 9 bits of 0.1 degree per count, the following equation for the number of bits needed in the buffer can be solved (n = number of buffer bits):

$$\begin{aligned} (10) 2^n &= 1000 \{ [0.5 + (0.38)(0.354)] - [0.5 - (0.38)(0.354)] \} \\ &= 1000 [2(0.38)(0.354)] \\ &= 1000(0.269). \end{aligned} \tag{14}$$

Thus, $2^n = 269/10 \approx 27$.

The integer value of n that will give the value closest to 27 is 5, and $2^5 = 32$. Since the realizable value of 2^n is 32 instead of 27, the number of samples needed to null-out the 1-degree error is greater than 1000. Let X = the total number of samples required to produce a net count of $10(2^5) = 320$, or

$$X(0.269) = 320. \tag{15}$$

$$X = \frac{320}{0.269}$$

= 1190 samples at one sample per second.

This gives an effective time constant of 1190 seconds. Since the system time-constant requirement is 1000 seconds, 1190 seconds is more than adequate.

VI. TESTING

A. Testing of Circuits

The various sections of the electronic circuitry were bread-boarded and tested individually, and necessary changes in the design were made throughout the work. The servo loops were tested using an adjustable earth-sun signal simulator built especially for this purpose. This early testing demonstrated that the system could search for, find, and lock on a simulated earth signal.

Two types of differential preamplifiers were designed, bread-boarded, and tested with the photovoltaic detector. One used a conventional PNP-type transistor; the other used a field effect transistor. In addition to the laboratory testing, a computer program was developed for comparing the performance characteristics, under various operating conditions, of the different transistors considered for the preamplifier. As a result of the testing and the computer analysis, a field effect transistor was chosen for use in the differential input stage.

Early testing of the servo loops had used simulated earth signals that were essentially noise free. The servo loops and the signal preamplifier were then integrated and subjected to tests with a simulated earth signal approximately equivalent to that from the fully illuminated earth at 10×10^6 n.mi. Satisfactory operation was demonstrated in the presence of noise. The search and acquisition functions were next integrated into the bread-board. Tests at this stage showed that the system was capable of searching for, acquiring, and tracking a simulated earth signal (fully illuminated) at 10×10^6 n.mi. in the presence of noise. At this point, one amplifier was deleted from the system, the track-check Schmitt trigger was added to provide a higher search rate for the position servo, a shaping network was incorporating preceding the filtering and amplifying of the outputs of monostables 3 and 4, and an "and" gate was added to prevent the position servo from locking on sub-multiples of the spin rate. All of these circuits were tested, but only the shaping network was integrated into the breadboard.

As has been discussed, it was found that dc offsets in the system integrating amplifiers, rather than noise, were the limiting factor so far as operating range was concerned. Several amplifiers had been studied for use as the integrating amplifiers, but all were found deficient with respect to drift characteristics. A circuit for a self-calibrating amplifier that offered promise of minimizing dc drifts was designed and breadboarded, but testing demonstrated that an amplifier design that could satisfy the requirement of the EAS did not appear realizable. As another approach to solution of the drift problem, the position and width integrating amplifiers of the earlier design were replaced by a digital integrator. This system was partially breadboarded

and tested, with results indicating that the design could satisfy the system range goal of operation at 5×10^7 n.mi. This new circuit was then integrated into the breadboard in preparation for system testing.

B. System Testing

Testing of the coherent system breadboard was performed with the test setup shown in Figure 42, using electronically simulated signals. The purpose of this testing was to demonstrate performance capability with signal inputs approximating those expected at 5×10^7 n.mi. The earth-pulse amplitude could be accurately simulated because the output of the earth-pulse generator could be attenuated to any desired level. The noise level at the signal-preamplifier output, however, was not quite as high as will be seen when the optics and electronics are integrated. This was due primarily to the fact that the signal was electronically simulated and therefore the noise that would normally be contributed by the silicon photovoltaic detector was not present.

To determine how well the system could measure the earth-pulse width, and therefore aspect angle, three points were monitored: the unattenuated earth pulse, the output of monostables 3 and 4, and the aspect-angle output voltage. During normal operation, it is necessary to monitor only the angle output voltage to determine aspect angle. For testing, however, the earth-pulse and monostable waveforms were monitored to provide a check on system accuracy. By testing in this manner, if a change occurs in the angle output voltage, the earth-pulse and monostable waveforms can be checked to see if the voltage change is due to an error in the system or is instead due to a change or malfunction in the simulator circuitry.

When the test was performed, the following simulator and circuit conditions were pre-set and remained unchanged throughout the test:

- 1) Function generator frequency = 1 cps, to simulate a spin rate of 1 rps.
- 2) Earth-pulse duration = 40 ms, to simulate an approximate aspect-angle null condition.
- 3) Earth-pulse amplitude into signal amplifier = 4 μ V, to simulate a 5×10^7 n.mi. earth.
- 4) Scale factor of aspect-angle output voltage = 350 mV/deg.
- 5) Preamplifier gain = 7×10^3 .
- 6) Peak earth signal from preamplifier \approx 28 mV (not distinguishable because of noise).
- 7) Wideband peak-to-peak noise from preamplifier \approx 1.2 V.

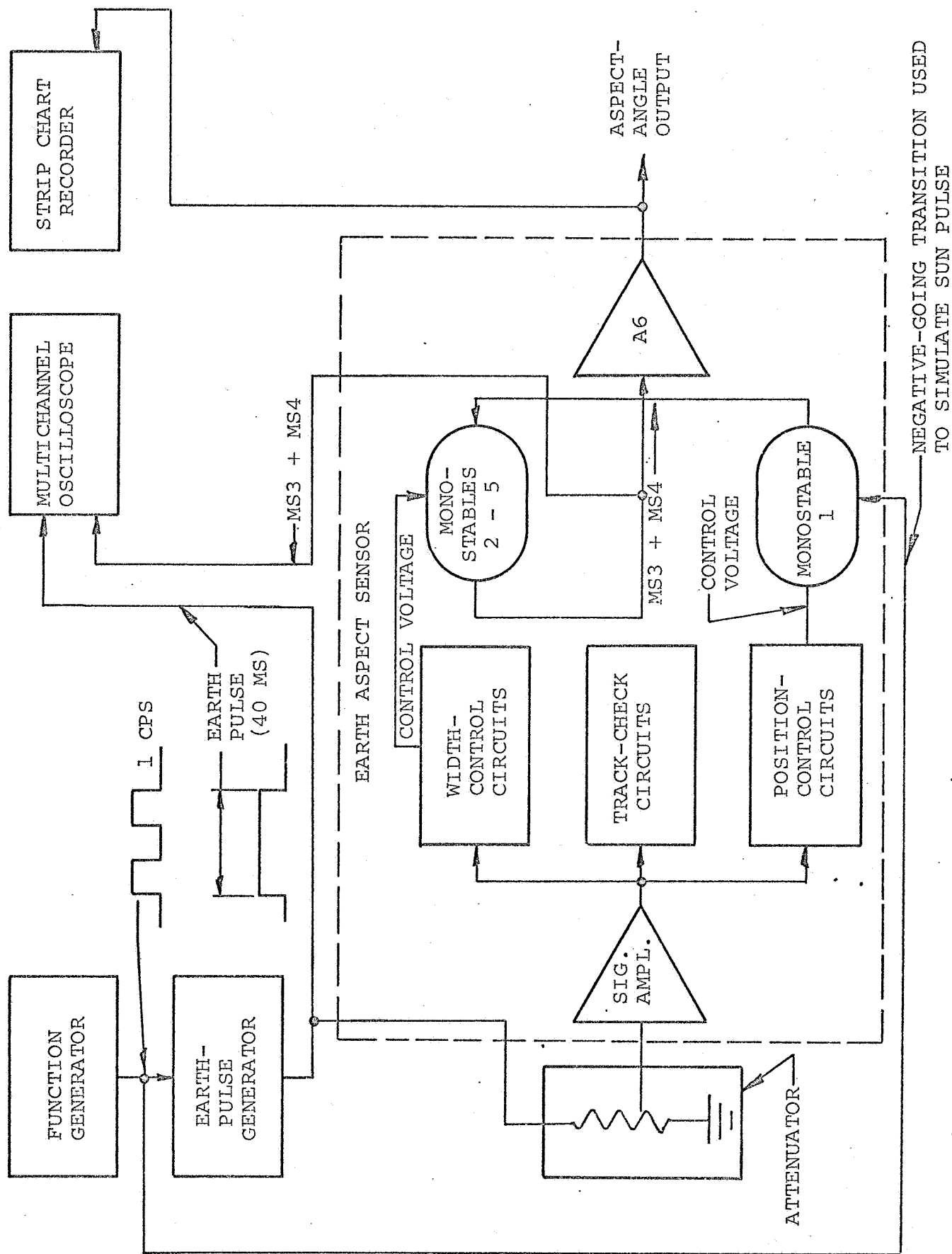


FIGURE 42. SYSTEM TEST SETUP

At the beginning of the test, after application of power, the system successfully demonstrated its ability to search for and acquire the earth pulse and to supply a track-check signal to indicate that the earth pulse had been acquired. After earth-pulse acquisition, the strip chart recorder was connected to the aspect-angle output and the performance of the width servo and the angle output amplifier was observed and recorded.

System accuracy was tested continuously for approximately 18 hours. During this interval, the system measured the earth-pulse width to within -0.1 to -0.5 degree; this appeared as a variation in angle output voltage of 150 mV peak to peak. Figure 43 is a $4\frac{1}{2}$ -hour section of the 18-hour strip chart record, showing the peak-to-peak excursion of the output voltage and also the 35-mV ripple component.

A photograph of the system breadboard is shown in Figure 44.

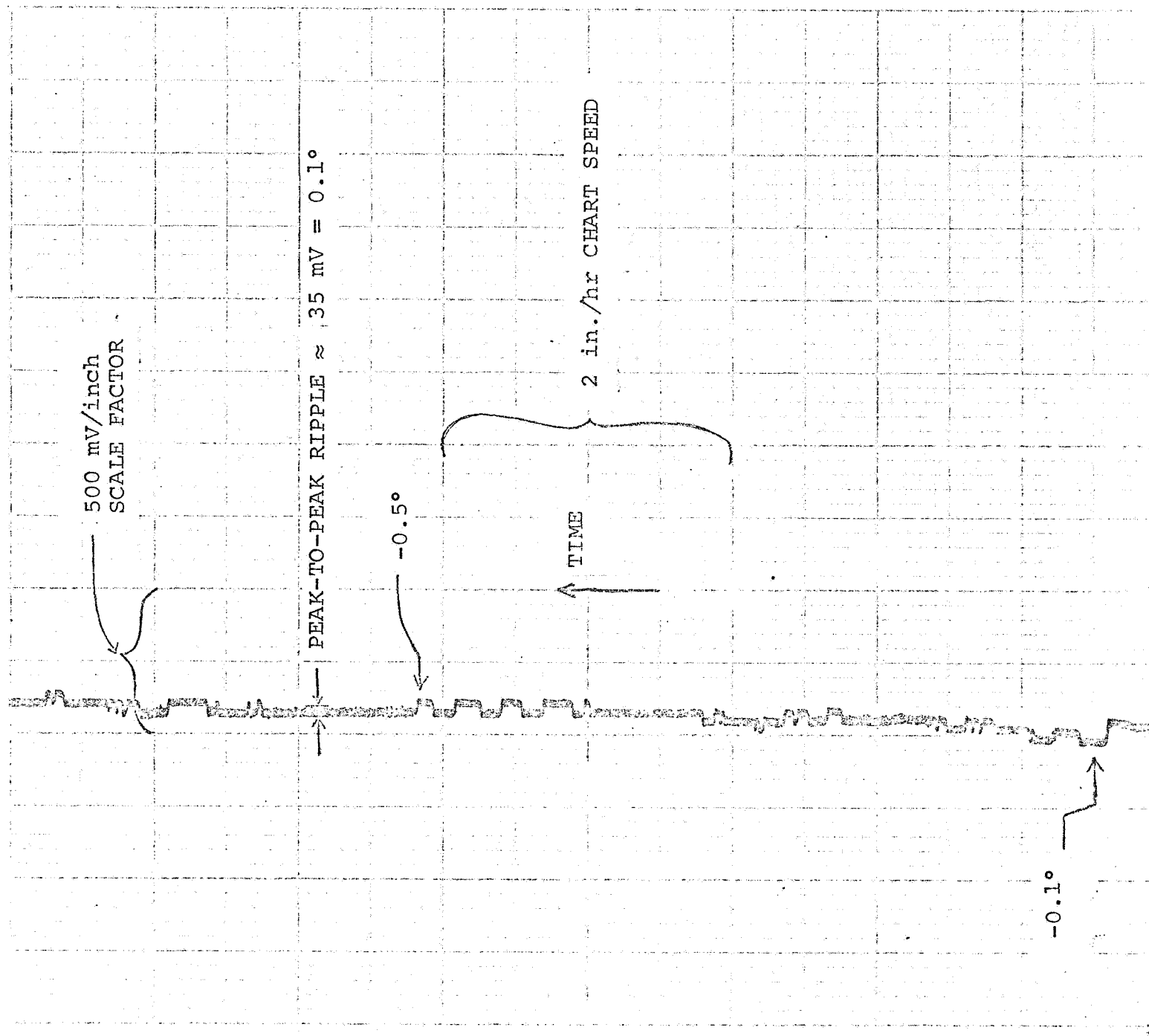
C. Target Simulator

The target simulator consists basically of a large, plane, front-surface mirror mounted on a turntable. The mirror is positioned in front of the EAS aperture and rotated, by means of the turntable, about an axis perpendicular to the EAS line of sight. A scan of this type limits the azimuth range over which the EAS can view simulated targets to considerably less than 360 degrees (about 105 degrees in the present unit). It might be supposed that an inclined mirror rotating about an axis parallel to the sensor line of sight would be better, since it could give a 360-degree azimuth sweep. In this mode, however, the direction of travel of the target image across the sensor reticle would vary as a function of azimuth position and would therefore be entirely unsuitable.

The major mechanical component of the simulator is the turntable, which is seated in a 9-inch-diameter bearing track. The table is driven by a 30-rps synchronous motor. The primary drive wheel, mounted on the motor shaft, transmits the rotation to the speed-change wheel on the turntable drive shaft. The final drive wheel, mounted on the top end of this shaft, drives the turntable. There are three interchangeable wheels to provide three different speeds: 0.25, 2, and 5 rps. The motor is pivot-mounted to accommodate the different wheel sizes. A photograph of the completed unit is shown in Figure 45.

The targets themselves will consist of filters placed over circular apertures behind which will be light sources. In addition to the red filters purchased for the sensor itself, some blue filters were obtained. Thus, it will be possible to generate blue, red, and white targets to qualitatively simulate the earth and the planets.

The turntable was fabricated, assembled, and tested, and found to operate successfully. However, an evaluation of the entire simulator cannot be made since the program was terminated before tests could be conducted of the optical head integrated with the electronics



RECORD OF SYSTEM TEST

FIGURE 43

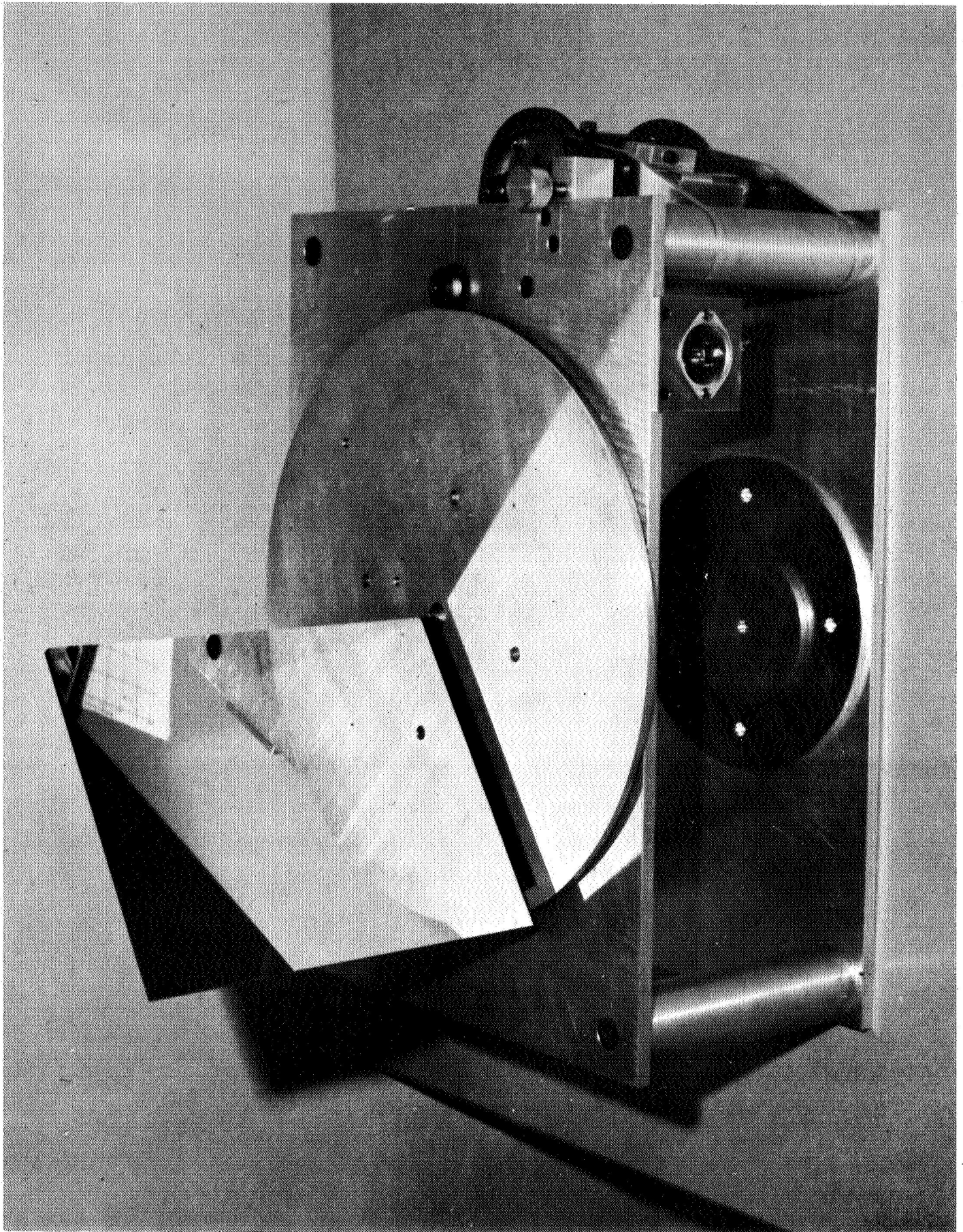


FIGURE 45. TARGET SIMULATOR

VII. MAJOR REMAINING TESTING AND DESIGN TASKS

The testing that was done with the system breadboard electronics proved the feasibility of the coherent signal-processing approach. The next logical step, had the effort continued, would have been to integrate the electronic breadboard with the optical head and conduct system tests, using the target simulator built for that purpose (ref. Figure 45). This testing would demonstrate the feasibility of the complete system, as well as that of the optical approach, in particular the "blue minus red" target-discrimination method. In addition, testing of the system as a whole would provide information for a more accurate prediction of how well the system would perform in an actual flight environment.

From a design standpoint, the major tasks remaining are 1) the packaging design, and 2) optimizing and refining the electronic circuit design for operation in the space environment. Significant reductions could be made in the parts count and electronic package size by using the new multifunction logic circuits now available instead of the single-function circuits used in the breadboard. This is particularly true in the case of the up-down counters in that the 26 TO-5 cans needed for a 13-bit counter could be replaced with four multifunction flat packs.

Quantic Industries, Inc.,
Electro-Optical Division,
1011 Commercial Street,
San Carlos, California, 1 June 1968.

APPENDIX A

DEFINITION OF D*

D* (called D-star) is defined as the detectivity normalized to unit area and unit bandwidth. Detectivity is the signal-to-noise ratio produced with unit radiant flux incident in the detector.

The units of D* are $\text{cm-cps}^{1/2}/\text{watt}$. For most detector types, the detectivity of a given detector is related to D* as follows:

$$D = D^* / (A \Delta f)^{1/2};$$

where D = detectivity (watt^{-1}),

A = detector area (cm^2),

Δf = bandwidth (cps).

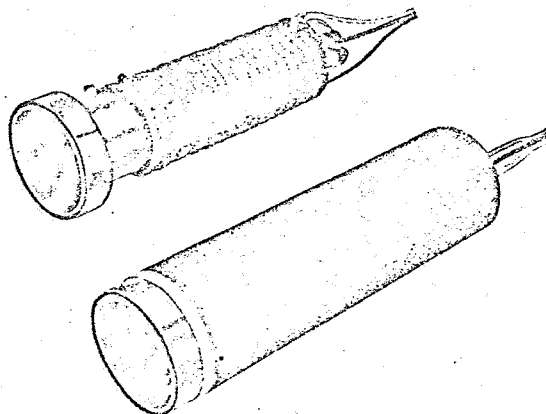
D*_{mm} is defined as D* at the peak wavelength, the optimum bias value, and the peak detective modulation frequency.

The notation $D^*(\lambda_p, f, \Delta f)$ used in this report is defined as D* at wavelengths of peak response, a modulation frequency f, and a bandwidth $\Delta f = 1$.

For detailed definitions of these and related detector terms, see reference 15.

SPECIFICATION DATA

MULTIPLIER PHOTOTUBE MODEL 543F-05-14



GENERAL

The EMR Model 543F-05-14 ASCOP Multiplier Phototube is an end-on, sapphire window tube with 14 stages and a 1.7-inch-diameter cesium telluride photocathode. The spectral sensitivity of this tube extends from 1450 Å, the cutoff of the selected ultra-violet-grade sapphire, to the photocathode threshold at approximately 3500 Å, a broad-band response characteristic exhibiting good long-wavelength rejection. Tubes with this response characteristic which are very sensitive to the short wavelength region but are insensitive to longer wavelength solar radiation through the atmosphere are referred to as SOLAR BLIND. This tube is custom-made, individually tested and calibrated, and delivered with complete test-data sheets for all major performance parameters.

The 43-mm-diameter useful cathode of the Model 543F-05-14 has a typical quantum efficiency of 6.5% at 2537 Å, and a typical room-temperature dark current of 7×10^{-11} ampere at a multiplier gain of 10^6 . Operating temperature is limited only by the photocathode, which is rated to $+100^\circ\text{C}$. The tube features a unique design of venetian-blind dynodes and a hard-glass Kovar ring construction in an encapsulated package and is capable of withstanding 50 g shocks of 11-millisecond duration.

Interstage resistors are potted with the tube in a fiberglass housing $7\frac{3}{16}$ inches long and 2 inches in diameter. These resistors are welded to the Kovar rings prior to potting; insulation problems are eliminated and the result is a resistor-chain mounting that is as rugged as the tube itself. Unless specified otherwise, 3.9-megohm resistors are used and the phototube is supplied as a potted assembly, with three color-coded leads brought out from the rear of the housing, for signal, cathode, and high voltage connections.

PHYSICAL CHARACTERISTICS

Number and type of dynodes:
Maximum overall length (unpotted):
Typical weight (unpotted):
Window material:
Cathode sensitive area:
Cathode type:

14; venetian blind; Ag-Mg
6.5 inches (17 cm)
190 grams
Selected ultraviolet grade sapphire (Al_2O_3)
1.7 in. (43 mm) dia.; area = 2.3 in.²
Semitransparent: Cesium Telluride

PHOTOCATHODE CHARACTERISTICS

Quantum efficiency (Q) at 2537 Å:
Cathode radiant sensitivity at 2537 Å (σ_k):
Quantum efficiency (Q) at 3500 Å:

MULTIPLIER PHOTOTUBE CHARACTERISTICS

Voltage required for current amplification (G), of: 10^5
 10^6
 10^7
Dark current (i_D) at 20°C at a current amplification of: 10^5
 10^6
 10^7
Anode radiant sensitivity (σ) at a current amplification of 10^6 @ 2537 Å:
Equivalent anode dark current input at 20°C at current amplification of 10^5 —
Radiant at 2537 Å, (ϵ_D):
Equivalent noise input at current amplification of 10^6 at 20°C —
Radiant at 2537 Å, (ϵ_N):

MAXIMUM RATINGS

Supply voltage:
Anode current:
Ambient temperature:

ENVIRONMENTAL

Shock:
Vibration:
Temperature:

Minimum	Typical	Maximum	Units
4.5	6.5		%
0.009	0.013		amp/watt
	0.045	0.09	%
	1800	2100	volts
	2400	2800	volts
	3000		volts
	9.0×10^{-12}		amps
	7.0×10^{-11}	6×10^{-10}	amps
	6.0×10^{-10}		amps
9,000	13,000		amps/watt
	5.4×10^{-15}	6.0×10^{-14}	watts
	3.6×10^{-16}	1.5×10^{-15}	watts
		3600	volts
		100	μ amps
		100	°C

50 g, 11 millisecond duration
20 g, 20 to 3,000 cps
-55°C to 100°C

PACKAGING

Potted weight (typical):

Normally packaged in a 2" (51 mm) O.D. x 7 $\frac{1}{4}$ " (18 cm) long fiberglass housing.
Approximately 430 grams

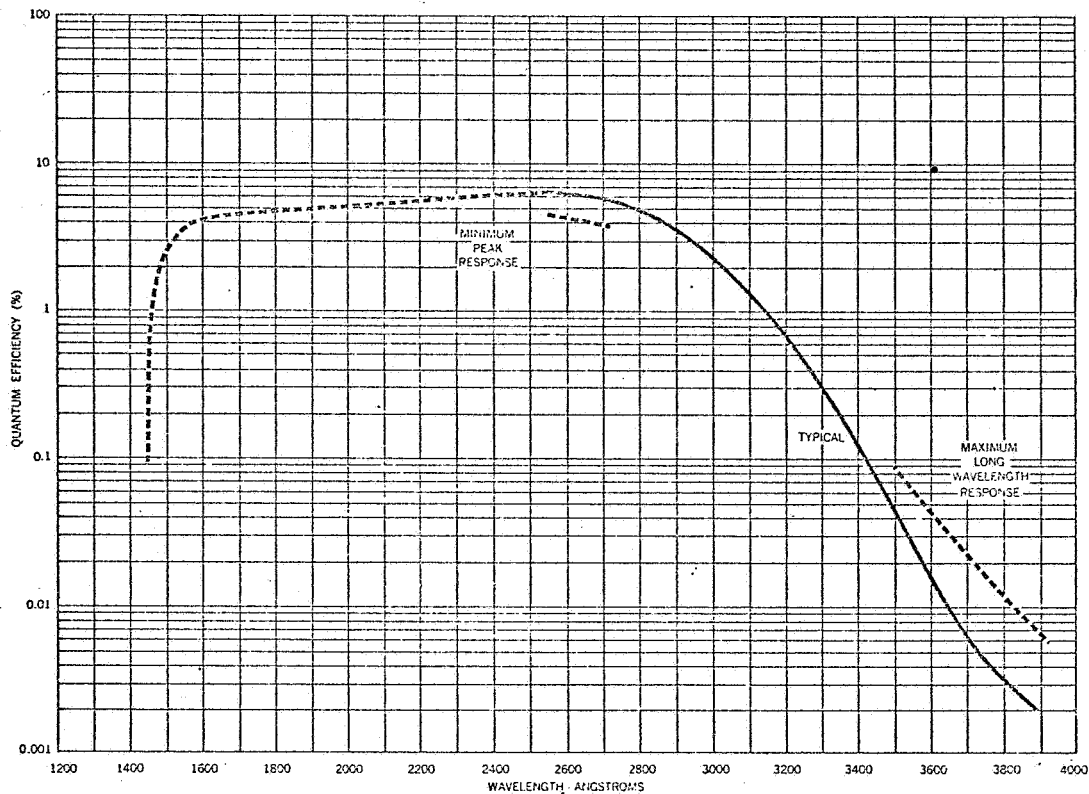


FIGURE 1.
SPECTRAL RESPONSE
CHARACTERISTICS

The typical quantum efficiency (emitted electrons per incident photon) is given as a function of wavelength in Angstroms. Also shown are the minimum peak sensitivity and the maximum long-wavelength response.

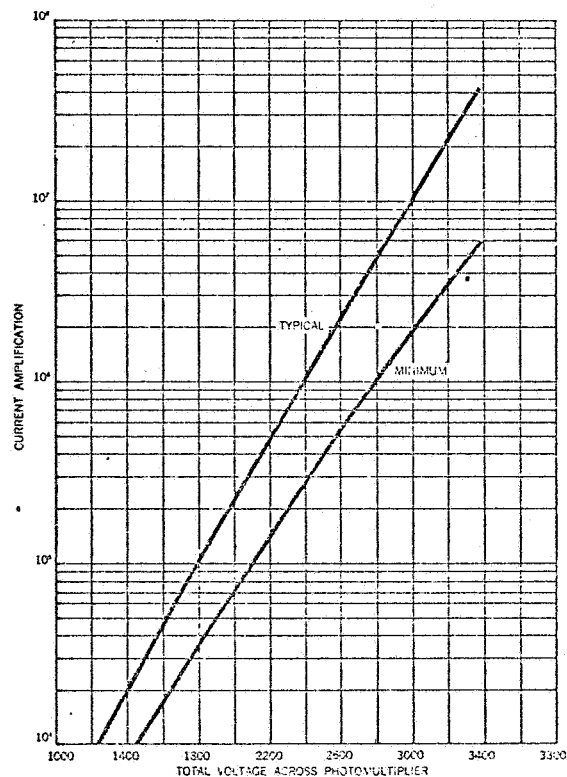


FIGURE 2
CURRENT
AMPLIFICATION

The dependence of current amplification on voltage is shown for the complete tube, from photocathode to last dynode. Curves are given for typical and minimum tube performance.

EMR warrants each tube for all of the characteristics identified in these specifications. However, EMR will not restock or give any financial consideration on tubes which meet these specifications but do not perform in accordance with uncontrolled characteristics which are unique to a specific customer. If control of special characteristics is desired, specific agreement regarding these characteristics must be achieved prior to acknowledgment of an order.

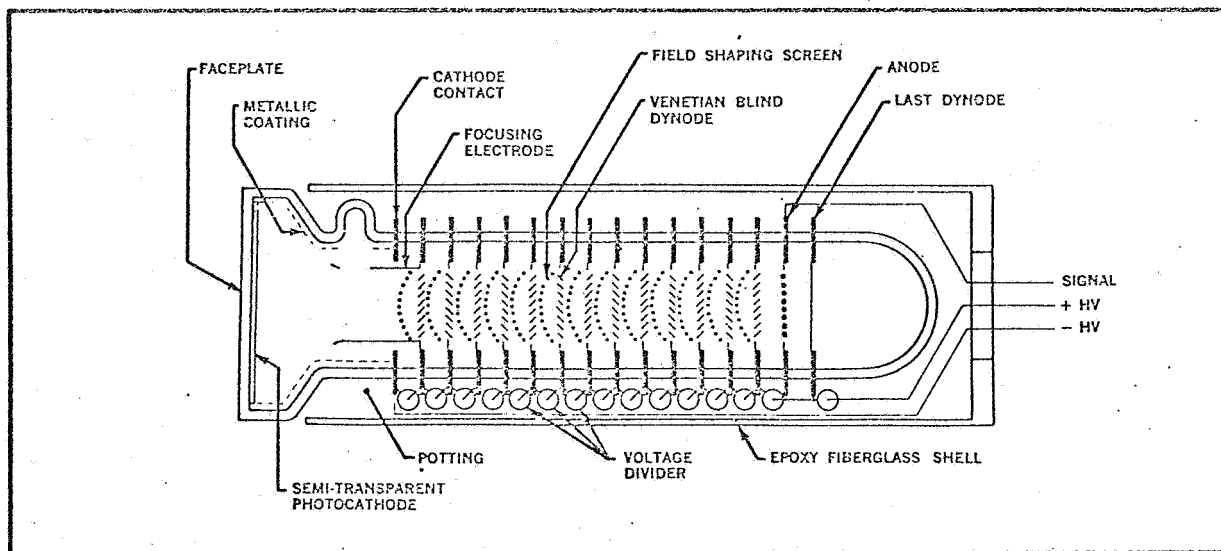


FIGURE 3

FUNCTIONAL DIAGRAM

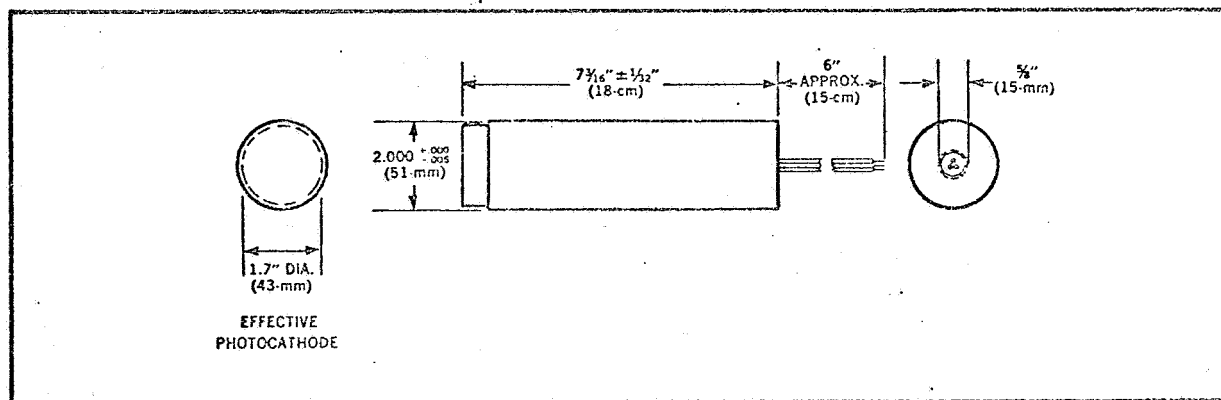


FIGURE 4

OUTLINE DRAWING

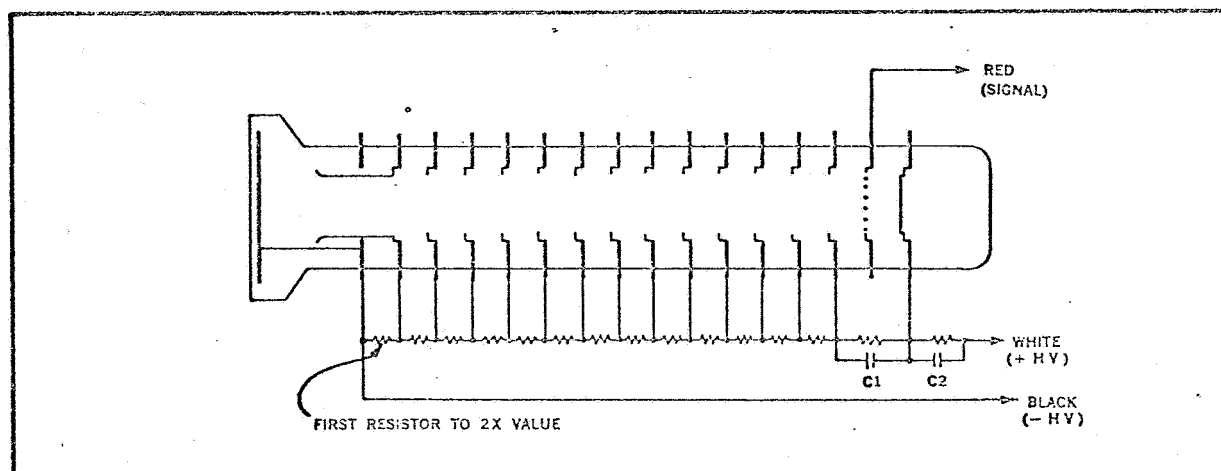
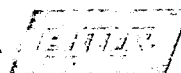


FIGURE 5

SCHEMATIC DRAWING

Resistor values are equal throughout.

ELECTRO-MECHANICAL RESEARCH, INC.



P. O. BOX 41, PRINCETON, N. J.

APPENDIX C

OPTICAL CONCEPTS BASED ON PULSE-WIDTH MEASUREMENT

The evolution of the pulse-width optical concept finally selected for detailed design is sketched briefly here. The various approaches differ primarily in the configuration of the detector array.

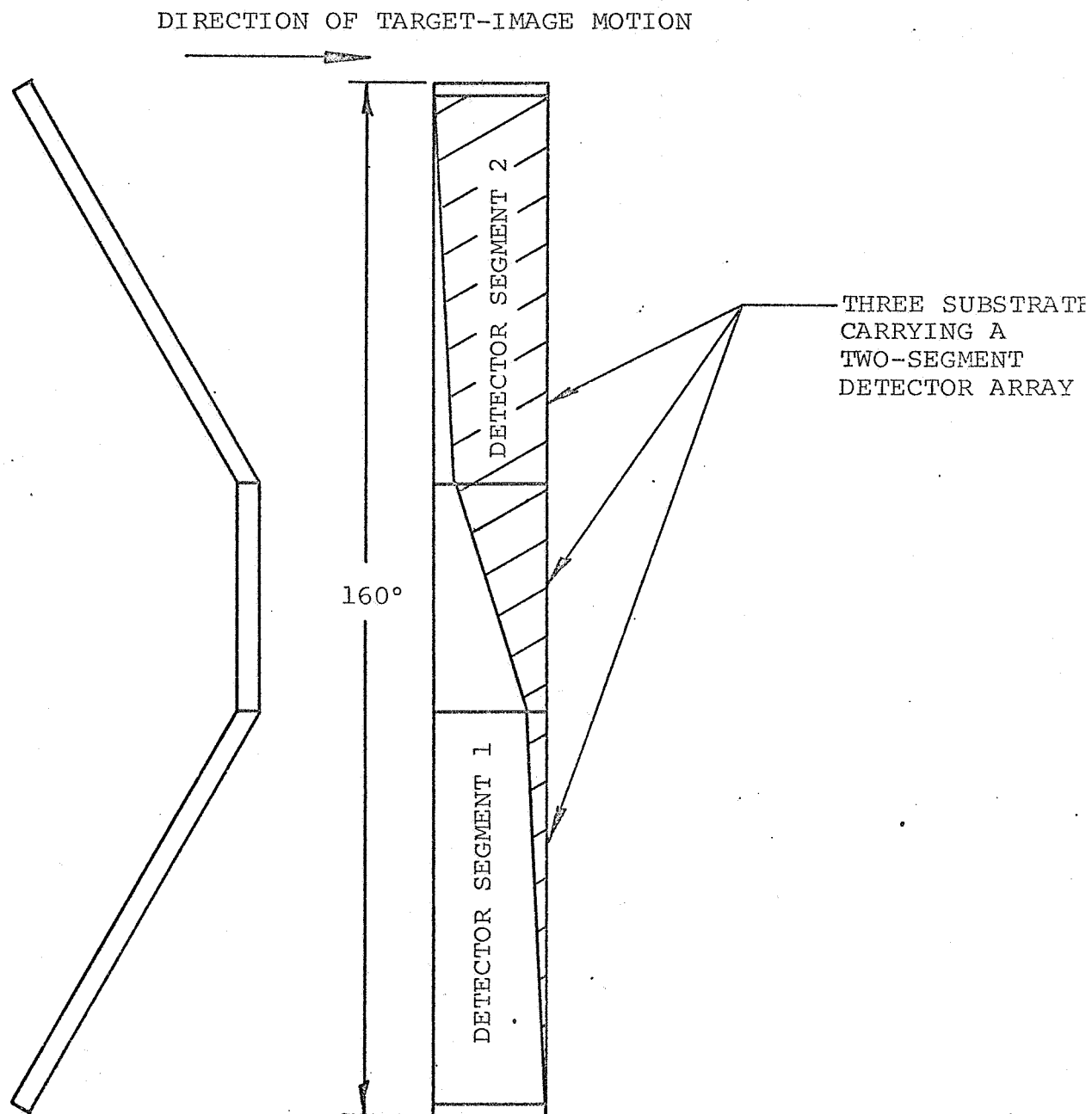
1. Three-Substrate Split-Rectangle Array

The first concept, that proposed prior to initiation of the EAS program, envisioned a detector array of the configuration shown in Figure C-1, placed at the focal plane of a wide-angle lens. The purpose of the three substrates set at angles to each other is to simplify the lens, since the substrates could follow the curved surface of best focus of the lens selected for the design. A two-segment detector is formed on the substrates. As the vehicle spins, the images of the earth, the moon, and the other planets sweep across the detector pattern from left to right, producing pulses from the two segments. If an image passes over the exact center of the array, the two segments will produce pulses of equal length. However, if the image passes over the array above the center, the pulse from the first detector segment will be slightly shorter than the pulse from the second detector segment, and vice versa. These pulses are processed in the system electronics (see Appendix D), and the resulting output is an accurate linear indication of the vertical position of the target image on the detector array. The output is relatively unaffected by the spin rate of the vehicle, the angular diameter of the target, or poor image quality of the lens.

The major disadvantages of this approach are that two optical channels are required (i.e., two sets of lenses, filters, housings, etc.) to provide for transmission in the long and short wavelengths (red and blue filters will perform this function), and that color discrimination must rely on the difference in the outputs of two completely separate detector arrays. A relative change in responsivity of the detectors would result in incorrect color measurement.

2. X-Detector Array

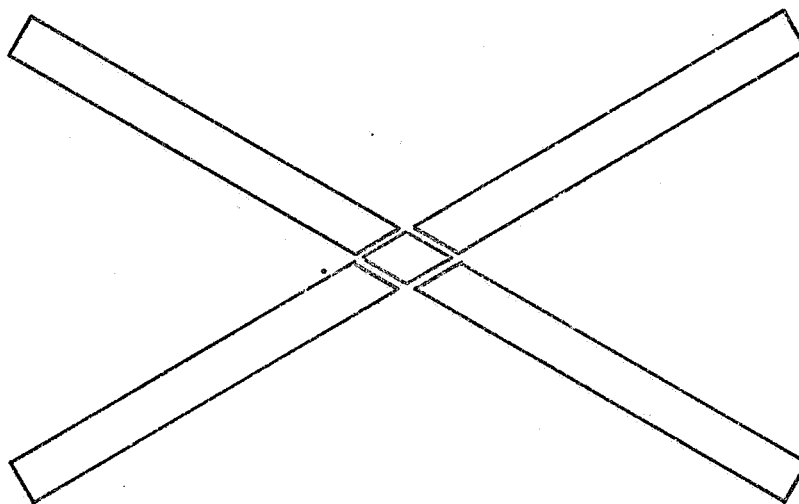
The detector pattern for this approach is illustrated in Figure C-2a. Five detector segments form an "X" at the focal plane of the lens. As the vehicle spins, the target image crosses the detectors in the direction indicated, producing pulses for signal processing (again see Appendix D). If the target image is centered vertically on the "X", pulses occur simultaneously from the two legs; if the image is not centered, pulses from one leg or the other will occur first. The time difference between the occurrence of the pulses provides a measure of the vertical position of the image on the detectors.



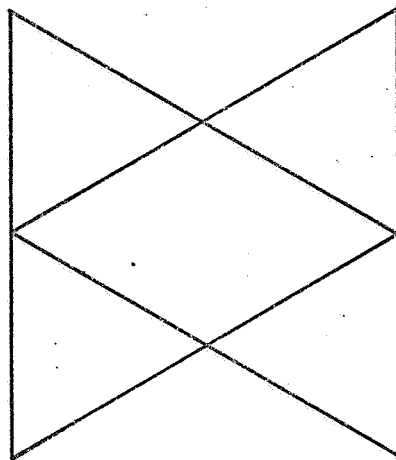
THREE-SUBSTRATE, SPLIT-RECTANGLE DETECTOR ARRAY
(ONE CHANNEL)

FIGURE C-1

DIRECTION OF TARGET-IMAGE MOTION



a. X-Detector Pattern



b. Superimposed-Triangle
Detector Pattern

FIGURE C-2

This approach has the same disadvantages as the three-substrate, split-rectangle array described above in that two optical channels are necessary and two detectors are required for color discrimination. Also, the associated electronic circuitry is somewhat more complex. An advantage is that detector noise would be somewhat less.

3. Superimposed-Triangle Array

The detector pattern for this approach is illustrated in Figure C-2b. Five detector elements are arranged to form two triangles superimposed on each other. As before, pulses are produced as the target image passes across the detectors during vehicle spin, the pulse widths varying with the vertical location of the image crossing. Again, the difference between the pulse widths is a measure of the vertical position of the image on the detectors.

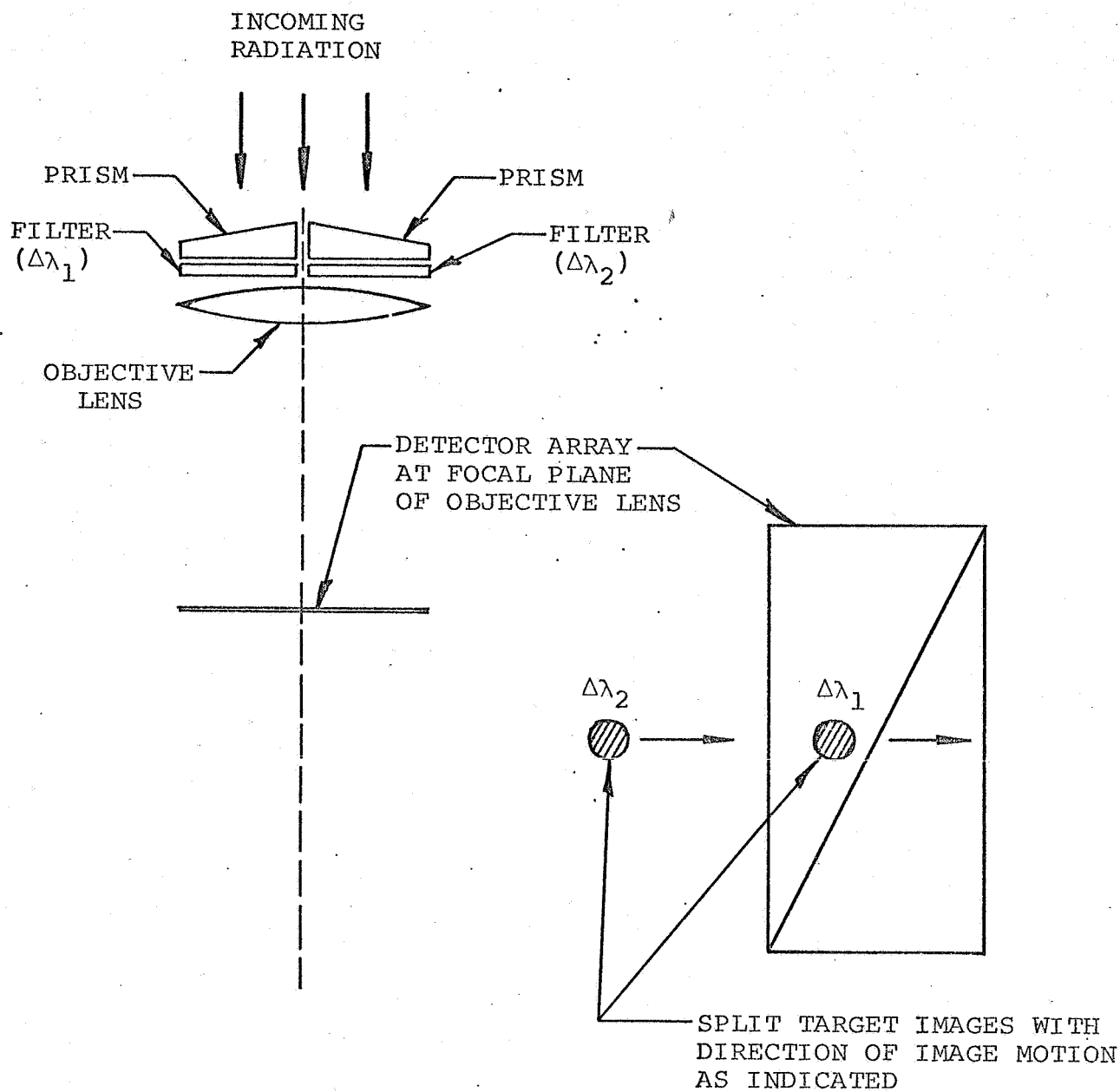
This approach has a slight advantage over the three-substrate, split-rectangle approach in that a change in target-image size introduces no null error whatever. However, in addition to the somewhat more complex detector pattern, it has the same basic disadvantage of requiring two optical channels and two detectors for color discrimination. As with the X-detector array, there is some additional electronic complexity.

4. Prism/Filter Approach

This concept was generated in an effort to provide color discrimination with a single detector and to eliminate the need for two separate optical channels. In this approach (see Figure C-3), two prisms are positioned immediately in front of the objective lens, one prism bearing (or having adjacent to it) a blue filter and the other a red filter. A detector array, which can be a split-rectangle or any of the other patterns described above, is placed at the focal plane of the objective lens. Instead of a single target image sweeping across the detector array, two images will cross the array in sequence, one red and one blue. This arrangement provides both aspect and color information from a single array. The two images must be sufficiently separated that the first image will be off the detector before the second one starts across.

As already noted, this approach has the advantages of requiring only one optical channel and a single detector. The first advantage will result in reduced system size and weight. The second advantage will provide the same detector responsivity and thus correct color measurement.

This approach has two disadvantages. First, the minimum angle of separation between the target and interfering targets is greater than with the three-substrate, split-rectangle approach. Second, since color information is present in sequential rather than simultaneous signals, the complexity of the electronics is somewhat increased.



OPTICAL SCHEMATIC
PRISM/FILTER APPROACH

FIGURE C-3

5. Separate-Color-Detector Approach

This approach eliminates the need for prisms while still using only a single optical channel. A detector array in the form of a split rectangle bounded by a blue and a red filter is placed at the focal plane of the objective lens (see Figure C-4). As the target image sweeps across the detector array, pulses are generated for processing to indicate aspect angle by measuring pulse width in the same manner as for the approaches already described. In addition, as the target image sweeps first across the blue and then across the red filter, radiation is transmitted and condensed onto a separate color detector, which coincides with the image of the objective lens formed by the condensing lens. Thus two pulses are generated in sequence on the color detector, and the relative pulse amplitude is a measure of target color.

Again the advantages are only one optical channel, with color information available on one detector instead of separate detectors. In addition, aspect-angle signal-to-noise ratio is higher than with the three-substrate, split-rectangle approach, since the optical bandwidth is relatively wide.

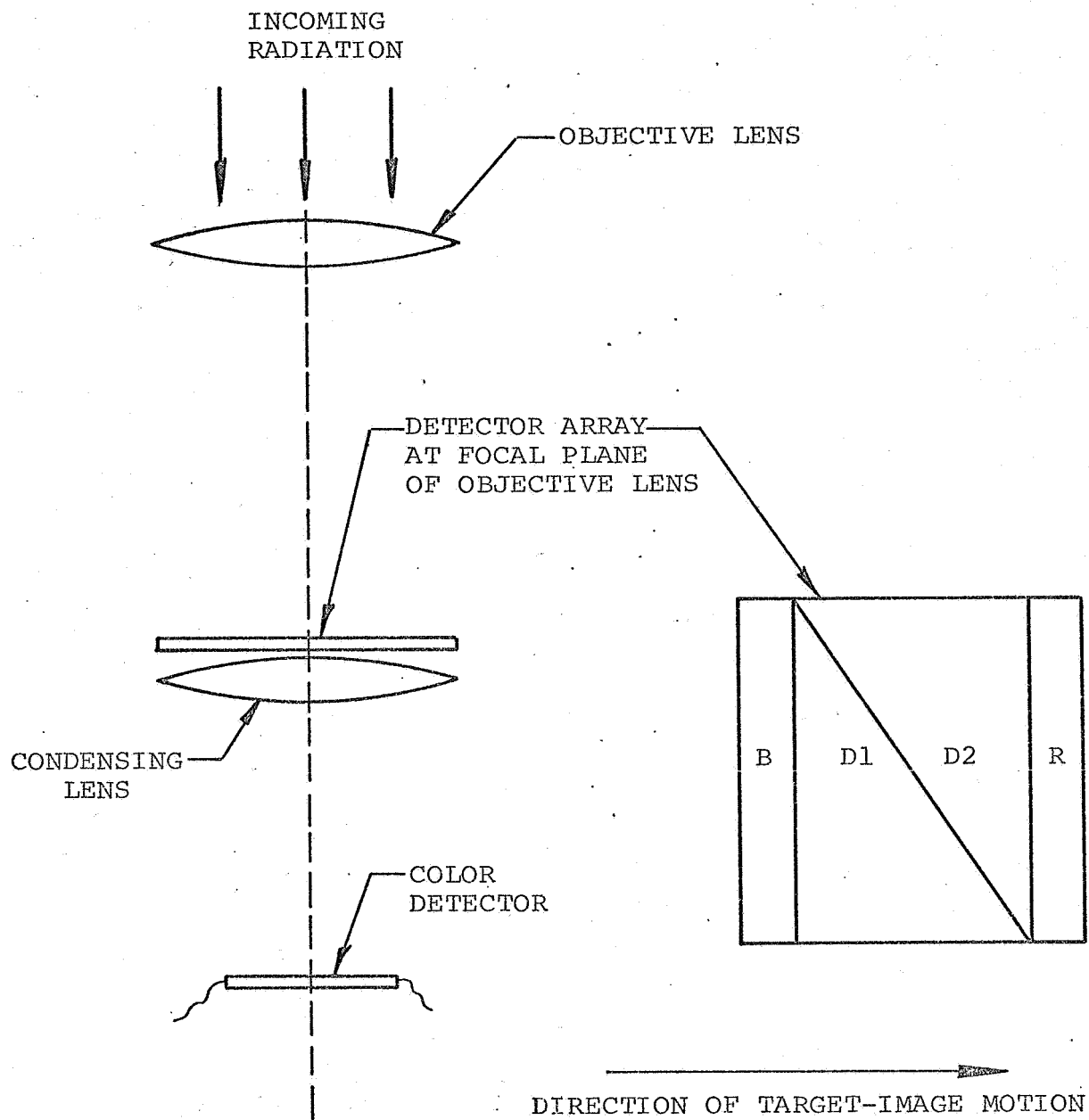
Disadvantages are that color signals are sequential, resulting in higher electronic complexity than for the three-substrate, split-rectangle approach, and minimum angle of separation between the target and interfering targets is slightly increased.

6. Single-Detector Approach

This approach was generated in an attempt to combine the best features of the five approaches described above. A blue and a red filter, shaped as indicated in Figure C-5, are placed at the focal plane of the objective lens. A condensing lens forms an image of the objective lens on a single detector. As the target image sweeps across the field of view, two pulses are generated in the detector. The relative width of these pulses is a function of aspect angle; the relative amplitude is a measure of target color. To prevent overlapping of the two signals at close distances to the target, the filters must be sufficiently separated that no image overlap occurs.

Advantages of this approach are a single optical channel, a single detector rather than an array, and a reduction in over-all electronic complexity over the system with the separate color detector.

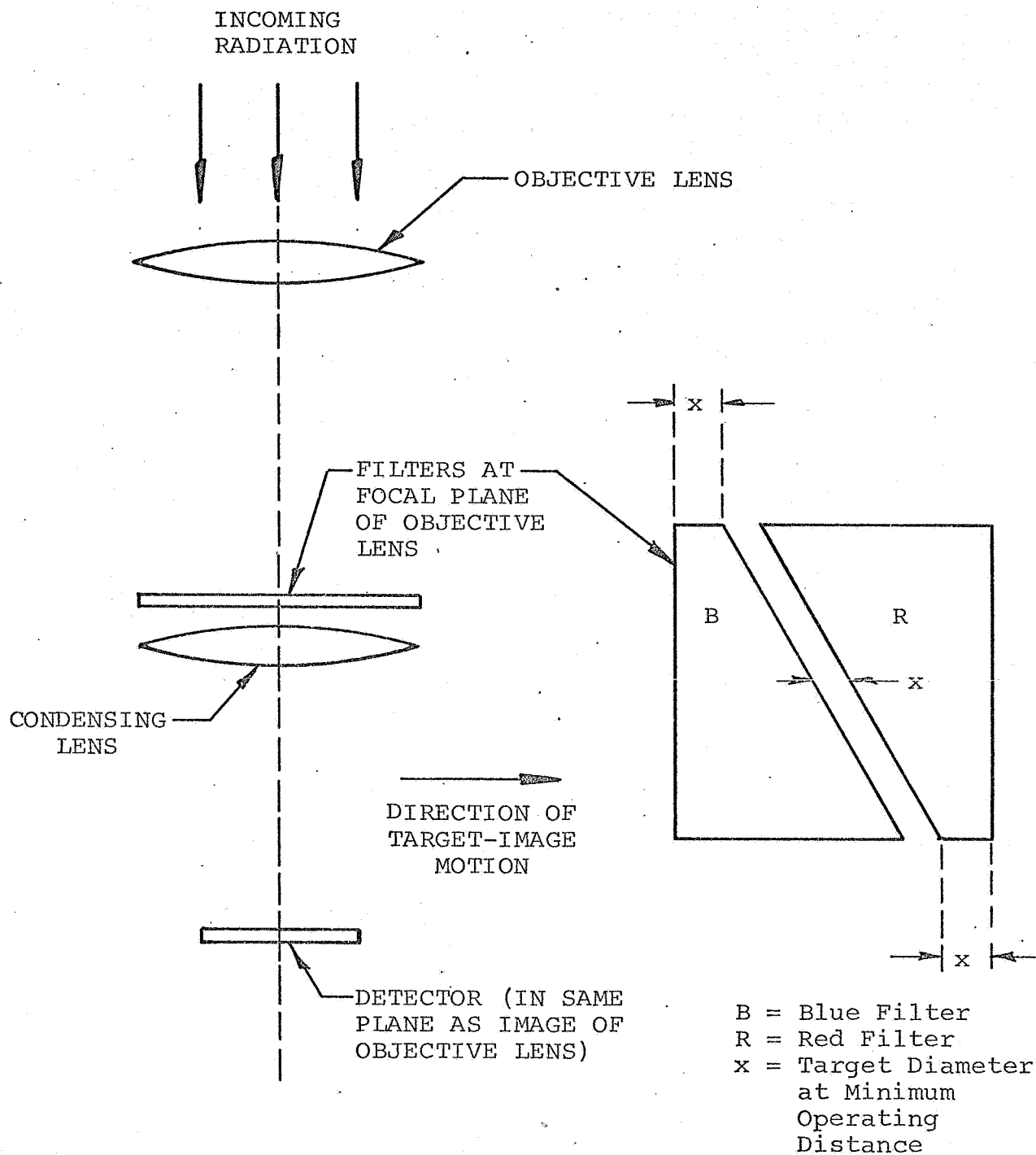
The major disadvantage is that the minimum angle of separation between the target and interfering targets is greater than in the three-substrate, split-rectangle approach.



D1 & D2 = Aspect-Angle Sensing Detectors
 B & R = Blue and Red Filter, respectively

OPTICAL SCHEMATIC
 SEPARATE-COLOR-DETECTOR APPROACH

FIGURE C-4



OPTICAL SCHEMATIC
SINGLE-DETECTOR APPROACH

FIGURE C-5

7. Selected Optical Concept

The approach finally selected for detailed design is described in Section IV.A. of this document, with the system itself described in detail in Section V. It is to some extent a combination of the split-rectangle detector array approach (C.1 above) and the single-detector approach (C.6). The selected system offers several significant advantages over the approaches described above. First, only one relatively simple optical channel is required. Second, radiation is completely defocused on the detectors; thus variations in sensitivity over the detector surfaces will have no effect on sensor operation, since only the average detector sensitivity is significant. Third, the detector configuration is relatively simple with stock items of the shape specified available. Fourth, electronic complexity is less because red and blue color information is presented to the electronics simultaneously rather than sequentially.

APPENDIX D

SIGNAL-PROCESSING CONCEPTS

The signal-processing concepts related to the various optical concepts based on pulse-width modulation (ref. Appendix C) are described first. The signal processing for the pulse-width-modulation approach selected for detailed design (ref. Section IV.A.1) is of course described in the body of the report (ref. Section IV.B and Section V.B).

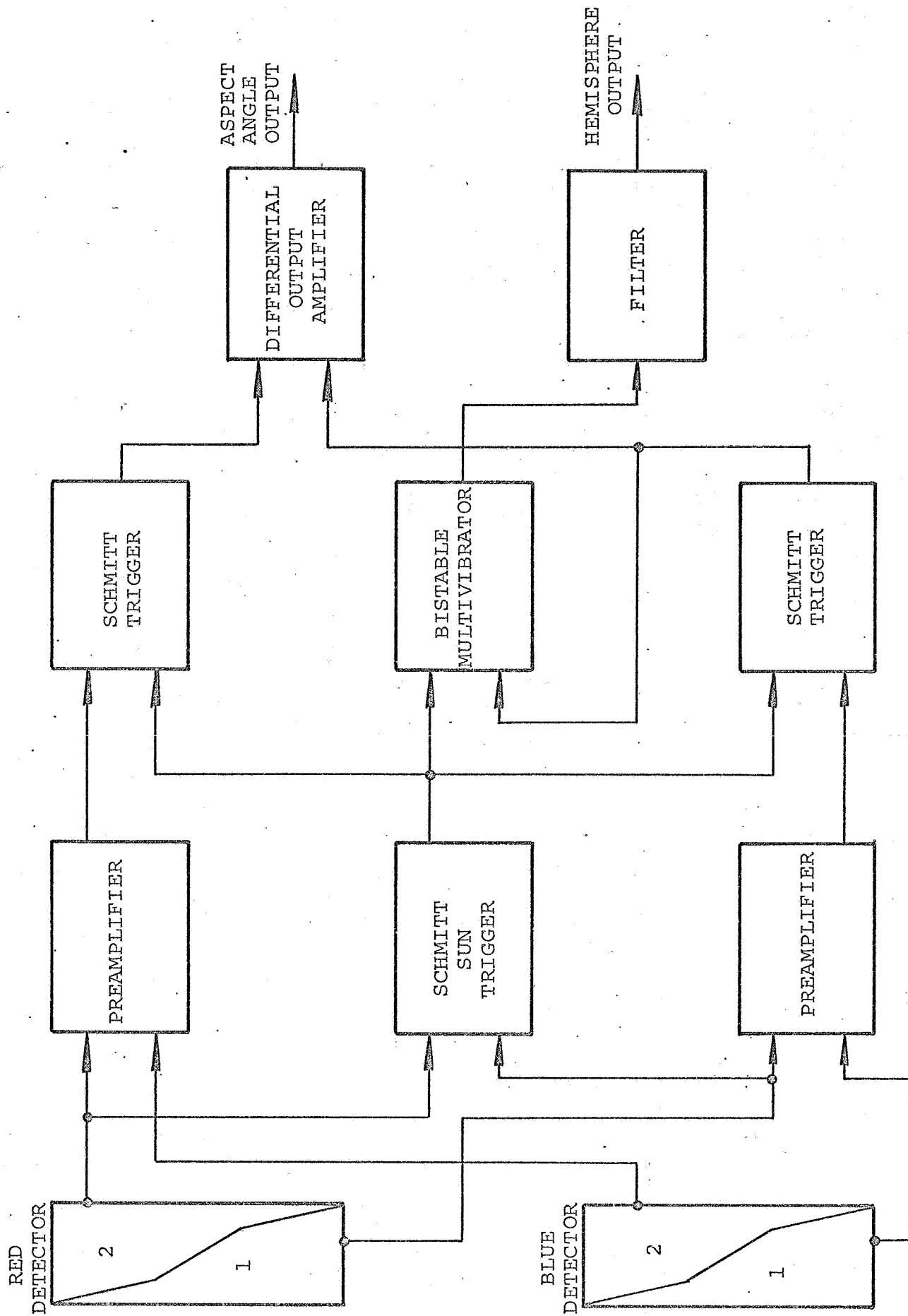
1. Pulse-Width Modulation

a. Three-Substrate Split-Rectangle Array

Refer to the block diagram, Figure D-1, and the detector schematic, Figure C-1. The outputs from the two detectors (one red and the other blue) are passed through separate preamplifiers and into separate Schmitt triggers. The triggering threshold on the triggers is set fairly low so that triggering occurs at the edges of the pulses. The earth look angle is computed as the filtered difference between the two Schmitt trigger outputs. For the idealized case (ideal point image sweeping across the detectors at a fixed spin rate), the dc component in a Schmitt trigger output would be proportional to pulse width and so the difference in the dc components of the Schmitt outputs would again represent earth look angle. If the spin rate increases, the pulse widths from both Schmitts would decrease but the pulse repetition rate would increase by exactly the same percentage. The dc component therefore remains unchanged. If the spin rate drops below some minimum value, ripple would begin to appear in the earth look angle output at the spin frequency. However, the dc or mean value of the output would remain accurate. If the angular width of the image increases, a constant would be added to the width of both detector output pulses. This constant increment of pulse width would cause a constant additional dc term to appear in both Schmitt outputs, but since the earth look angle is computed as the difference in dc outputs of the two Schmitts, the additional dc term would cancel out when the difference is taken. Again, no error will occur.

The width of the two Schmitt trigger outputs is compared by applying the outputs to a differential output amplifier. The voltage appearing at the amplifier output will be the difference between the two inputs, and hence proportional to the earth look angle (or aspect angle).

The output amplifier consists of a standard dual-transistor differential input stage followed by an integrated circuit amplifier. A two-section RC feedback network minimizes drifts and provides the necessary filtering. In addition, two Zener diodes and two resistors form a voltage divider in the feedback. This divider is inoperative until the amplifier output



SIGNAL PROCESSING FOR
THREE-SUBSTRATE SPLIT-RECTANGLE ARRAY

exceeds the breakdown level of the Zeners, at which time the gain of the amplifier increases by the ratio of the two resistors in the divider. By proper selection of these two resistors, the increase in scale factor can be made to compensate for the decrease in scale factor caused by the change in the interface angle of the two detector segments. The result is a constant scale factor over the full 160-degree range of the sensor.

Correction for errors introduced by the illuminated lunar surface is provided by scaling the two detector outputs so that when the illuminated lunar surface is in the FOV, the red detector output is canceled by the blue detector output. Partial cancellation of the earth signal also occurs, but since the earth-signal ratio of the two channels is different from the lunar-signal ratio, the net earth signal is much larger.

To eliminate errors introduced by the sun in the FOV, a Schmitt trigger is connected directly to the outputs of the detectors. Its triggering level is set so that it will not change state under any level of earth illumination, but when the sun crosses the FOV, the very large signal produced will trigger the sun Schmitt. The sun Schmitt output is coupled to the voltage-comparing Schmitts to prevent triggering by the outputs from the preamplifiers.

Hemisphere determination is derived by including an integrated-circuit bistable multivibrator that is placed in its "sun state" by the output from the Schmitt sun trigger and in its "earth state" by the output from either of the voltage-comparing Schmitt triggers. The bistable output takes one form when the vehicle spin axis is pointing into one hemisphere and the reverse form when the spin axis is pointing into the other hemisphere. By filtering the bistable output, a dc logic level is established that tells which way the spin axis is pointing, thus determining the hemisphere.

Should detector drifts cause marginal operation of the system described above, the signal processing could be modified by eliminating the Schmitt sun trigger and adding two integrated Schmitt triggers. The triggering voltage would be the difference between the blue and red detector outputs, with the detector outputs scaled so that they would cancel when the earth is in the FOV, thus preventing triggering from earth signals. When either the sun or the moon enters the FOV, the Schmitts would trigger and their outputs would be used to prevent the voltage-comparing Schmitt triggers from being switched by the outputs from the preamplifiers.

A further modification would add another output amplifier, which would provide information on sun look angle, in addition to earth look angle and hemisphere determination. The sun look angle would be derived in exactly the same way as earth look angle, that is, by comparing the widths of the two trigger outputs

in a differential-input feedback amplifier. This configuration is attractive in that a separate sun sensor could be eliminated or replaced by another earth-solar aspect sensor, thus providing redundancy and correspondingly greater reliability.

b. X-Detector Array and Superimposed-Triangle Array

Refer to the detector schematic, Figure C-2. Although the signal processing for these two arrays is similar to that for the split-rectangle array just discussed (ref. Figure D-1), it is somewhat more complex because in each case one segment of the array is common to both channels.

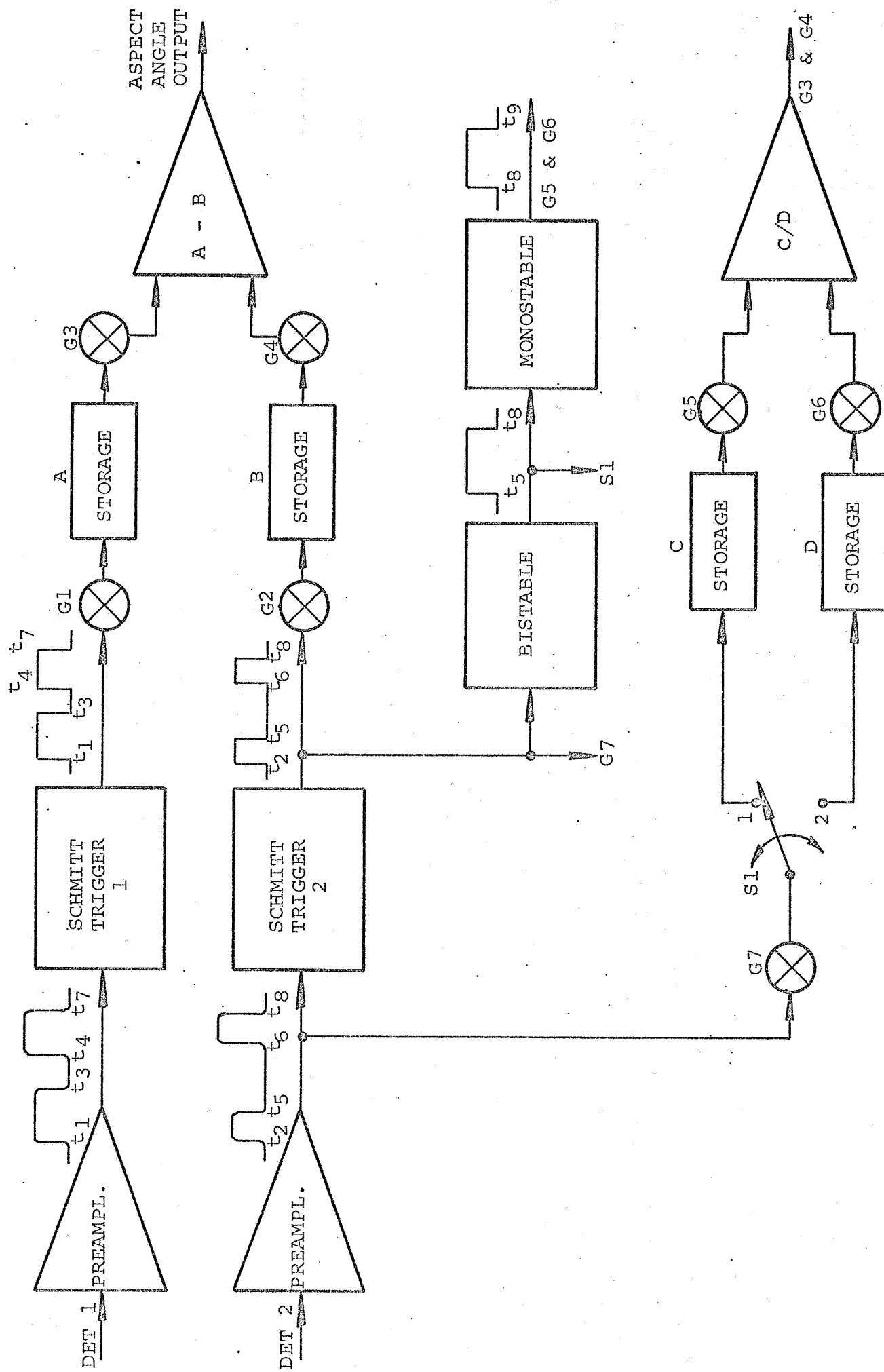
In the case of the X-detector array, the detectors are connected to two preamplifiers such that one of the preamplifiers receives inputs from one leg of the X while the other receives inputs from the other leg. The preamplifier outputs are applied to Schmitt triggers such that a state change is caused by passage of the earth-image leading edge over the detectors. The outputs of the two Schmitts then turn a flip-flop on and off; the duty cycle of the flip-flop is a measure of earth-image location independent of spin rate. An additional trigger monitors which of the two legs is crossed first and thus controls the polarity of the outputs.

In the case of the superimposed-triangle array, the five detectors are connected to two preamplifiers such that one receives signals from the three detectors forming one triangle while the other receives signals from the three detectors forming the other triangle. (As can be seen in Figure C-2b, the center detector is common to the two triangles.) The remainder of the signal processing is identical with that for the X-detector array.

The common detector requires some signal and impedance matching at the detector outputs. The resulting additional complexity over the electronics for the split-rectangle array is significant in that the signal level is reduced. This means that the maximum operating range of the X-detector and superimposed-triangle arrays would be smaller than that of the split-rectangle array.

c. Prism/Filter Approach

Refer to the block diagram, Figure D-2, and the optical schematic, Figure C-3. The signal processing for this approach is much the same as that for the split-rectangle system in that the pulse widths of the detector outputs are compared indirectly. The method of target discrimination is different, however, in that the amplitude of two sequential pulses must be compared to determine



SIGNAL PROCESSING FOR
WEDGE/FILTER APPROACH

FIGURE D-2

which target (earth or planets) is in view. Since the pulses are sequential, the first one must be stored until the second one occurs. In addition, storing must be done in the angle-computing section because the target cannot be identified until the second pulse has occurred. If the signal is from the earth, the stored information is then transferred to the differential output amplifier.

The following sequence of events occurs in the electronics when a target image passes over the detector array:

- t_1 - Leading edge of first image passes over leading edge of detector 1.
Schmitt trigger 1 output goes positive, opening G1.
- t_2 - Leading edge of first image passes over leading edge of detector 2.
Schmitt trigger 2 output goes positive, opening G2 and G7.
- t_3 - Trailing edge of first image leaves detector 1.
Schmitt trigger 1 output goes negative, closing G1.
- t_4 - Leading edge of second image passes over leading edge of detector 1.
Schmitt trigger 1 output goes positive, opening G1.
- t_5 - Trailing edge of first image leaves detector 2.
Schmitt trigger 2 output goes negative, opening G2 and G7.
Bistable output goes positive, changing S1 from position 1 to position 2.
- t_6 - Leading edge of second image passes over leading edge of detector 2.
Schmitt trigger 2 output goes positive, opening G2 and G7.
- t_7 - Trailing edge of second image leaves detector 1.
Schmitt trigger 1 output goes negative, closing G1.
- t_8 - Trailing edge of second image leaves detector 2.
Schmitt trigger 2 output goes negative, opening G2 and G7.
Bistable output goes negative, returning S1 to position 1.

Monostable output goes positive, opening G5 and G6.

If C/D ratio indicates earth, G3 and G4 open.

t_9 - Monostable output goes negative, closing G3, G4, G5, and G6.

All quantities stored in storage blocks are dumped.

It is noted here that in most of the systems described, logarithmic amplifiers would be used to amplify the detector outputs, because of the wide variations in signal strength between near-earth and far-earth conditions. In other words, some sort of limiting must be done if the amplifiers are to have sufficient gain for weak signals and yet not saturate on strong signals. Logarithmic amplifiers fulfill the limiting requirement. In addition, the amplitude of the output pulse from logarithmic amplifiers is dependent on the amplitude of the input pulse, which makes amplitude discrimination of the amplified signals possible.

d. Separate-Color-Detector Approach

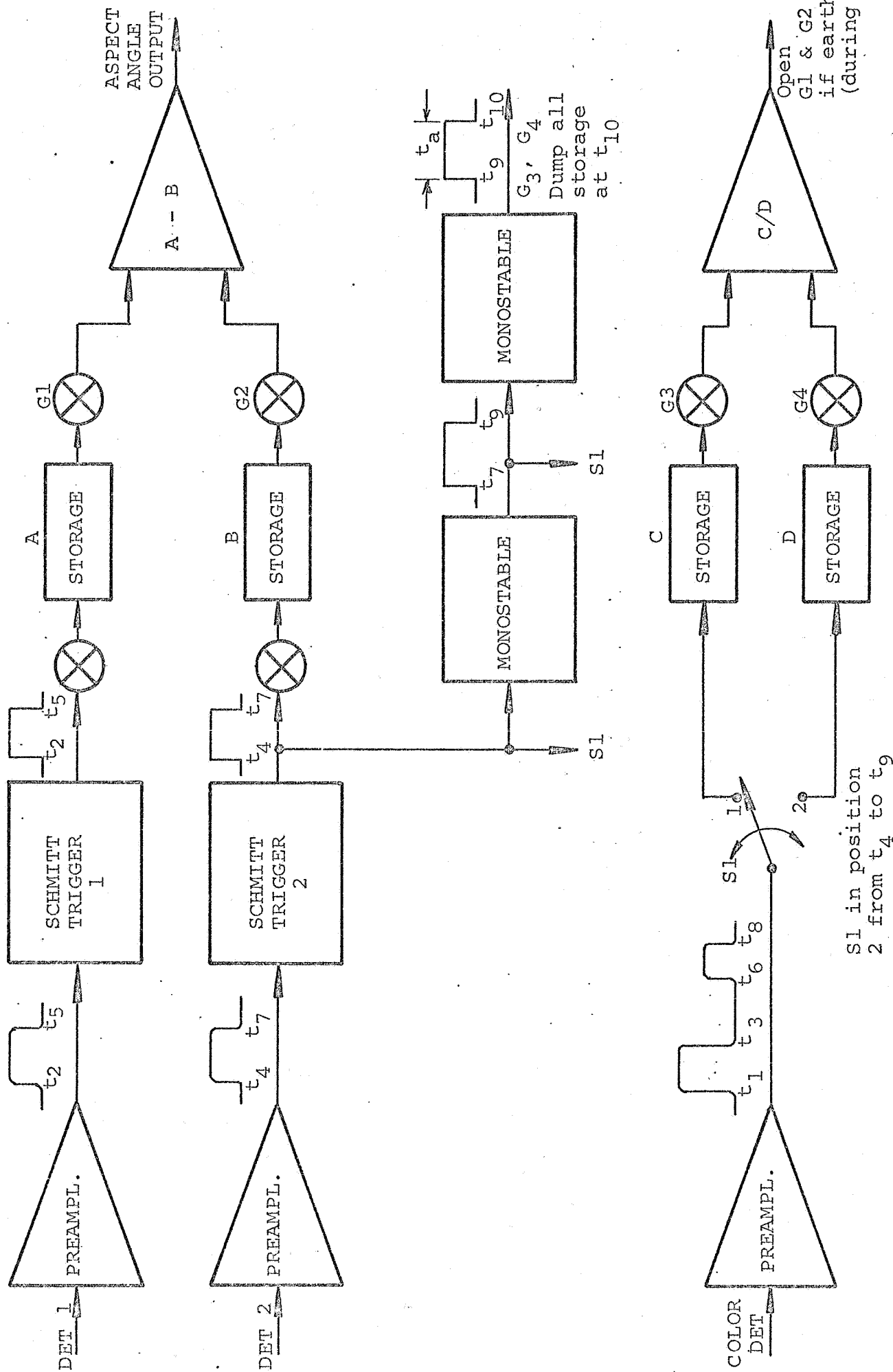
Refer to the block diagram, Figure D-3, and the optical schematic, Figure C-4. Computation of aspect angle and target discrimination in this system is almost identical with that for the wedge/filter approach just discussed. The principal difference is the addition of a separate color-detector amplifier. The sequence of events is substantially the same as for the wedge/filter approach.

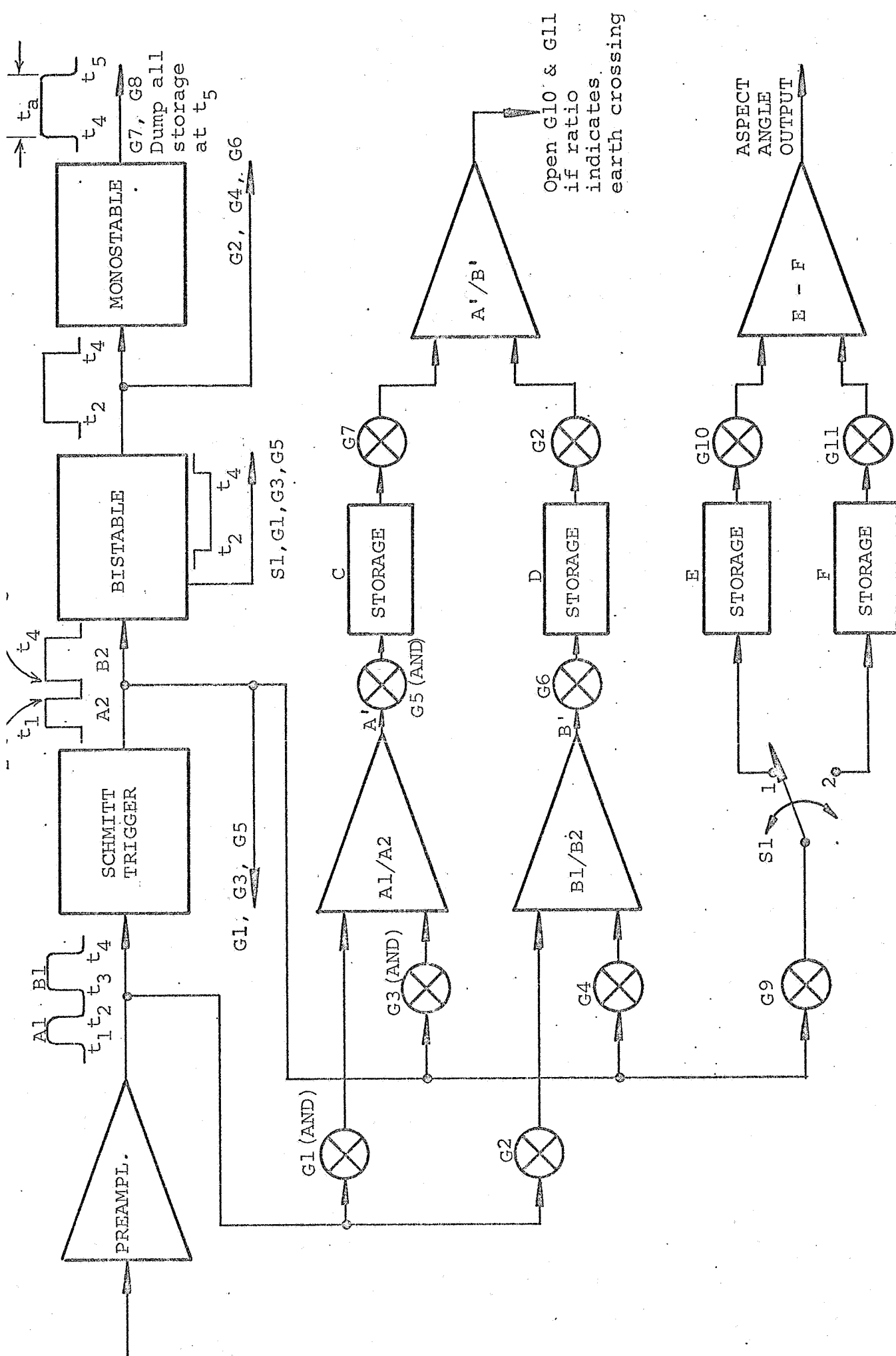
e. Single-Detector Approach

Refer to the block diagram, Figure D-4, and the optical schematic, Figure C-5. Aspect angle is computed in the same way as for the wedge/prism and separate-color-detector approaches. Target discrimination, however, is considerably different because a two-step ratio-taking process is involved, considerably increasing the electronic complexity. This is particularly true because the A1/A2 and B1/B2 blocks are analog devices and could be quite complex within themselves in order to supply the necessary accuracy. The A'/B' block is the same as the C/D blocks in the wedge/prism and separate-color-detector systems, and again the sequence of events is similar.

2. Pulse-Amplitude Modulation

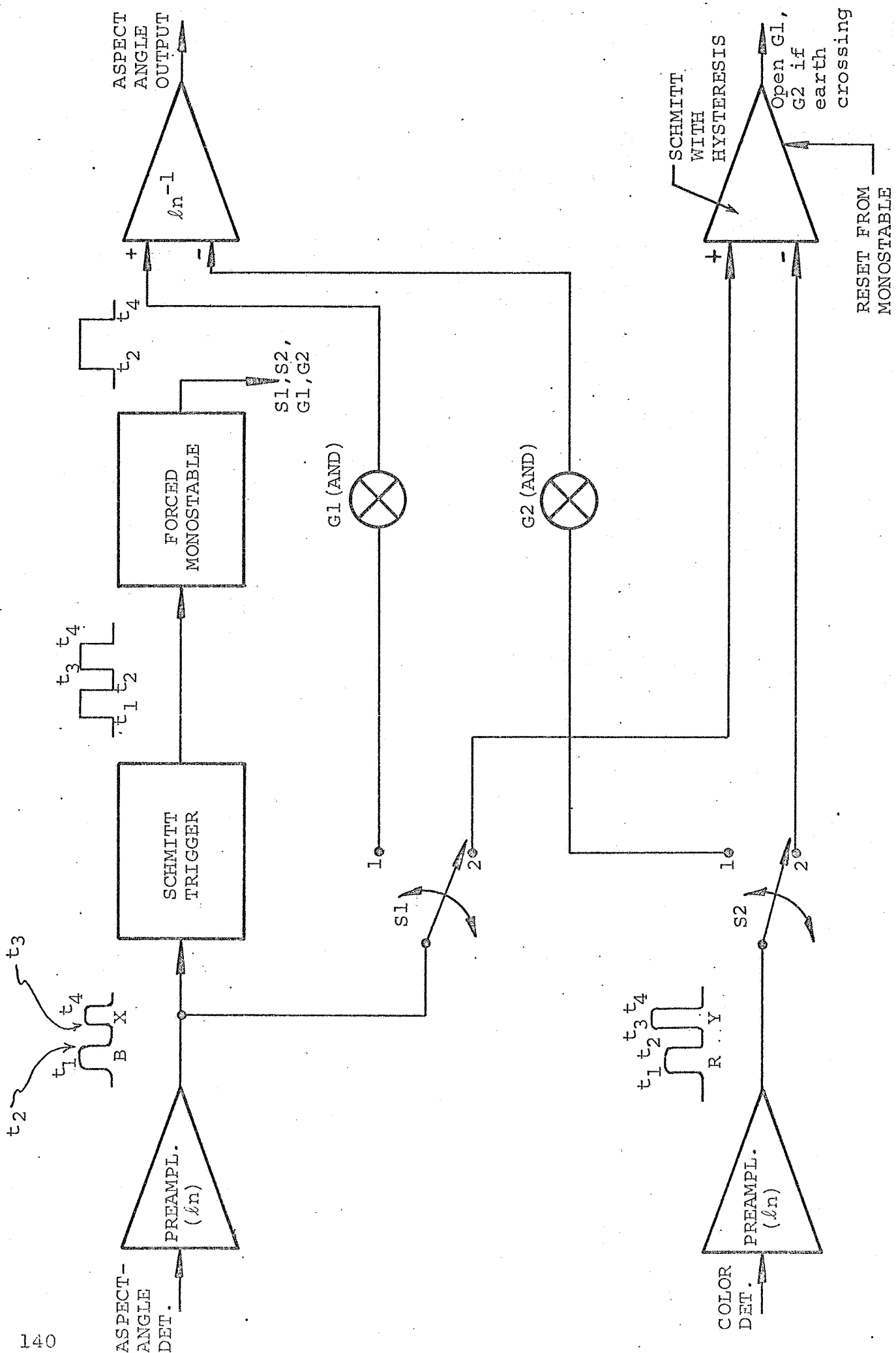
Refer to the block diagram, Figure D-5, and the optical schematic, Figure 23 (Section IV.A.). In this system, aspect angle is computed by comparing pulse amplitude instead of pulse width as in the systems discussed above. Target discrimination, however, is computed in the same way. Although the block diagram appears the least complex, electronically, of the systems described thus far, the actual complexity would depend on the complexity





SIGNAL PROCESSING FOR
SINGLE-DETECTOR APPROACH

FIGURE D-4



SIGNAL PROCESSING FOR
PULSE-AMPLITUDE CONCEPT
(VARIABLE-TRANSMISSION NEUTRAL-DENSITY FILTERS)

required to achieve the exponential function in the output circuit. Circuits of this type can be realized through the proper use of operational amplifiers and diodes.

3. Direct-Digital Concept.

a. Binary Coded Mask

Refer to the block diagram, Figure D-6, and the schematic, Figure 24a. This system, for small targets, is relatively simple electronically. Only four coded tracks are shown, but the system block diagram remains the same regardless of the number of tracks.

In operation, as the image sweeps across the field of view, the $e_b - e_r$ amplifier amplifies the outputs of detector segments 1, 2, 3, and 4. If the image passes over an unshaded area, a pulse is generated; if the image passes over a shaded area, the output remains unchanged. These individual pulses are then steered, by means of a steering gate, to the stage of the shift register corresponding to the detector segment that produced the pulse; i.e., the pulse from segment 1 is steered to register state 1, pulse 2 to state 2, etc. This steering, or commutating, is accomplished by amplifying the pulses from detector segments 5, 6, and 7 and using the amplified pulses to switch the $e_b - e_r$ amplifier output to successive register stages at the occurrence of each pulse.

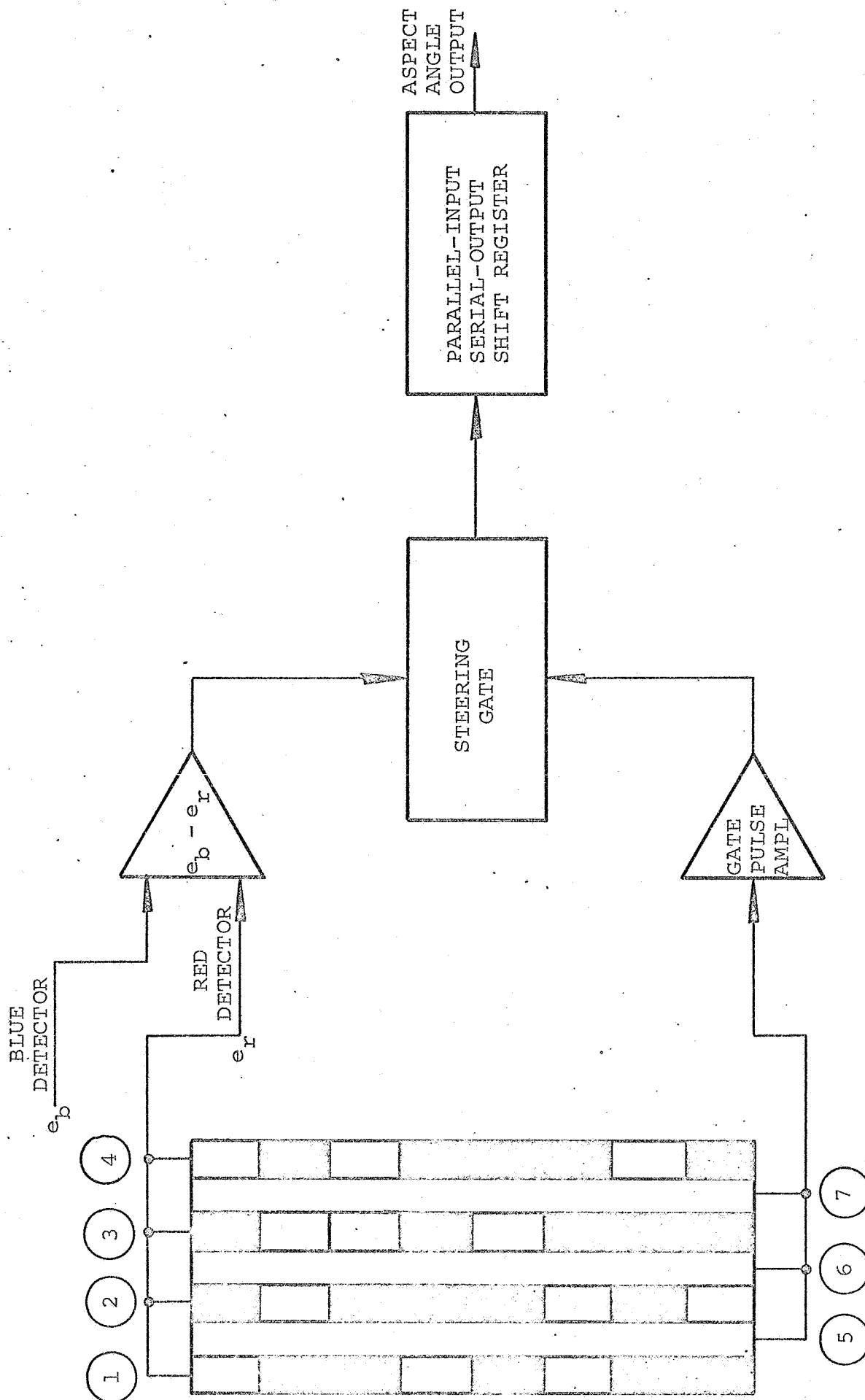
Target discrimination is accomplished in the same manner as in the split-rectangle system, that is, by comparing the outputs of two identical detector arrays having different colored filters in front of them. The comparison is made at the input to the $e_b - e_r$ amplifier.

As was mentioned before, this system works well for small targets. However, for large targets such as a 7-degree earth, the track coding becomes rather complex and a large number of tracks would be required to give the desired accuracy. Also, since a 7-degree target could cover more than one code track at a time, separate amplifiers would be needed for successive tracks.

b. Pulse Counting

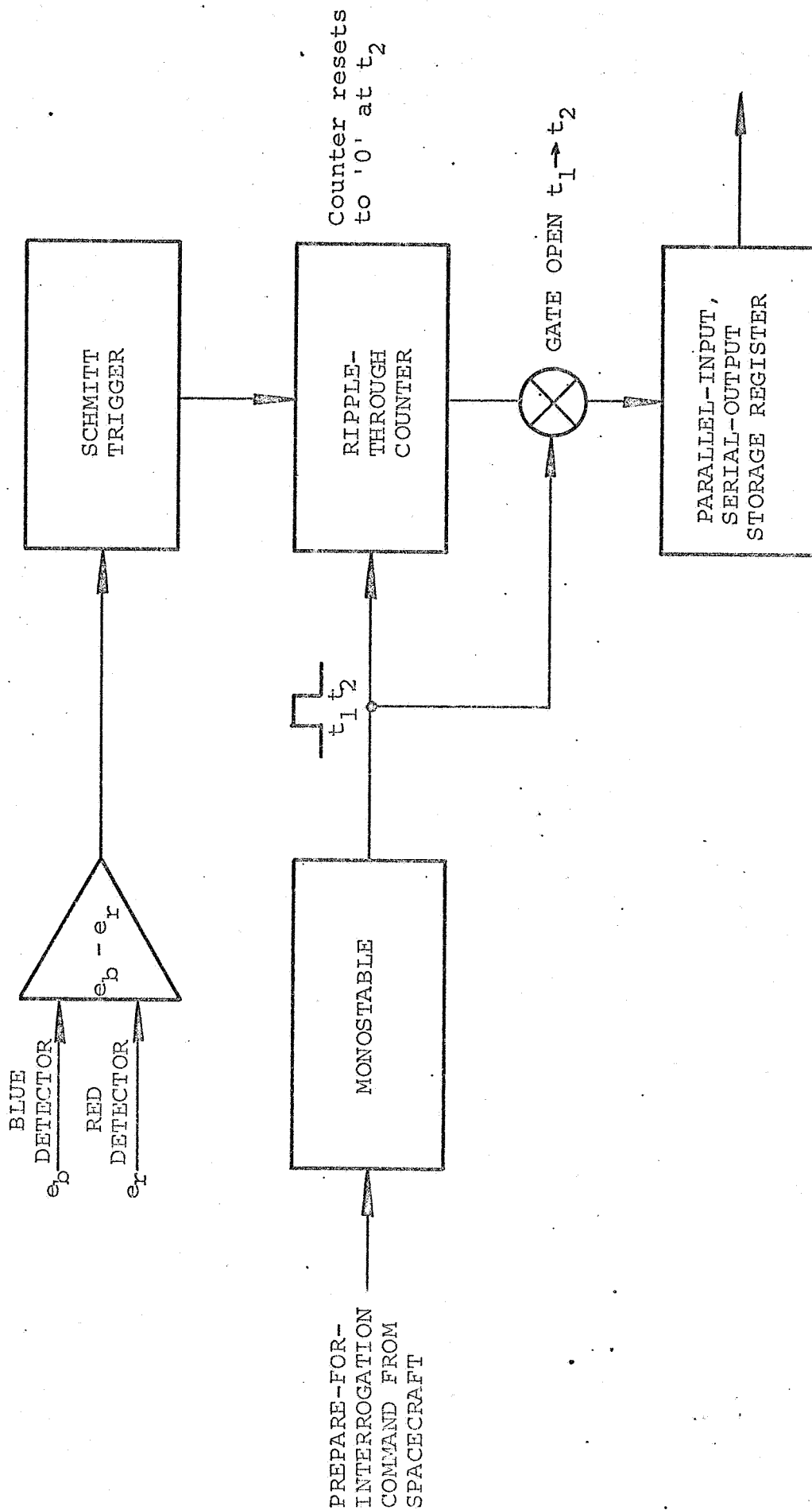
Refer to the block diagram, Figure D-7, and the schematic, Figure 24b. This system also works well for small targets and is somewhat simpler than the coded-mask system.

When an image sweeps across the sensor FOV, a pulse train is generated with the number of pulses being an indication of aspect angle. These pulses are "squared up" in a Schmitt trigger and then drive a ripple-through counter. When the spacecraft sends the prepare-for-interrogation command to the sensor, the monostable opens a gate, allowing the counter information to be sent to the storage register.



SIGNAL PROCESSING FOR
BINARY-CODED-MASK DIRECT-DIGITAL CONCEPT

FIGURE D-6



SIGNAL PROCESSING FOR
PULSE-COUNTING DIRECT-DIGITAL CONCEPT

FIGURE D-7

Target discrimination is accomplished in the same way as in the binary-coded-mask system.

The pulse-counting system has the same disadvantage as the binary-coded-mask system in that neither works well on large targets.

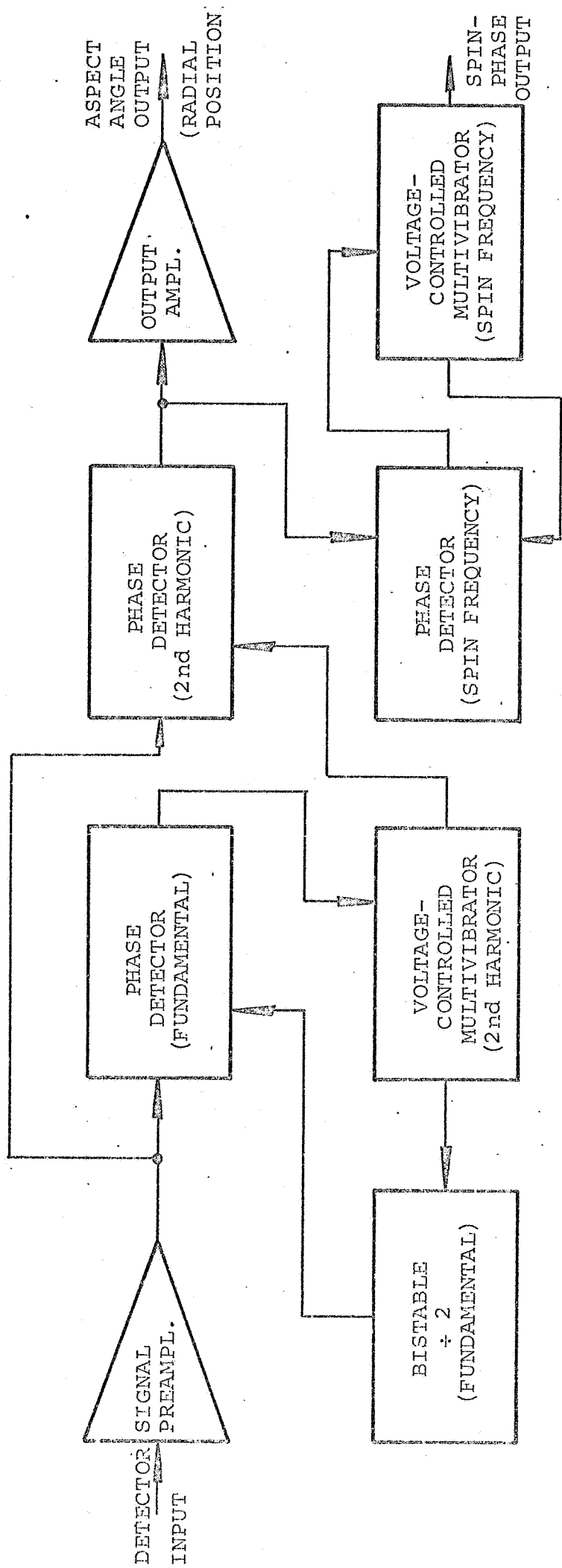
4. Star Sensor

Refer to the block diagram, Figure D-8, the optical schematic, Figure 25, and the reticle schematic, Figure 26. As the vehicle spins, the image of Canopus (when the vehicle is properly oriented) will appear to describe a circular path around the annular ring of the reticle. The average duty cycle is a function of the angular distance of Canopus off the sensor optical axis (which coincides with the vehicle spin axis). When the optical axis is aimed at the south ecliptic pole, the Canopus image will describe a circle 14 degrees off-axis and the average duty cycle will be 50%. If the axis is closer to Canopus than 14 degrees, the duty cycle will increase, and when the axis is greater than 14 degrees off Canopus, the average duty cycle will be less than 50%. Although the average duty cycle is a function only of the angular distance of Canopus from the sensor optical axis (and vehicle spin axis), the width of individual "on" pulses at a given angular distance from the axis varies as a sinusoidal function of the reticle phase (which will have a known phase relationship with control jets on the vehicle). As noted before, the reticle illustrated in Figure 26 is only schematic; an actual unit would have about 100 cycles instead of 10.

The radial position of Canopus is determined by measuring the second-harmonic content in the signal generated by the reticle modulation of the star light. This signal is first amplified in the signal preamplifier and then phase-detected in the second-harmonic phase detector. The phase-detector output is then filtered and scaled in the output amplifier, whose output is a dc analog voltage proportional to radial position of the image with respect to the vehicle spin axis.

Spin-phase determination is obtained by use of the lock loop consisting of the spin-frequency phase detector and the voltage-controlled multivibrator. Coding of the reticle is such that the output of the second-harmonic phase detector is modulated at the spin frequency; the lock loop locks to this spin-frequency component and the transitions of the multivibrator provide an accurate indication of spin phase.

To lock the frequency and phase of the sensor second-harmonic phase detector to the amplified detector output, a second voltage-controlled multivibrator is used. The frequency of this device is controlled by the filtered output of the fundamental



Note: Fundamental refers to the fundamental frequency of the amplifier output which is:
 Spin Rate (in rps) \times Number of Teeth on Reticle 2nd Harmonic = $2 \times$ Fundamental.

SIGNAL PROCESSING FOR STAR SENSOR

FIGURE D-8

phase detector. This is essentially a closed-loop servo with the only stable condition occurring when the fundamental bistable frequency is locked to the signal frequency.

Electronically, this system is one of the least complex and the most "solid" because it is completely coherent. It also has the smallest noise equivalent angle in the final output since the bandwidth can be as narrow as the expected vehicle tilt rates will allow.

APPENDIX E
OPERATING RANGE

Note: As was discussed in Section IV.B, it was found, during design of the coherent signal-processing electronics, that the limiting effect as far as long-range operation is concerned is dc offsets at the inputs to the integrating amplifiers rather than noise. The following discussion of the study of signal-to-noise ratio and operating range is included here as indicative of the encompassing investigations undertaken in connection with the design program.

Signal-to-noise (S/N) calculations were made and maximum operating ranges predicted for four versions of the EAS:

- 1) Non-coherent electronics with solid-state detector.
- 2) Non-coherent electronics with photomultiplier tube.
- 3) Coherent electronics with solid-state detector.
- 4) Coherent electronics with photomultiplier tube.

Since the maximum operating range of any system that measures reflected sunlight is a function of phase angle, maximum ranges versus phase angle were calculated, based on the assumed conditions listed below. The effect of the periodic pulse of solar flux was ignored.

Diameter of objective lens	18 mm (0.71 in.)
Transmission of objective lens	90%
Transmission of condensing lens	90%
Transmission of blue and red filters	90% within design bandpass 0% outside design bandpass
FOV width	10° (+ 1.5° for tolerance)
Earth condition	"Red" (conservative case). Range will be greater with earth in average ("blue") condition.
Photomultiplier tube	EMR 541D-05-14
Solid-state detector	ENL 601-10

S/N: Non-coherent system

10/1 peak signal to
0-to-peak noise

Coherent system

3/1 peak signal to
rms noise

Temperature

Ambient (20 to 25°C)*

Mission

In or close to ecliptic
plane

Results of these calculations are shown in Figures E-1 through E-3. As can be seen, several factors besides S/N limit operating range. With the photomultiplier-tube systems, the operating region is entirely bounded by these other factors, which are described briefly below.

1) At distances where the V-magnitude of the earth is -1 or greater, the earth signal drops to a level comparable to the signal of some of the brighter stars. These stellar color temperatures vary widely; some appear redder than the earth, some bluer, and some about the same. Although discrimination against stellar targets could be incorporated, the complexity of such a device exceeds that of the EAS as conceived at the time.

2) The EAS will not operate when the angular separation of the earth and the sun, as seen from the spacecraft, is equal to or less than the width of the sensor FOV (along the spin direction).

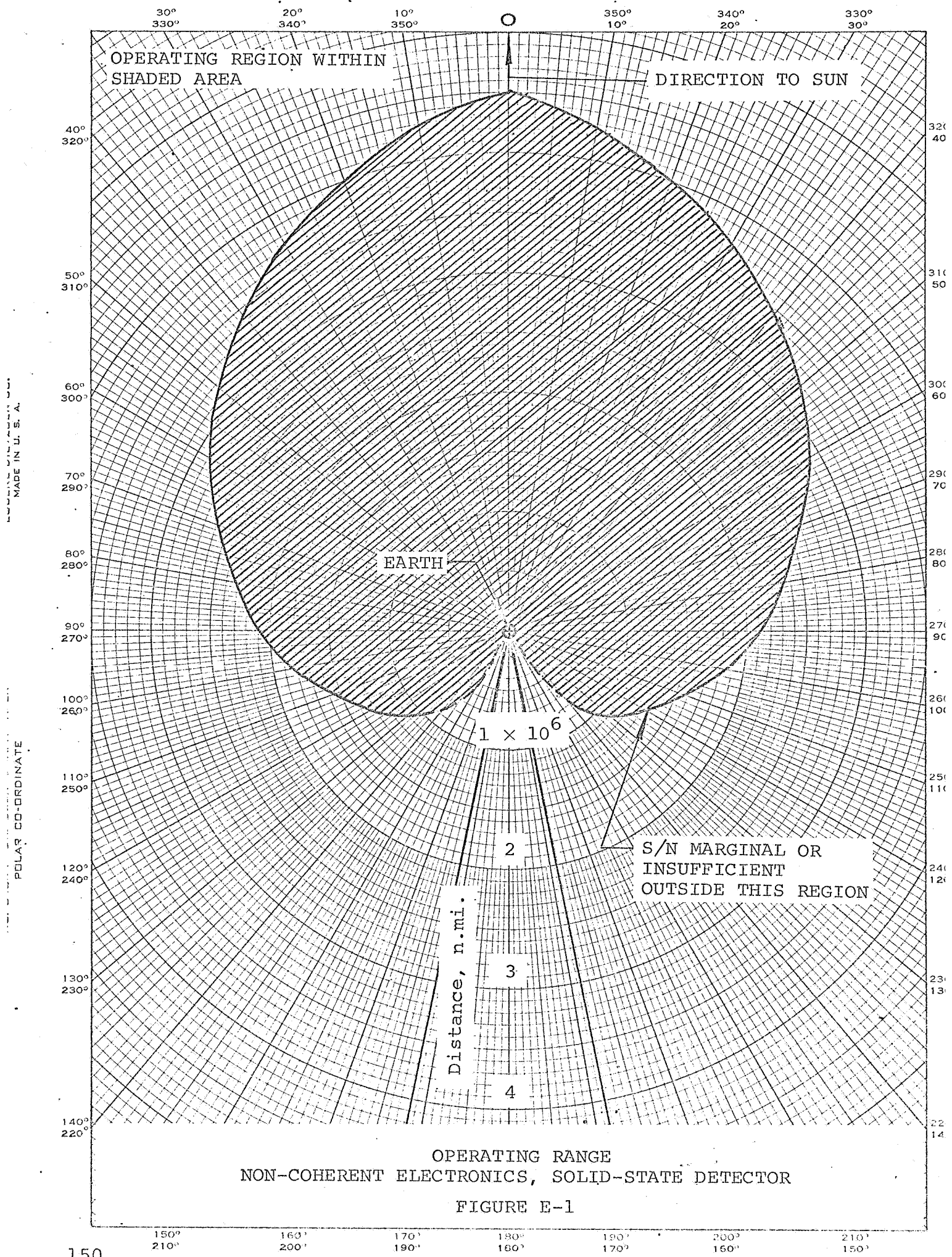
3) There is a limit on how close to the sun the sensor (and the spacecraft) can approach and still operate. This limit depends to a large extent on spacecraft thermal design, etc., and was not considered in the above calculations.

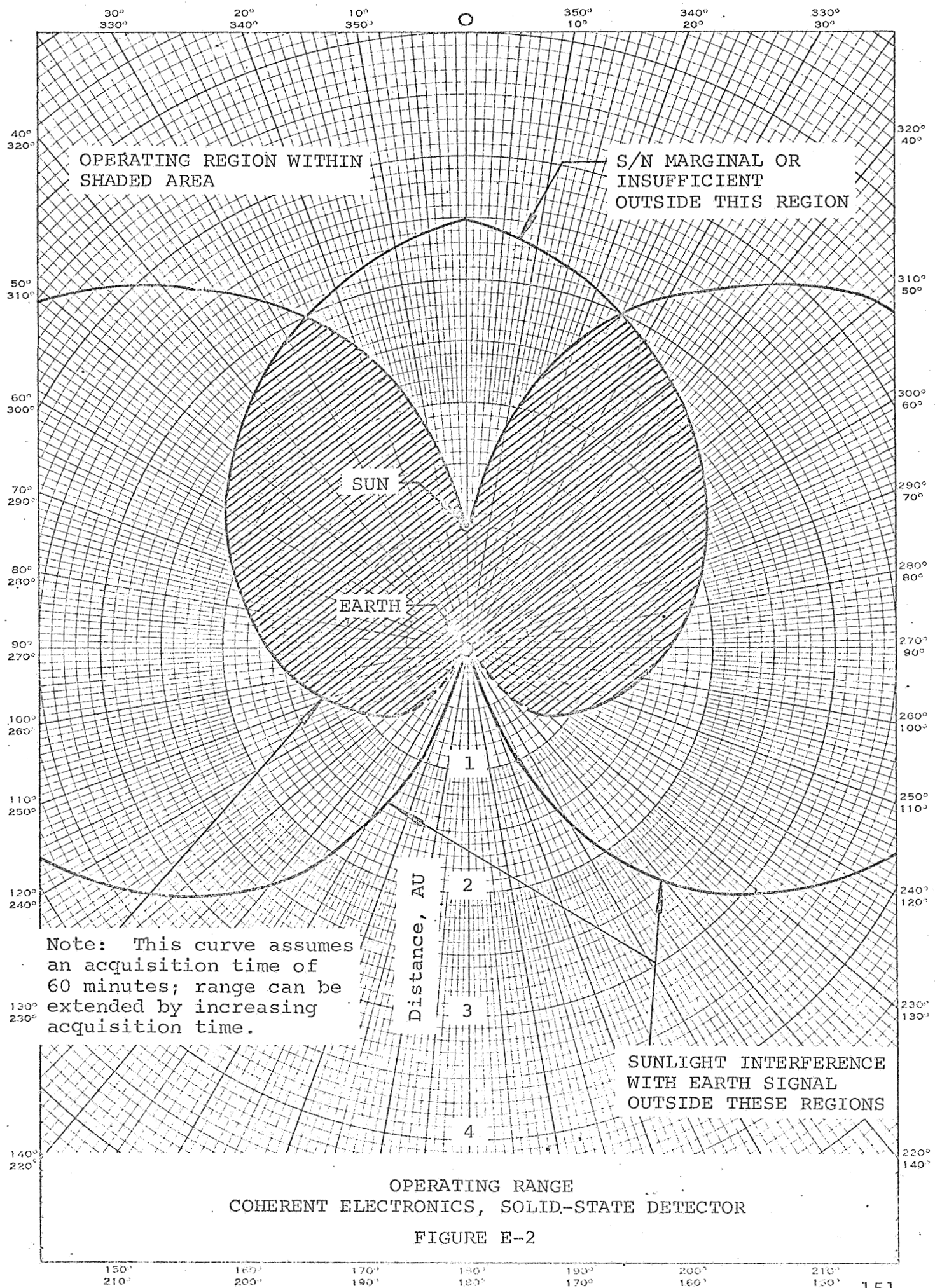
Another factor that influences operating range is the exponential decay of the solid-state detector output after the sun has passed from the field of view (ref. Section IV.C.2.d). In the non-coherent signal-processing system, the sun-generated 20.4-mV exponential decay would not increase the region of sun interference enough to change the operating region and range, as shown in Figure E-1. This is particularly true since the voltage is appearing simultaneously at both inputs to the differential preamplifier (both detector segments are exposed to the sun at the same time). The equivalent net input is then only a function of the unbalance between light falling on the two detector segments.

* At lower temperatures, down to -10°C, the S/N will stay the same or improve slightly. At higher temperatures, up to 50 or 60°C, the S/N will be reduced by about 50%. However, these high ambient temperatures should occur only during close approaches to the sun when the earth is about 1 AU distant at phase angles greater than 90 degrees.

In the coherent signal-processing system, however, the effect is more severe, since the minimum earth signal can be as low as 0.5 μ V at the maximum operating ranges. The manner in which the operating region of the coherent system is affected is somewhat complex, as is reflected qualitatively in Figure E-4. The reason for this complexity is that the detector output, because of its exponential characteristics, does not cause a fixed increase in the sun interference angle* but instead has a varying effect that is dependent on the signal amplitude and is therefore a function of not only range but also of phase angle.

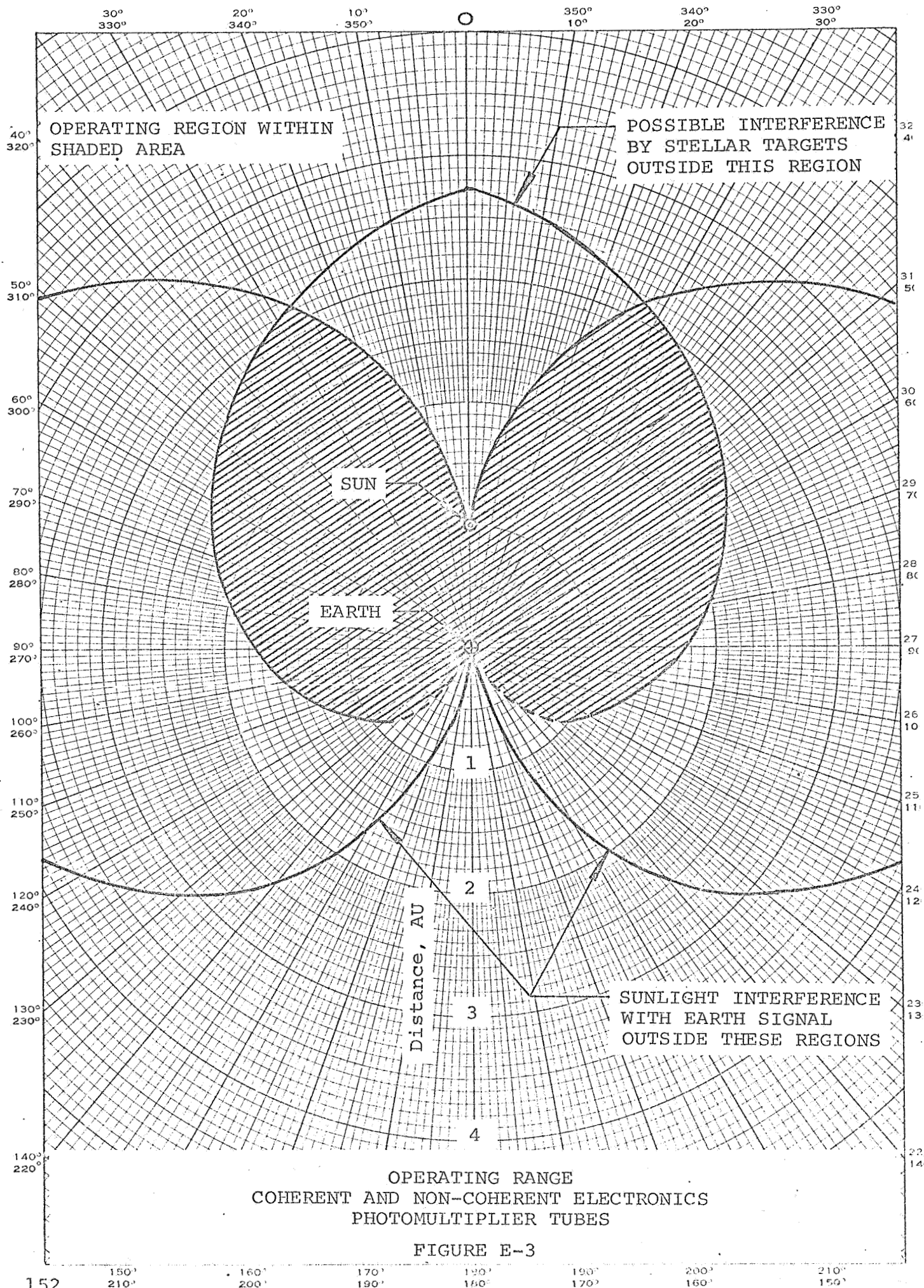
* Sun interference angle is defined as the minimum angle that can exist between the earth and sun look lines without impairing system performance.

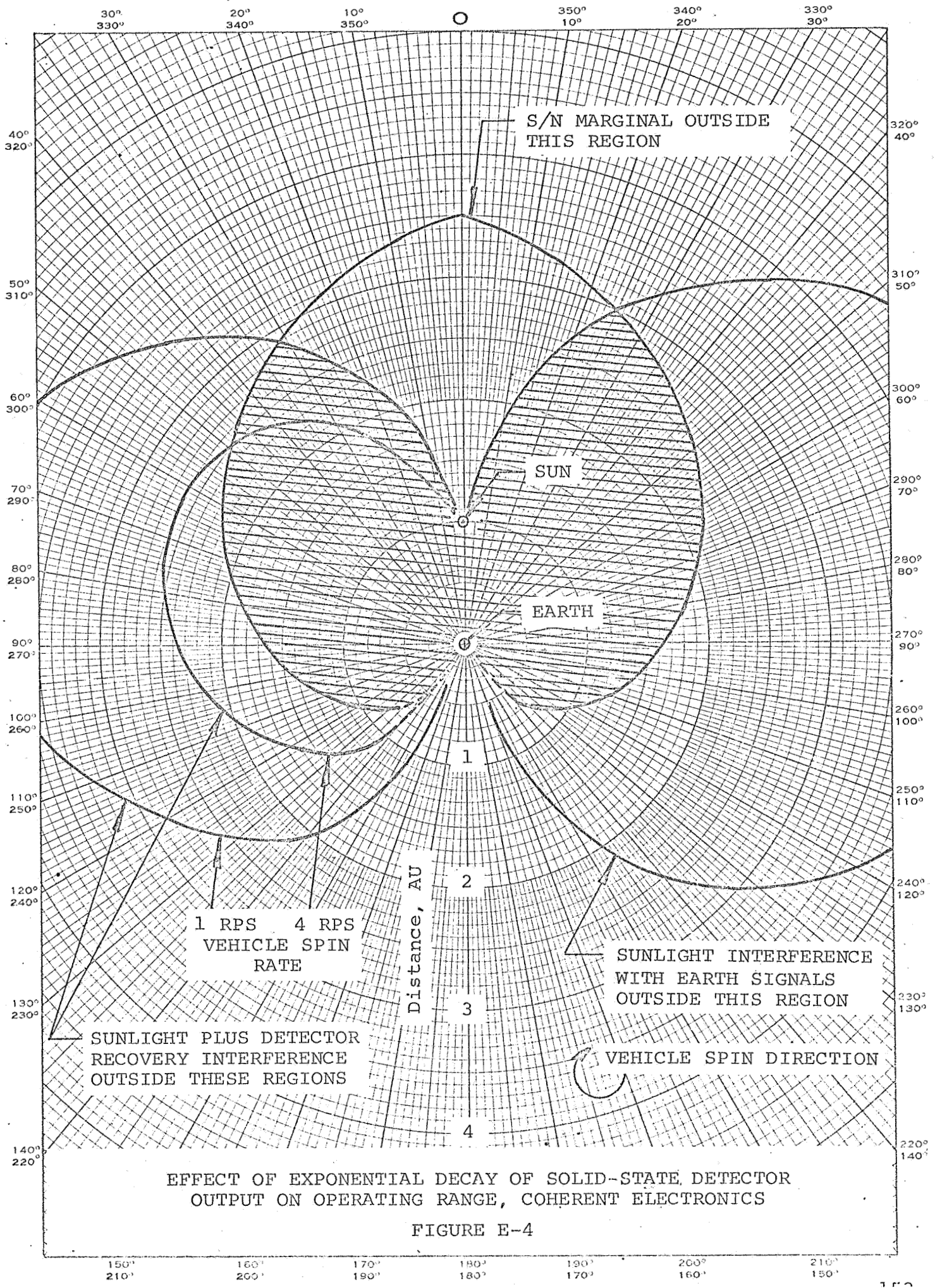




EUGENE L. DIEZEL, INC.
MADE IN U. S. A.

POLAR CO-ORDINATE





PRECEDING PAGE BLANK NOT FILMED.

APPENDIX F

WIDE-ANGLE FOV CONCEPTS

As noted in the main text, the optical configuration under consideration did not appear suitable for wide-angle FOV applications (>50 degrees) without modification. For an FOV of 50 degrees, the diameter of the detector sensitive area must be approximately twice the diameter of the objective lens, even with a very fast condensing lens system ($f\text{-no.} \approx 0.7$). The detector size increases rapidly with FOV at angles larger than 50 degrees.

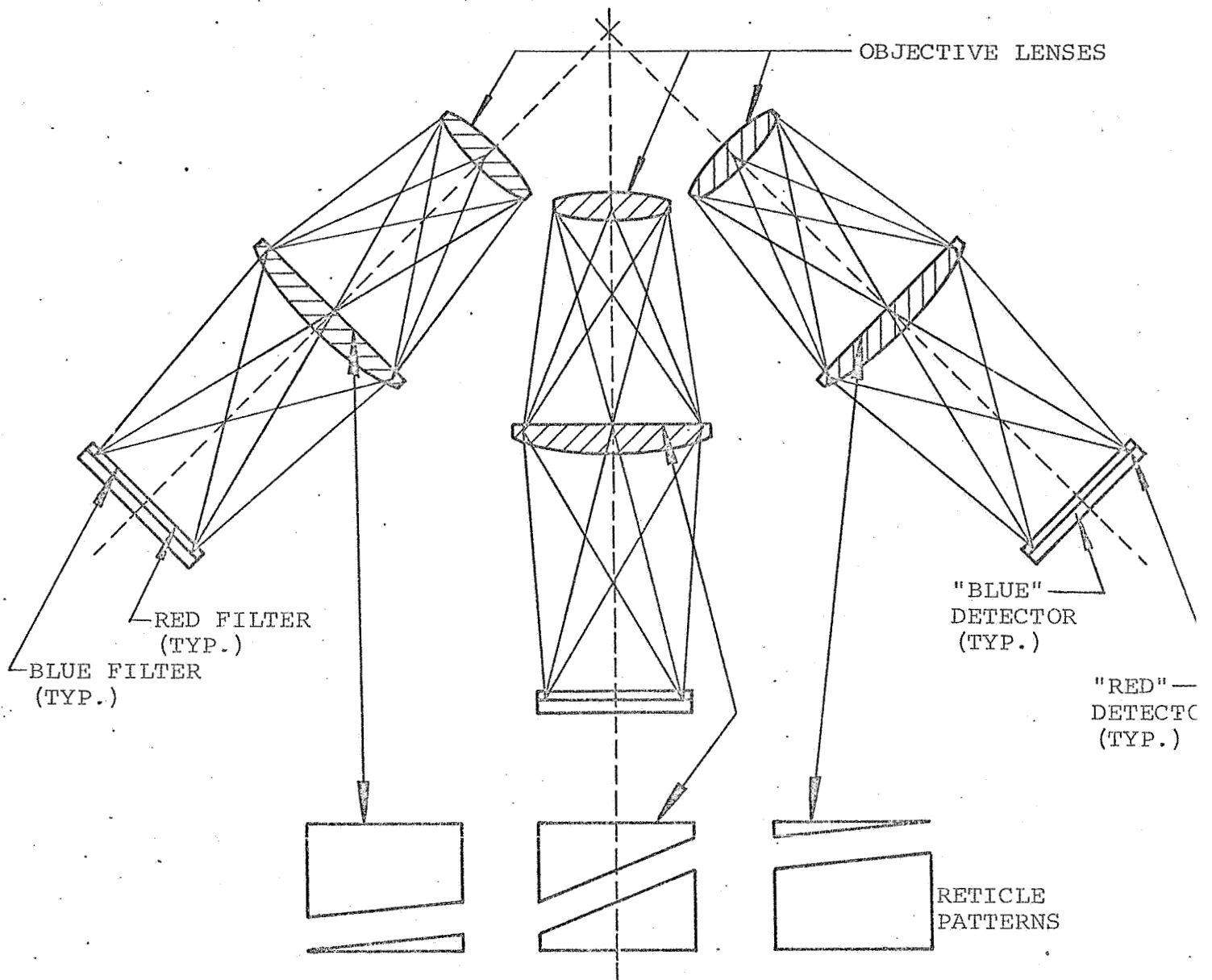
1. Initial Designs

Schematics of two versions suitable for a wide-angle EAS are shown in Figures F-1 and F-2. The configuration of Figure F-1 would be suitable for use with solid-state detectors. In this approach, the wide FOV is covered by using three optical channels, identical except for the reticles, oriented as indicated. The "blue" detectors (one in each optical channel) are connected in parallel, as are the "red" detectors. The three channels lie in a plane perpendicular to the vehicle spin direction. A more compact configuration, with the three channels not lying in this plane, would result in a formidable sun-shielding problem. The approximate reticle patterns (for a non-coherent signal-processing system) are also shown in Figure F-1.

Since the above wide-angle approach requires multiple detectors, it is not practical for a sensor using photomultiplier tubes. Figure F-2 is a schematic of a wide-angle system using a fiber-optics condenser. This system consists of a single optical channel with a wide-angle objective lens. A slightly curved focal surface is indicated, since a flat-surface wide-angle lens would require more elements and be bulkier. The reticle pattern at the focal surface is a composite of the three shown in Figure F-1. The entrance aperture of the fiber-optics bundle is located somewhat behind the focal surface so that the earth image is sufficiently defocused that the blur circle is large in comparison with the size of the individual fibers. As indicated, alternate fibers in the condenser entrance aperture are directed to the red and blue filters in front of the detector, which could be either a photomultiplier tube or a solid-state detector. The maximum range of this approach would probably be slightly smaller than that of a narrow-angle version using an equivalent objective-lens aperture and a conventional condensing lens, due to light losses in the fibers and cross talk between adjacent fibers alternately directed to the red and blue channels.

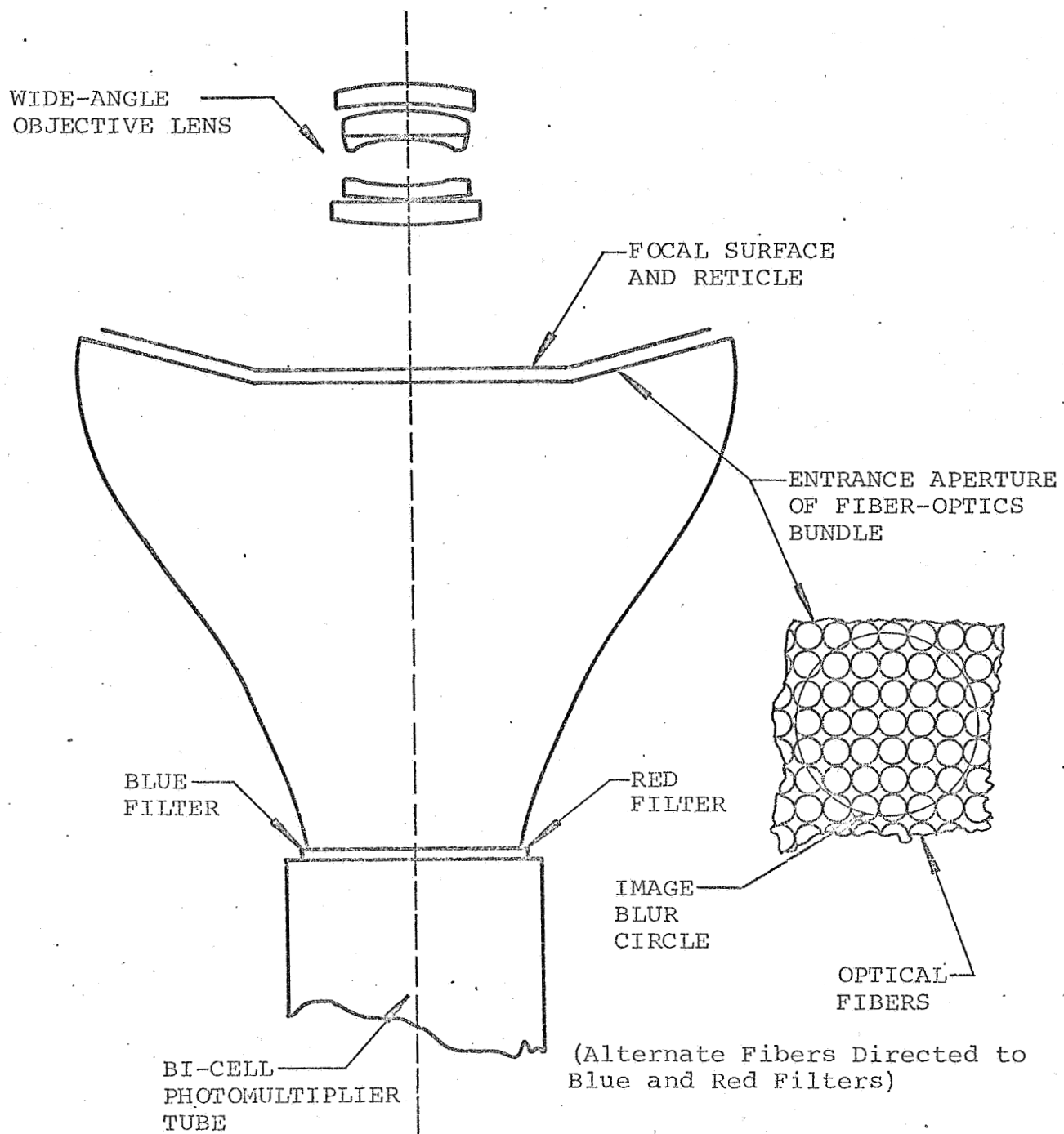
2. Improved Design

A less bulky wide-angle design approach is shown in Figure F-3. The optics are the same in concept as for the system shown in Figure 22 (Section IV.A), but the design differs somewhat.



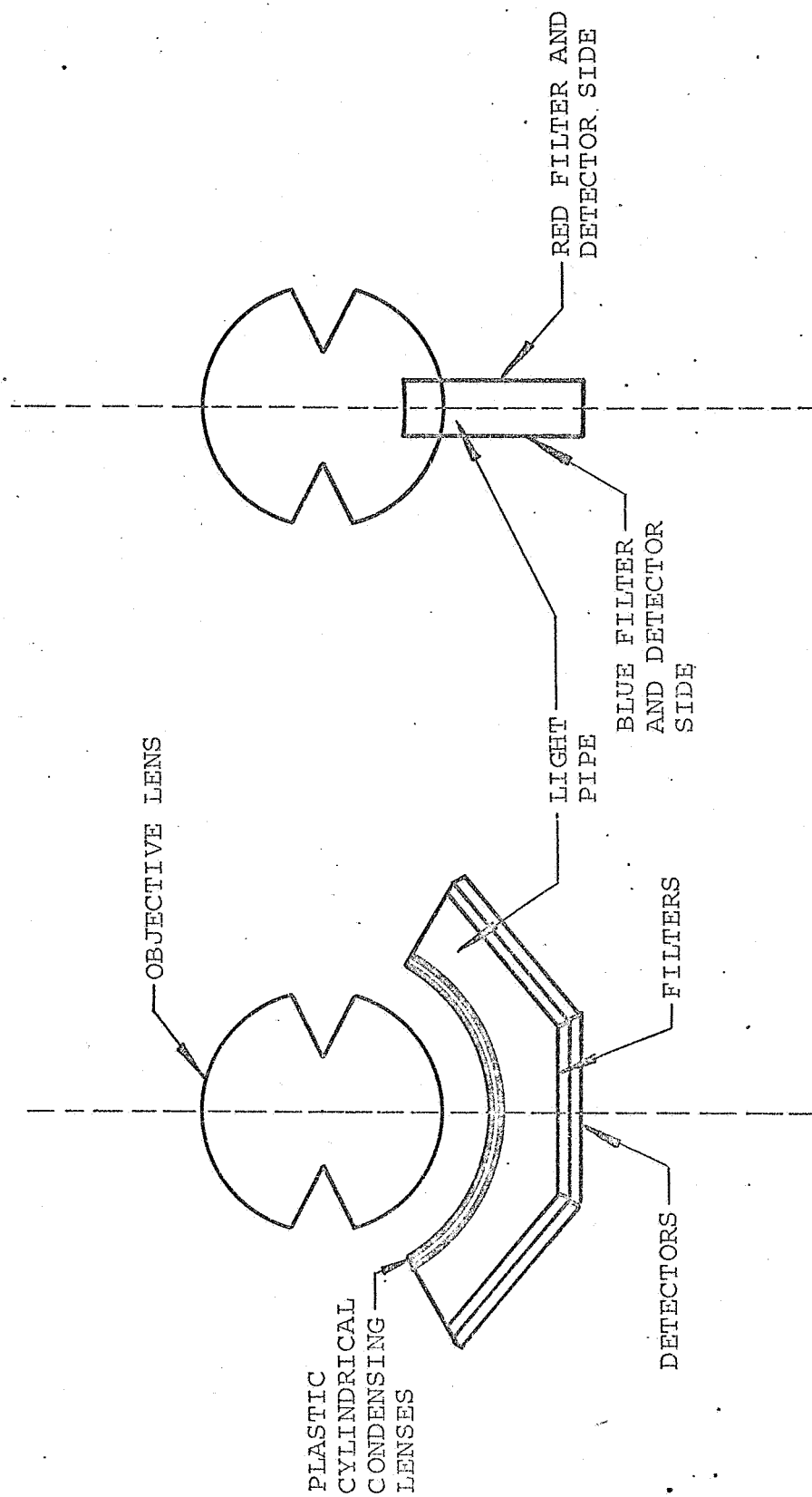
OPTICAL SCHEMATIC
THREE-CHANNEL WIDE-ANGLE OPTICS USING SOLID-STATE DETECTORS

FIGURE F-1



OPTICAL SCHEMATIC
WIDE-ANGLE OPTICS USING FIBER-OPTICS CONDENSER
(WITH PHOTOMULTIPLIER TUBE)

FIGURE F-2



OPTICAL SCHEMATIC
WIDE-ANGLE OPTICS WITH LIGHT-PIPE CONDENSER

FIGURE F-3

in physical appearance. The objective lens is a single-element concentric lens capable of providing an FOV of $120^\circ \times 19^\circ$ with adequate resolution over the entire field.

The surface of best focus for concentric lenses is spherical. The split-rectangle reticle and the entrance aperture of the condensing system are coincident with this spherical surface as indicated.

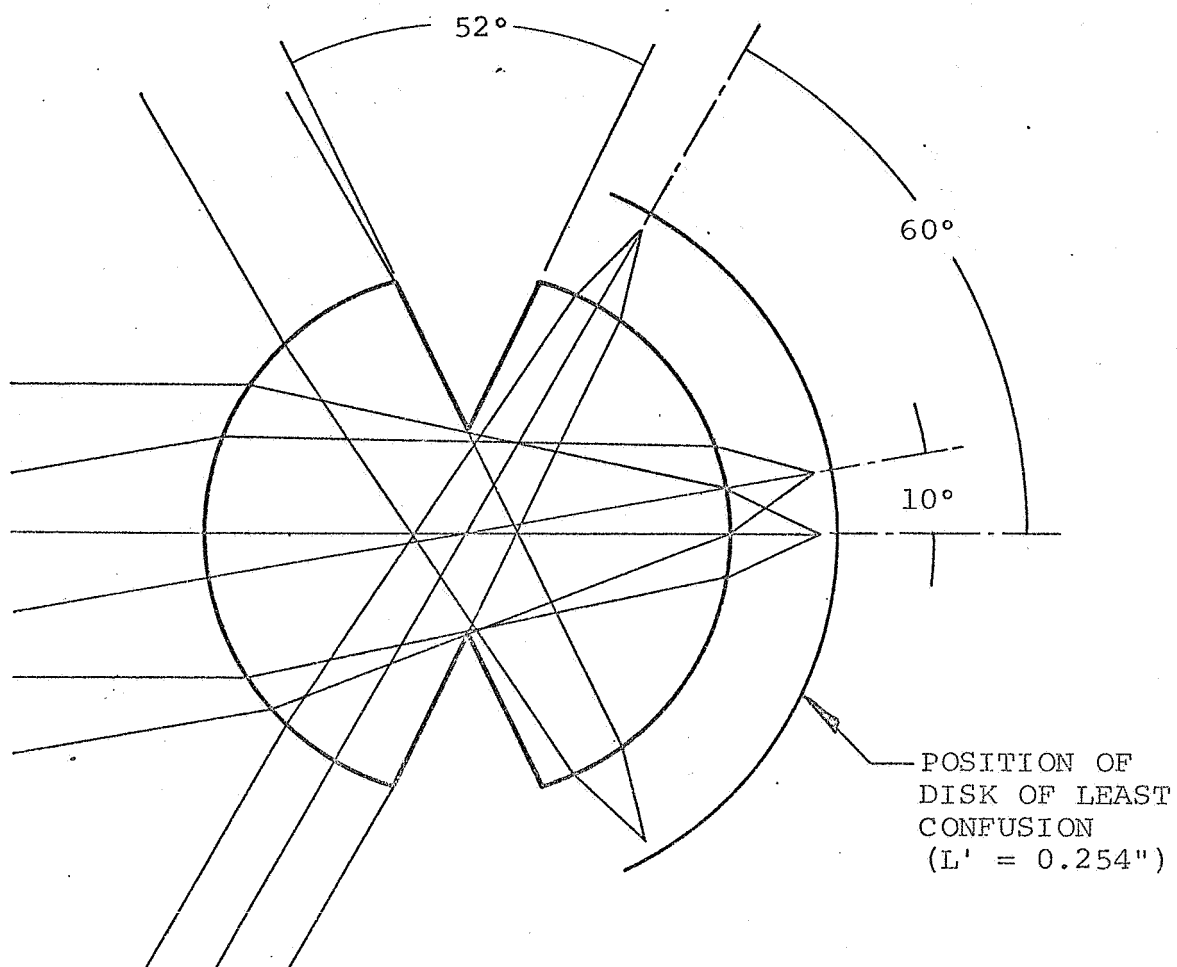
The purpose of the condensing system is to form an image of the objective-lens aperture on the plane of the detectors. If the detector array consists of parallel rectangular segments, it can be seen that a conventional two-dimensional image is not required as long as the rays from one side of the objective lens are incident on one of the detector segments while the rays from the other side of the objective lens are incident on the other segment. An alternative to this would be for rays from all parts of the objective lens to be random with respect to which of the two detector segments they strike, regardless of the position of the target image in the focal plane. It can be shown that this cannot be accomplished with a light pipe of finite length. Hence a cylindrical condensing lens arrangement is installed in the pipe so that the objective lens is imaged along the dimension perpendicular to the long side of the detector segments. A blue filter is placed on one detector segment and a red filter on the other.

The requirement for an FOV of 120 degrees (in a direction perpendicular to target motion) can be satisfied by the simple concentric lens shown in Figure F-4 (on which a nominal design is given). Some of the attractive features of the lens are the following:

- a) It vignettes approximately as $\cos \theta$, where θ is the angle of departure from the optical axis,* instead of $\cos^4 \theta$, as is the case for most conventional lenses. Thus a target 60 degrees off-axis would image one-half the energy it would if on-axis, instead of about 28% as is the case with more conventional lenses.
- b) All angles in the object space are reproduced faithfully in the image space; i.e., the distortion is zero by definition.
- c) The weight of the lens (glass only) is 1.59 ounces.
- d) The resolution is almost constant over the entire field with a circle of confusion of 0.45 degree.

Several design variations for the condensing system were considered, all involving combination light pipes and condensing lenses. A light pipe, shaped as indicated in Figure F-3, with flat internally reflecting walls will serve several purposes. First,

*The axis in this case is defined as the common center of curvature of the two surfaces, also containing the center of the circular aperture stop. Otherwise, a concentric lens has no optical axis.



Focal Length (to Disk of Least Confusion) = 0.935 in.
 Diameter of Disk of Confusion = 0.00780 in.
 = 0.0078 rad
 = 0°45'

Diameter of Lens = 1.363 in.
 f-no. = 1.25

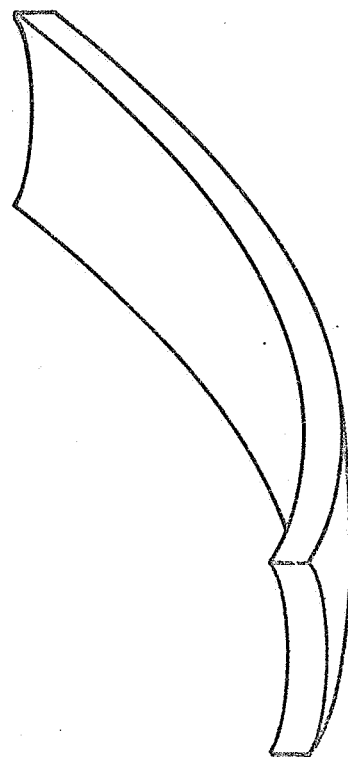
SPHERICAL OBJECTIVE LENS FOR WIDE-ANGLE OPTICS

FIGURE F-4

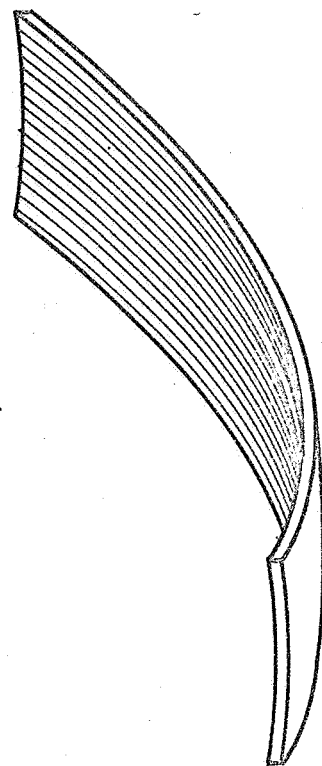
in the direction in which cylindrical lenses have no power, the end walls of the pipe will reflect incident rays and prevent beam divergence in this direction. Second, the side walls of the pipe will reflect some of the extreme rays that would normally fall well outside the image region. This will be particularly true if Fresnel equivalents of the cylindrical lenses are used. Third, the light pipe can serve as a structure for the mounting of the condensing lenses. A conventional version of the cylindrical condensing lenses is shown in Figure F-5a and the Fresnel equivalent in Figure F-5b. Because of the unconventional shape of these lenses, they would be made of molded plastic (probably an acrylic). Although the lens design was not detailed, probably two strips would be required. It can be seen that the surface of best focus is not in a plane but in a cylindrical surface. A detailed design would determine whether or not the placement of the detector array in a plane would be satisfactory. If not, the detector could be segmented as indicated in Figure F-3.

The split-rectangle reticle pattern will fit within an FOV of about $120^\circ \times 19^\circ$. The slope of the split rectangles near the null position is designed to produce as low a scale factor as possible and still yield a noise equivalent angle of $\pm 1/2$ degree (with a safety factor allowance). A higher scale factor would result in a smaller noise equivalent angle but would require a wider electrical bandwidth, thus reducing maximum operating range. At positions away from null, the slope is such as to allow decreased accuracy, again in order to hold to a narrow electrical bandwidth.

Since the operating range of the EAS is less than 15 million miles, signals from planets other than the earth need not be considered since they will not reach the threshold level to trigger the Schmitt in the signal-processing electronics. Therefore, only the moon need be considered in choosing the filters for color discrimination. The filters required to produce a slightly negative lunar-signal output from the differential amplifier are a short-wavelength pass filter with a sharp cut-off at approximately 0.725μ ("blue") and a long-wavelength pass filter with a sharp cut-off at approximately 0.725μ ("red").



a. "Conventional" Version



b. "Fresnel" Version

CYLINDRICAL CONDENSING LENSES FOR WIDE-ANGLE OPTICS

FIGURE F-5

APPENDIX G

SUN SHIELDING

The purpose of a sun shield is to enable an earth sensor to perform properly when the sun is in the vicinity of, but not within, the FOV. The reason drastic sun-shielding measures must be taken can be understood when one considers that the ratio of solar irradiance to the irradiance of the fully illuminated earth at a distance of 5 million miles is about 4×10^6 . At greater distances from the earth, this ratio becomes higher. Although it was not within the scope of the contract to build a sun shield, the problem was investigated briefly to determine the amenability of the EAS being designed to sun shielding.

Traditionally, solar glare is alleviated by means of a blackened conical shield, sometimes with internal concentric rings also black and with sharp edges. Not only are these incomplete, they are also unpredictable because the amount of residual reflection cannot be defined accurately and because the path and intensity of diffuse reflection are very difficult to calculate quantitatively.

The device shown in Figure G-1 is based on two principles, once the blue sky background has been eliminated by space:

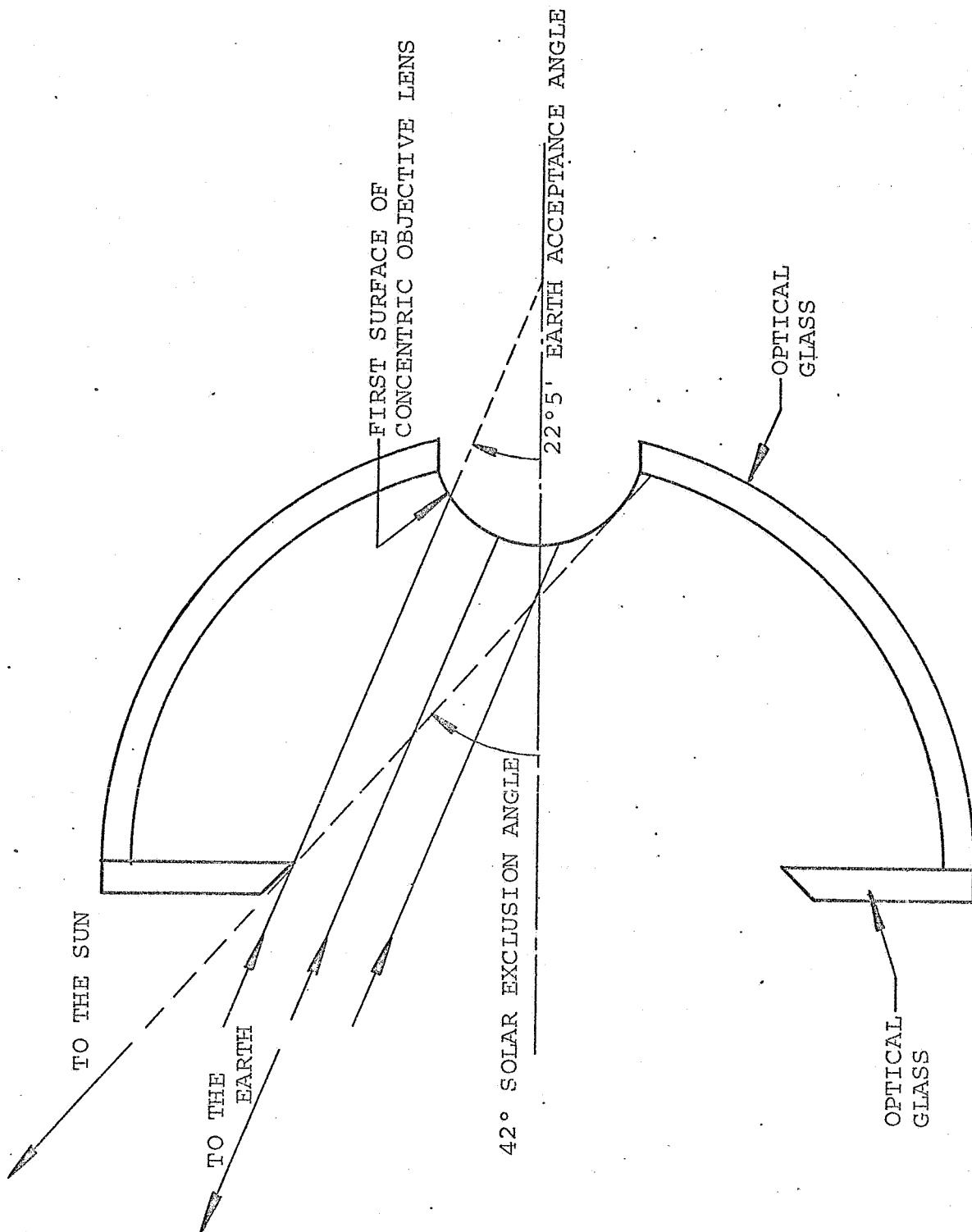
- 1) Specular reflection can be calculated exactly.
- 2) A hemisphere with its aperture at its center of curvature will form an image of this aperture stop at the real aperture stop, and thus all light falling on the specular hemisphere will return to its place of origin.

As with any solar-glare shield, this one would be effective only when direct sunlight is not incident on the objective lens.

The outer surface of the hemisphere is coated with a transparent black whose dyed base has the same index and dispersion as the optical glass. The coated inner surface reflects only about 1/2% of the incident light. Of this very small fraction of sunlight that is reflected, essentially all returns through the shield aperture to space. Thus, when the sun is outside the solar exclusion angle, the only solar rays that can strike the objective lens are those reflected from such glint points as dust on the glass or defects in the glass.

A somewhat modified concept that would result in weight saving could be used with the EAS. If the vehicle spin axis is perpendicular, or close to perpendicular, to the vehicle sun line, the solar look angle will be at or close to 90 degrees and the solar image will sweep by the image surface of the objective lens at the null position. Thus, no shielding would be required for solar positions at large solar look angles. The modified concept would

consist of two cylindrical reflectors that would prevent glare in the 19-degree FOV direction and ignore protection in the 120-degree FOV direction. The shield would have the appearance of curved "horse blinders."



SOLAR-CLARE SHIELD

FIGURE G-1

PRECEDING PAGE BLANK NOT FILMED.

REFERENCES

1. Planetary Coordinates for the Years 1960-1980. H. M. Nautical Almanac Office (London).
2. Kuiper, G. P.; and Middlehurst, B. M.: Planets and Satellites. University of Chicago Press, 1961. Chapters 6 and 8.
3. Kuiper, G. P.: The Earth as a Planet. University of Chicago Press, 1954. Chapter 15.
4. Allen, C. W.: Astrophysical Quantities, Athlone Press, 1963.
5. D. Ya. Martynov, Sov. A, 3, 633.
6. Hardie, R. H.: Private communication (November 15, 1965). Dyer Observatory, Vanderbilt University.
7. Band, H. E.; and Block, L. C.: Spectral Radiance Measurements of the Earth from High Altitudes. Applied Optics, vol. 4, no. 3, Mar. 1965, p. 355.
8. Green, A. E. S.: Attenuation by Ozone and the Earth's Albedo in the Middle Ultraviolet. Applied Optics, vol. 3, no. 2, Feb. 1964, p. 203.
9. Hrasky, W. C.; and McKee, T. B.: Radiance of the Earth and Its Limb in the Middle Ultraviolet. NASA TN D-2355, 1964.
10. Heddle, D. W.: The Spectral Radiance of the Moon in the Near U.V. The Observatory, vol. 83, no. 936, p. 225.
11. Boggess, A., III; and Dunkleman, L.: Ultraviolet Reflectivities of Mars and Jupiter. Astrophysical Journal, vol. 129, 1959, p. 236.
12. Johnson, H. L.; and Mitchell, R. I.: A Completely Digitized Multi-Color Photometer. Comm. of the Lunar and Planetary Laboratory, vol. 1, no. 14, June 1962, p. 73.
13. Eisenman, W. L.; and Cussen, A. J.: Properties of Photoconductive Detectors. Photoconductive Detector Series, 31st Report, NAVORD Report 4649 (NOLC Report 404), U. S. Naval Ordnance Laboratory, Corona, Calif., December 1957.
14. Investigation of Dark Current in ASCOP 541F Multiplier Phototubes After Exposure to High Light Level. Final Report, Electro-Mechanical Research, Inc., for NASA/Goddard Space Flight Center (Contract NAS5-9089).
15. NOLC Report 558, U. S. Naval Ordnance Laboratory, Corona, Calif., January 1962.